INFORMATION TO USERS

This reproduction was made from a copy of a document sent to us for microfilming. While the most advanced technology has been used to photograph and reproduce this document, the quality of the reproduction is heavily dependent upon the quality of the material submitted.

The following explanation of techniques is provided to help clarify markings or notations which may appear on this reproduction.

1. The sign or "target" for pages apparently lacking from the document photographed is "Missing Page(s)". If it was possible to obtain the missing page(s) or section, they are spliced into the film along with adjacent pages. This may have necessitated cutting through an image and duplicating adjacent pages to assure complete continuity.

2. When an image on the film is obliterated with a round black mark, it is an indication of either blurred copy because of movement during exposure, duplicate copy, or copyrighted materials that should not have been filmed. For blurred pages, a good image of the page can be found in the adjacent frame. If copyrighted materials were deleted, a target note will appear listing the pages in the adjacent frame.

3. When a map, drawing or chart, etc., is part of the material being photographed, a definite method of "sectioning" the material has been followed. It is customary to begin filming at the upper left hand corner of a large sheet and to continue from left to right in equal sections with small overlaps. If necessary, sectioning is continued again—beginning below the first row and continuing on until complete.

4. For illustrations that cannot be satisfactorily reproduced by xerographic means, photographic prints can be purchased at additional cost and inserted into your xerographic copy. These prints are available upon request from the Dissertations Customer Services Department.

5. Some pages in any document may have indistinct print. In all cases the best available copy has been filmed.

University
Microfilms
International

300 N. Zeeb Road
Ann Arbor, MI 48106

Aly, Samy H.

SM-CO BASED FERROMAGNETIC FILMS SYNTHESIZED DIRECTLY BY RF SPUTTERING

City University of New York PH.D. 1985

PLEASE NOTE:

In all cases this material has been filmed in the best possible way from the available copy. Problems encountered with this document have been identified here with a check mark _✓_.

1. Glossy photographs or pages _____
2. Colored illustrations, paper or print _____
3. Photographs with dark background ✓
4. Illustrations are poor copy _____
5. Pages with black marks, not original copy _____
6. Print shows through as there is text on both sides of page _____
7. Indistinct, broken or small print on several pages ✓
8. Print exceeds margin requirements _____
9. Tightly bound copy with print lost in spine _____
10. Computer printout pages with indistinct print _____
11. Page(s) _____ lacking when material received, and not available from school or author.
12. Page(s) _____ seem to be missing in numbering only as text follows.
13. Two pages numbered _____. Text follows.
14. Curling and wrinkled pages _____
15. Other _____

Sm-Co BASED FERROMAGNETIC FILMS SYNTHESIZED DIRECTLY BY RF SPUTTERING

by

SAMY H. ALY

A dissertation submitted to the Graduate Faculty in Physics in partial fulfillment of the requirements for the degree of Doctor of Philosophy, The City University of New York.

1985

This manuscript has been read and accepted for the Graduate Faculty in Physics in satisfaction of the dissertation requirement for the degree of Doctor of Philosophy.

February 22, 1985 — Date
Fred J. Cadieu — Chairman of Examining Committee

Feb. 22, 1985 — Date
[signature] — Executive Officer

Prof. Jacob Neuberger
Prof. Fred J. Cadieu
Prof. Maryim Sarachick
Prof. Joseph Kreiger
Dr. Ron Pirich
Supervisory Committee

The City University of New York

ABSTRACT

Sm-Co BASED FERROMAGNETIC FILMS SYNTHESIZED DIRECTLY BY RF SPUTTERING

by

Samy H. Aly

Adviser: Professor F. J. Cadieu

The light rare earth intermetallic ferromagnetic compounds exhibit both high saturation moment and high crystal anisotropy energy. Also, they have high critical temperature for magnetic ordering. These properties made them excellent candidates as permanent magnet materials.

The purpose of this work is to study the magnetic properties of ferromagnetic films of the Sm-Co based system. The films are synthesized by selectively thermalized RF sputtering onto heated substrates without any further heat treatment for promoting their magnetic properties.

In the first chapter we review the basic mechanisms responsible for the outstanding properties of these materials. The second chapter deals with the experimental procedures for synthesis of the ferromagnetic films by RF sputtering. The effects of different sputtering parameters on the films physical and microstructural properties are discussed.

In the third chapter the method of x-ray energy dispersive fluorescence analysis used to study the composition of our films is presented. The fourth chapter covers the x-ray diffraction techniques used to study the crystal structure of the films, to determine the grain size and the

states of preferred orientations of certain crystal planes developed in the films.

In the fifth and last chapter we present our results and discuss them on the light of the previous chapters. Magnetization, coercive forces, and energy products of the films as obtained from hysteresis loop measurements are discussed. In addition, a tentative model of the possible magnetization reversal processes in our films is suggested. A discussion of the preferred textures exhibited by these films closes the chapter.

ACKNOWLEDGMENTS

I am grateful to my supervisor, Professor Fred J. Cadieu, for his continuous support and encouragement throughout this work. Thanks are also due to all the members of our research group; in particular Dr. Tak D. Cheung, Lee Wickramasekara, Hossin Abdeldayem, and Patt Harington for several helpful contributions in one way or another.

I would also like to thank the members of my committee, in particular Dr. Ron Pirich of the Grumman Aerospace Corporation for being able to perform some magnetic measurements in his lab and for useful discussions.

It is my pleasure to also acknowledge the helpful assistance of our machine and electronics shop group and to all my teachers, colleagues and friends.

My thesis is part of a research program studying rare earth transition metal permanent magnet systems which has been principally supported by the U.S. Army Research Office. During part of my studies as a graduate student, I was supported by the U.S. Army Research Office contract funds. I was also supported in part by funds from the PSC-BHE Faculty Research Award Program Grants of Professor Cadieu.

TABLE OF CONTENTS

Page

Page

LIST OF TABLES

LIST OF FIGURES

1.1.1) RARE EARTH ELEMENTS

1.1.2) THE ELECTRONIC CONFIGURATION:

The ground state of those elements has a configuration given by :(Xe) $4f^x$ $5d^y$ $6s^2$, in which (Xe) refers to the full shell core of Xenon.[1] The 5d and 6s electrons are responsible for bonding while the 4f electrons are inner electrons with their quantum mechanical probability peaks closer to the nucleus than do the d and the s electrons, so these 4f electrons play a minor role in bonding and hence the magnetic properties of rare earth elements are attributed to them. Being well localized the 4f electrons behave almost like electrons in free ion, i.e. approximately unaware of the surroundings. The ground state configuration is given by Hund's rule, however the total angular momentum is a good quantum number because of the relatively strong spin orbit interaction. The lowest J multiplet is normally populated at room temperature. The value of J for more than and less than half filled f shell is given by L+S and L-S respectively.

1.1.3) MAGNETIC PROPERTIES OF FREE IONS

The interaction that a rare earth atom experiences in a crystal are electrostatic in origin, they are the crystal field and exchange interactions. These two interactions are of energy smaller than the spin orbit coupling energy and are $\lesssim$ KT at room temperature.

The magnetic interaction between the moments and a magnetic field H is given by:[2]

$$\sum_i u_B (\vec{L}_i+2\vec{S}_i).\vec{H} = u_B (\vec{L}+2\vec{S}).\vec{H}$$

and for the lowest multiplet $\vec{L}\sim(2-\lambda)\vec{J}$ where λ is Lande factor. For rare earths $\lambda<2$ (except for Gd and Eu) and thus $\vec{L}$ is always parallel to $\vec{J}$, however since $\vec{S}\sim(\lambda-1)\vec{J}$ for the lowest multiplet and since $\lambda<1$ for more than half filled shell and $\lambda<1$ for less than half filled shell (except for La, Ly and other non-triplet ionized atoms), the spin is parallel to the total angular momentum for Gd and heavier elements but antiparallel to it for light rare earths, i.e. those of less than half filled f-shell, the saturation moment is given by $\lambda u_B J$ per atom if the environmental forces are considered to be null which is not the case.

1.1.4) EXCHANGE INTERACTIONS BETWEEN IONS

Exchange interaction and not the crystal field interaction that a rare earth ion undergoes must be responsible for magnetic order which is a cooperative phenomenon. The exchange between two electronic spins is given by the following isotropic hamiltonian: $H_{ex}=J_{ex}\vec{s}_i\cdot\vec{s}_j$, but for atoms i, j of several electrons each the hamiltonian reads $H_{ex} = J_{ex}\,\vec{S}_i\cdot\vec{S}_j$ where the total spins are involved. The exchange constant J_{ex} as appears in the above hamiltonian is assumed not to depend on orbit, in fact J_{ex} does depend on the overlap of atomic orbitals as well as on the crystal structure but it does not vary much along the rare earth series.

The mechanisms responsible for the interaction given by H_{ex} can be isotropic or anisotropic relative to the crystal axes. If the

exchange is due to direct overlap between charge clouds of nearby atoms it should depend on the orientation of the involved charge distributions relative to some reference axis, e.g. the crystal axis and this might cause anisotropic terms to appear in the exchange hamiltonian. Moreover the electrostatic interactions, being anisotropic can lead also to some anisotropy in H_{ex}, however these interactions are more important in the light rare earths because the electronic multipoles are larger for them because of the lanthanides contraction, i.e. the decrease in the charge cloud spread as the atomic number increases.

It is important to notice that the crystal field effects are the opposite of the exchange interactions effects. At temperatures of the order of the crystal field splitting the crystal field can destroy or at least diminish the orbital contribution to the magnetic moment of the ion, but since the spin orbit coupling is strong, the spin contribution and not only the orbital contribution to the total magnetic moment is diminished.

1.1.5) MAGNETIC ANISOTROPY

The magnetic anisotropy energy in most of the rare earths is very large and is considered to be important perturbation to the exchange, this in contrast to the 3d transition elements as it will be seen. The heavy rare earths in particular have very large anisotropy, this is due to the interaction between the crystal field and the non-spherical 4f cloud multipole moments, the large spin orbit locks the spin direction to the orbital angular momentum direction (Gd is an exception).

1.2.1) THE 3d TRANSITION ELEMENTS

Those are the elements from SC^{21} of outer most electronic configuration $4s^2\ 3d^1$ to Zn^{30} :$4s^2\ 3d^{10}$, the atoms of those elements have the 3d inner shell of higher energy than the 4s outer shell, the filled shell 1s, 2s, 2p, 3s and 3p do not contribute to the magnetism of these atoms. In the 3d elements the 4s electrons are the ones mostly responsible for bonding and hence the 3d electrons are outer electrons subjected to the inhomogeneous crystal field, so the 3d atoms can retain their magnetic moment as they compose the crystal. The directions of $\vec{L}$ and $\vec{S}$ however, and hence the directions of their perspective magnetic moments are influenced by factors like spin orbit interaction and of course the application of an external magnetic field. The effect of the crystal field on those ions is to quench the orbital momentum and thus reduces the orbital contribution to the total magnetic moment.[1,3] In contrast to the crystal field effects, the spin orbit coupling causes the electronic orbital wavefunction to be polarized, i.e. introducing some component of the orbital motion depending on the strength of LS coupling. Ferromagnetism is only observed in Fe, Co and Ni of the 3d series.

The theories that try to explain the existence of ferromagnetism in those elements vary among themselves regarding the nature of the 3d electrons behavior in the solid, namely whether they are itinerant or itinerant but with their motion correlated by coulomb interactions.[3,4] The theory based on complete localizability of the 3d-electrons has its drawbacks, for example the expected ionic moment must be integer multi-

ple of Bohr magneton, however the experimental values for Fe, Co and Ni for example are 2.2, 1.7 and 0.6 Bohr magnetons respectively assuming that 4s electrons contribute nothing to the magnetism. According to the band theory explanation of ferromagnetism the "magnetic electrons" must lie in partially filled bands, i.e. vacant energy levels must be available to accommodate unpaired spins, also high density of states and sufficient overlap between atomic orbitals are another condition for the occurence of ferromagnetism. The ionic radii of the divalent 3d ions vary from about 0.9 to about .7 angestroms as one goes across the series from Ti to Ni, i.e. the d orbitals become more localized across the series and the d bands become more narrow. In terms of curie temperature Fe, Co and Ni have 1394, 1043 and 631 degress kelvin respectively. The question of using pure cobalt as permanent magnet will be investigated later, being uniaxial and of high induction and high curie temperature, in addition to relatively high anisotropy recommended its use for permanent magnets, however problems of instability of the required hexagonal phase and certain particle size requirements made rare earth cobalt compounds much more superior as will be discussed next section.

1.3.1) RARE EARTH INTERMETALLIC COMPOUNDS WITH COBALT

1.3.2) INTRODUCTION

For a material to be a good candidate for permanent magnets particular qualifications should be present in order to guarantee high performance, those are high Curie temperature to be useful at high

working temperatures, relatively high remanent magnetization which is a prerequisite for high induction and high anisotropy field which is the field required to twist the magnetic moment from the easy to the hard direction of magnetization. The latter requirement is necessary to hold the magnetization in place after removal of the magnetizing field.[1,5]

Among RCo_5 intermetallic compounds[1,5,6] only Gadolinum and heavier rare earths couple antiferromagnetically with the cobalt sublattice, the lighter elements, however couple ferromagnetically with cobalt. The $SmCo_5$ system in particular has been investigated[7,8] to study the nature of coupling between the very small moment of samarium (about $0.6u_B$) and the cobalt moment, the coupling is believed to be ferromagnetic, i.e. the moments of the two sublattices couple parallel to each other.

In RCo_5 and R_2Co_{17} compounds the anisotropy is determined by an interplay between the cobalt and the rare earth sublattices. In RCo_5 compounds the cobalt sublattice prefers large and positive values of the anisotropy constant k_1, i.e. cobalt sublattice prefers easy axis, the rare earth on the other hand favors easy axis for samarium[9] but an easy plane for other rare earths (e.g. Nd, Ho, Tb and Pr). In the R_2Co_{17} case the Co sublattice prefers easy plane, the anisotropy constant is one order of magnitude smaller than that of RCo_5 and is negative, however the rare earth sublattice anisotropy is dominant for Samarium even at room temperature and an easy axis preference is present for Sm_2Co_{17} even at room temperature.[10,11] Models have been proposed[9,12,13] to account for the important role played by the rare

earth sublattice in 1:5 and 2:17 cobalt compounds. In such models the rare earth is subjected simultaneously to a crystalline electric field and an effective exchange field.

The exchange field at rare earth ion is considered to be composed of rare earth-rare earth exchange and rare earth-transition metal exchange. Those two interactions and the transition metal-transition metal interaction are reviewed briefly in the following sections.

1.3.3) THE RARE EARTH-RARE EARTH EXCHANGE

As has been discussed before the interatomic distances between rare earth ions in the elements are large compared to the radius of the 4f shell, this situation is present as well in rare earth intermetallic compounds. The 4f electrons therefore are considered to be localized in those compounds as well and so dipole-dipole and direct exchange interactions represent but a small part of the magnetic interactions between rare earth ions in such compounds. It has been suggested by Kittel and others that the interaction takes place via the conduction electrons, this is known as the RKKY interaction.[12] Unlike the Heisenberg exchange between localized electronic moments or the exchange between itinerant or Bloch electronic moments the RKKY exchange takes place between f-f electrons through s-f exchange.

A spin polarization of the conduction electrons is induced because of the presence of the magnetic 4f electrons and through that polarization the localized 4f magnetic moment themselves interact. The oscillatory nature of the conduction electron polarization is not

uniform in space, rather its amplitude decreases with the distance from a given 4f moment. The coupling between the localized 4f moments could lead to parallel or antiparallel alignment of those moments depending on the location of the other 4f moments from the referenced one.

The R-R interaction is relatively weak, the low values of the ordering temperature, which is a measure of the interaction strength, observed in the R-M compounds where M is not a magnetic ion is an experimental evidence of the weakness of that interaction.[6]

1.3.4) THE M-M INTERACTION

The 3d wavefunctions are known to be of much larger spatial extent than the 4f wavefunctions, and hence the M-M interaction is much more stronger than the R-R interaction. The experimental evidence of that is the much higher ordering temperature observed for R-M compounds in which R is not magnetic.[6]

The strong overlap between the 3d wavefunctions suggested itinerant electron models based on the 3d band structure to be developed,[14] on the other hand more localized models have been suggested as well to explain the magnetic properties of these compounds.[15,16] Experimental work including NMR and Mossbauer on one side and magnetovolume effects on the other side gave indication of the localized and the itinerant nature of the 3d electrons respectively.

1.3.5) THE R-M INTERACTION

It has been already mentioned in the introduction to this section

that parallel and antiparallel coupling between the moments for light and heavy compounds respectively have been used to interpret the observed saturation moments.

The antiparallel coupling between the 3d and 4f spin magnetic moments has been accounted for using different models.[10,11] Due to the very small magnetic moment of Sm ion ($<=0.7\mu_B$), the nature of coupling between the Co and Sm sublattice is not quite clear although it has been suggested to be ferromagnetic.[7,8] The strength of that interaction is intermediate between R-R and M-M interactions.

1.3.6) MAGNETOCRYSTALLINE ANISOTROPY ENERGY

1.3.7) INTRODUCTION

In a ferromagnetic crystal the magnetization prefers to be directed along certain crystallographic axes called the directions of easy magnetization. It takes particular amount of energy to magnetize a crystal to saturation along an easy axis, it takes more energy, however, to saturate the same crystal along other axis called the hard axis of magnetization. The difference between these to amounts of energy is called the magnetocrystalline anisotropy energy or simply the crystal energy.

For a hexagonal crystal the expression of the anisotropy energy density is in general given by:

$$E_n = \sum_n k_n \sin\theta^{2n}$$

where θ is the angle that the magnetization makes with the easy axis

which is the c-axis of the crystal in the case of the hexagonal crytals under study. k_n are the anisotropy constants, they are independent of angle but are strongly temperature dependent.[1,17] The odd powers of sinθ are not considered because of magnetic and crystallographic symmetry considerations.

For $SmCo_5$ the anisotropy energy is determined mainly by k_1 only because other constants are negligibly small compared to k_1 in the temperature tange from about 0-1000 K.[17] The value of k_1 at 4.2 k was measured to be 2.62×10^8 erg/cc and 1.71×10^8 erg/cc at room temperature,[18] further more the anisotropy constants were found to be sensitive to the oxygen content of the sample.[9] The temperature dependence of k_1 for $SmCo_5$ has been studied in several works,[9,18-20] up to room temperature in some and to about 1000 K in others. k_1 was shown to be positive at all temperatures up to about 1000 K.[14]

A very essential parameter that distinguishes $SmCo_5$ is its very large anisotropy field. The anisotropy field is defined as the field required to saturate the material in the hard direction or equivalently the field required to rotate the magnetization vector into the hard direction. Such rotation requires a torque that is proportional to k_1 which is a measure of the material magnetic hardness.

The anisotropy field is given by:

$$H_A = 2k_1/M_s$$

assuming that magnetocrystalline anisotropy dominates over the other sources of anisotropy, e.g. shape and magnetostruction anisotropies, and that the magnetization reversal takes place only through coherent

domain rotation. M_s is the saturation magnetization of the sample, the value of H_A is estimated by extrapolating the hard axis curve to saturation.

For $SmCo_5$ H_A is about 600 kOe near absolute zero and about 400 kOe near room temperature.[21] In general R_2Co_{17} compounds have anisotropies much less than the corresponding RCo_5 compounds,[19] in particular Sm_2Co_{17} has an anisotropy field about one order of magnitude less than that of $SmCo_5$.[22,23]

1.3.8) ORIGIN OF MAGNETOCRYSTALLINE ANISOTROPY

The exchange energy is known to be isotropic relative to the crystal axes since it depends on the directions of the interacting spins relative to each other but not relative to the crystal axes themselves and thus it does not lead to any anisotropy. An old study by V. Vleck[24] showed that magnetic interactions such as dipole dipole interaction lead only to a small contribution to the observed anisotropies and thus cannot by itself stand as the only source of anisotropy.

Several studies[9,13,25] showed that the origin of the extremely large anisotropy of $SmCo_5$ lies in the combined effects of the crystalline electric field and the exchange field on the Sm single ions. The magnetic dipole dipole interaction in $SmCo_5$ is very small since it is proportional to the square of the magnetic moment, the latter is only $<=0.7\mu_B$ for Sm and thus it is justified to be entirely neglected.[25] The preferred direction of Sm sublattice magnetizations has been established to be along the c-axis in the entire temperature range

4 to about 1000 K[9] in agreement with the experimental data done on single crystals.

The hamiltonian used in such calculations contains the spin orbit coupling, the exchange field interaction with the spin magnetic moment of Sm and the crystal field interaction. An amount of energy called the stabilization energy of the Sm sublattice is taken as a measure of the relative stability of the Sm sublattice in those compounds. That amount is defined as the difference in the free energy of the system if the exchange field is taken parallel or perpendicular to the c-axis keeping all other interactions the same. That energy is equal to the absolute value of k_1+k_2 where these constants are associated with the Sm sublattice alone. It is worth mentioning that the hexagonal structure of this class of compounds and the type of point symmetry D_{6n} at the rare earth site for which there are six rare earth next neighbors in the plane of the reference atom and two neighbors along the c-axis are important factors of the prominent role that the crystal field effects do have in such compounds.

The cobalt contribution to the magnetic anisotropy in 1:5 compounds is a substantial one. The exchange field at Sm ion springs mainly from the Sm-Co exchange interaction and hence is proportional to the cobalt sublattice moment.[26] Several other works[27] showed that the anisotropy declines for more Co rich $CaCu_5$ type compounds. It has been shown using neutron diffraction[28] that the Co (2c) sites contribute the most to the magnetic anisotropy.

The structure of Sm_2Co_{17} is related to that of $SmCo_5$.[5,6] Figure 1 shows the crystal structure of the $CaCu_5$ compound. The reduction of

anisotropy upon increasing the Co content in RCo_5 compounds has been attributed to the introduction of what is called dumbbell pairs of Co atoms in some of the R sites in RCo_5, such introduction has the effect of reducing the symmetry at the 2c site and hence decreasing the anisotropy.[10,28,29]

1.3.9) MAGNETIZATION OF RE-TM COMPOUNDS

The saturation magnetization of $SmCo_5$ per atomic species is about 1.4 μ_B compared to 1.72 μ_B for elemental cobalt and 2.2 μ_B for elemental iron. So as far the magnetization itself is concerned $SmCo_5$ is not superior, as has been discussed in the previous section. It is the very large anisotropy that distinguishes that compound.

Sm_2Co_{17} on the other hand has magnetization higher than that of $SmCo_5$ due to the increase of the 3d atoms concentration. As in the case of RCo_5 compounds the magnetization of R_2Co_{17} compounds can be accounted for using two sublattice models in which the spin magnetic moment of R is antiparallel to that of the Co, with ferromagnetic coupling between the total moments in Sm_2Co_{17} compound.[30] The R_2Co_{17} compounds exhibit higher saturation magnetization and higher curie point than the corresponding RCo_5 compounds on one hand, and R_2Fe_{17} compounds on the other hand.

The saturation magnetization $4\pi M$ has been measured for $SmCo_5$ single crystals,[20] and varies from about 10.2 KG to about 9.65 KG in the temperature range from 80-300 K, i.e. from about 94 emu/gm to about 89 emu/gm for samples of density 8.6 gm/cc. A value of more

than 80 emu/gm has also been reported earlier[31] for a well aligned sample prepared by liquid phase sintering. The saturation magnetization calculated for hexagonal unit cells of $SmCo_5$ having a moment of 8.5 μ_B is about 100 emu/gm that is 10.8 kG. The Sm_2Co_{17} on the other hand has been reported to have higher saturation magnetization of 12 KG i.e. about 110 emu/gm.[30,32] The samples in those works were slightly richer in Co than the stoichiometric composition but magnetization data has been corrected for that.

1.3.10) COERCIVITY OF RE-TM COMPOUNDS

Coercivity is a measure of the material resistence to demagnetization. The instrinic (extrinsic) coercive force is defined as the field required to reduce the magnetization (induction B) to zero. The name coercivity, however, is used sometimes in the literature to denote the field required to demagnetize a practically saturated material. This terminology will be used in this work from now on. Clearly for permanent magnet applications a high coercivity is highly desired.

The materials with high anisotropy fields do have great potential to have high coercivity as well, however in order to take full advantage of high anisotropy fields, the microstructure of the material should be such that the magnetization is forced to reverse against the high anisotropy field rather than getting reversed through other mechanisms which lead only to small coercivities, e.g. domain wall rotation. The coercivity of the material is not a thermodynamic state function depending on temperature and pressure, but rather it depends

strongly on the microstructure[30,33-35] of the material which is sensitive to the synthesis method.

Many investigations[21,36,37] have been done to study the mechanisms of magnetization reversal in single crystals and sintered R-Co compounds, and to account for the observed coercivities of $SmCo_5$ in particular which is only one order of magnitude below the theoretical upper limit determined by H_A, i.e. only about 10% of the room temperature value of H_A for example (400 kOe) has been measured.[33] The effect of the magnetostatic demagnetization field which is oriented antiparallel to the spontaneous magnetization and thus causes reversed domains to be formed is only negligible in case of $SmCo_5$ magnets. For example at room temperature $4\pi M$ = 9.65 KG and H_A = 400 kOe, so the intrinsic force H_A = 400 - 9.65 kOe, this is about 390 kOe that is about 97% of H_A, this means that some other mechanisms are responsible for the observed coercivities.

1.3.11) ENERGY PRODUCTS

The function of a permanent magnet is to provide an external magnetic field and persist to do so in the presence of demagnetizing factors. The field provided by the magnet poles in a given air gap should be as large as possible for given gap and magnet volume. The relation between gap volume V_g, magnet volume V_m and the field in gap H_g is given by:[38]

$$B_m H_m = V_g H_g^2 / V_m$$

if equal cross sectional areas of air gap and magnet are assumed. The amount $H_g^2 V_g/8\pi$ represents the energy density stored in the air gap. It is independent of magnet volume and is proportional to BH which is called the energy product.

The magnet should be designed such that it operates at the point of maximum BH product $(BH)_{max}$ located on its demagnetization curve. It should be mentioned that the energy product just referred to is the static energy product for which the air gap is fixed in size. For materials with high anisotropy fields, one may show that:

$$_BH_c = B_s = 4\pi M_s$$

the maximum energy product in such cases is given by:

$$(0.5xB_s)(0.5x_BH_c) = (0.5xB_s)^2 = 4\pi^2M_s^2 = B_s^2/4$$

assuming perfect alignment, i.e. $B_r=B_s$ and packing fraction of unity, if the alignment, however, is not perfect, i.e. $B_r<B_s$ and that $_iH_c$ is numerically greater than B_r, the maximum energy product will be given by $B_r^2/4$.

It is worth mentioning that the intrinsic coercive force for R-Co alloys are much larger than the extrinsic coercive force. This is so since the theoretical upper limit of $_iH_c = 2K/M_s$ which is much larger than the limit of $_BH_c$ given by $4\pi M_s$, evidently because $k>>M_s$ for these materials. The maximum possible energy product for fully aligned and totally packed $SmCo_5$ of density 8.6 gm/cc is about 29 Mg-Oe.

Very high $_iH_c$ have been reported[33,39] but this high coercive force was associated with low energy product[33] of about 4 Mg-Oe for high rate

sputtered and then annealed $SmCo_5$ thick films. High energy products about 22 Mg-Oe has been achieved for $SmCo_5$ bulk slightly richer in Sm than the stoichiometric composition, with $_iH_c$ about 17 kOe.[40]

2.1.1) MAGNETIC THIN FILMS: EXPERIMENTAL PROCEDURE

2.1.2) INTRODUCTION

Radio frequency sputtering techniques[41-43] have been used for synthesizing our magnetic films. This technique is different from and has some advantages over the evaporation technique[43-45] and is more efficient and versatile than the D.C sputtering method.[42]

Its efficiency springs from the fact that using A.C source promotes the ionization of the sputtering gas and this in turn leads to self sustaining the discharge, which means that the number of generated secondary electrons is enough to produce more sputtering gas ions by collisions with the neutral gas atoms and those ions in turn produce the same number of electrons again. Its versatility even over other rare eath-transition metal permanent magnet preparation techniques stems from the variety of parameters involved in the sputtering process (see section 2.1.6) which offer a unique opportunity to study and optimize the factors that affect the material, chemical, physical and crystallographical state and hence affect its magnetic properties.

The major advantages of sputtering over the present techniques, e.g. poweder metallurgy has been reviewed in the literature, high rate sputtering has been suggested even for magnet production.[33] The coercive force of the R-Co compounds are still only an order of magnitude lower than $2k/M_2$. Effects of oxygen and material morphology on the magnetic properties of those compounds have been studied extensively.[21,33,34,36,40,46] The effect of both oxygen and argon incorporation in our magnetic films on their physical and crystallographical

states and hence their relation to the magnetic properties of the films will be discussed.[47-50]

2.1.3) TARGET PREPARATION

For preparing the targets from the material to be sputtered we have used an arc melter[51] which uses an inert gas like argon for effectively flushing contaminations during melting as well as for rapid quenching of the molten to room temperature. Also targets prepared by arc melting have the advantage over other methods, e.g. hot pressing of powder targets[41] which are very dense and hence minimize contamination problems.

Target materials have been melted more than once to assure their homogeneity; highly pure and well homogenized samples have been prepared from chunks and/or powder of research type elements of high purity (99.999% Co and 99.99% Sm). Preparing Sm targets was rather difficult because of the high reactivity of the Sm element. Tungsten rods have been used to support the targets and to mount them in the target holder inside the sputtering chamber. The purity and homogeneity of the targets have been checked by XFA (Chapter 3).

Targets are in the form of buttons of pure elements with a surface area of about 1 squared centimeter each. Three of them, two cobalt and one samarium, were used for trisputtering, i.e. for simultaneous sputtering from the three targets. The relative cobalt content of the targets is chosen to be more than the samarium content because of the Sm-Co compounds of interest for permanent magnets are Co rich compounds. The arrangement of the targets was such that a composition gradient was

established along the substrate length from cobalt rich subregions to samarium rich ones.[47-49]

The existence of subregions of different composition enabled a systematic study to be done relating the magnetic properties to composition and to crystal structure. In some stage of this work, films of single phase $SmCo_5$ were prepared from single phase nonaligned $SmCo_5$ bulk cylinder obtained from Crucible, Inc., three targets in the form of disks about 0.6 inches in diameter each were cut out from the cylinder.[50]

Figure (2) displays the x-ray diffraction pattern of one of the targets. The pattern agrees with that obtained from the powder file, but with different relative intensities of the lines. The lattice parameters obtained from that pattern are: c=3.966 and a=5.002 A. The purity of the targets has been checked by x-ray fluorescence analysis (Chapter 3). The density of the target material has been measured to be about 7.8 gm/cc while the x-ray density as determined from the lattice parameters given is 8.6 gm/cc.

2.1.4) APPARATUS DESCRIPTION

Figure (3) sketches the apparatus used for RF sputtering in this work. The chamber (from Varian) is made of stainless steel with different ports for gas inlet, vacuum gauges, powering targets and substrate, and several other ports for viewing the glow discharge and connecting any other equipments. Vacsorp pumps which use the principle of physical adhesion were used for pumping the system from atmospheric

pressure down to about one micron, then inert gas ion pumps and a titanium sublimation pump were used for pumping down to the base pressure of 10^{-8} to 10^{-9} Torr. Liquid nitrogen was allowed to pass during sputtering through a shroud for cooling down the cryopanel of the titanium pump for maintaining low contamination during film deposition.

The upper part of the chamber which is usually opened frequently for mounting targets and substrates, etc., is isolated from the lower part by an isolation valve. A dry nitrogen gas was allowed to pass through the system rather than passing moist air whenever the system was to be vented. In addition heater belts around both parts of the system were used to improve the degassing process and thus aided in bringing the system back to working vacuum conditions quickly and effectively.

The RF power supply output impedence (50 ohms) is matched with the glow discharge impedence, which is usually much higher using a matching LC circuit. It is well known that the power of RF generator is maximum if its output impedence is equal to the load impedence.[52] Using such matching circuits enabled maximum power to be dissipated in the glow discharge itself and hence minimizing the reflected power that could damage the generator. The high frequency of 13.56 Mhz of the radio source caused the target to be self biased with negative potential.[42] This is so in principle because of the different mobilities of the ions and the electrons in the plasma, a magnitude in the order of 1 kv has been used in this work.

The negatively self biased targets attract the positive ions of the sputtering gas. They impinge on the target surface and cause the sputtering phenomenon to take place. The targets were mounted such

that they face the substrate which is located a few centimeters away. The target-substrate distance could be varied if needed. Substrates of polished polycrystalline $A\ell_2O_3$ plates of dimensions 5, 1.8 and 0.6 centimeters were used in all this work to support the sputtered films. The substrate material is diamagnetic with an isotropic room temperature magnetic susceptibility of $-0.4\pm0.1\ 10^{-6}$ emu/gm, the total moment of a piece of 0.4 cm^2 area was measured to be $-4x10^{-4}$ emu at magnetic field of 14 kOe. This is about 1% of the magnetization of our samples and hence the substrate contribution to the moment has been neglected.

Subregions of the films were sectioned out for magnetic measurements by using a diamond pen. The cutting process is believed not to affect the magnetic quality of our samples. It may affect materials of low coercivity due to introducing some strains during cutting.

The substrate temperature in the range 600-1000 C has proved to be high enough to directly crystallize the sputtered films with no need to any heat treatment after deposition. The substrate was either heated by directly heating a substrate holder made of molybdenum which is known for its high thermal conductivity and low thermal expansion, or by using 600-1000 watt quartz lamps for this purpose. Measuring the substrate temperature in a vacuum system could be done either by attaching a thermocouple to the face of the substrate or by using infrared optical pyrometer, the latter has the advantage of having no material in contact with a substrate that might contaminate the system. It must be mentioned that during sputtering the substrate acquires some heat input from the glow disharge in addition to its own heat input from the heater. The

correction of such effects, however, are difficult to account for and has not been dealt with in this work.

A movable shutter was positioned facing the substrate and close to it to allow for presputtering the targets. The purpose of this is to clean the target surface specially from surface oxides and to getter the system background from impurities, in addition to maintain thermal equilibrium in the target before the actual deposition. The substrate was electrically floating in all runs, it therefore acquires some potential because it is immersed in the plasma, the shutter itself was grounded. The presputtering time depends on the situation at hand and was empirically set at about half an hour.

In order to promote alignment of the magnetic moments in a particular direction in the plane of the magnetic films an A&NiCo permanent magnet of field about 1750 Oe has been mounted in some stage of this work inside the chamber such that to expose the substrate surface to its magnetic field. The field was parallel to the substrate surface and perpendicular to its long axis.[49]

2.1.5) THICKNESS MEASUREMENTS

Three methods have been used to measure the thickness of our films. The first by weighing the substrate before and after deposition. This of course determines the thickness roughly since the deposit consists of different regions of different densities due to the existence of pure and/or mixed phases along the substrate. Furthermore the densities of the known phases differ although not appreciably from those of the corresponding bulk phases. The second method uses electron backscattering,

the number of which for a given electron energy is proportional to both the thickness and the atomic number of the sample under study. The electrons are detected using Giger counter mounted very close to the sample surfaces, different radioactive sources were used as electron sources and different standards are available for calibration. For long enough measuring time the uncertainty in film thickness was only a few percent. The third method uses scanning electron microscopy (SEM). Films of thickness in the order of 1 micron have been prepared in moderate time depending on sputtering parameters.

2.1.6) SPUTTERING PARAMETERS

The different parameters involved in the sputtering process and their relation to the physical, chemical and crystallographical properties of the films are now discussed. They are the sputtering gas, i.e. the gas species and the pressure used, the substrate temperature, the target power and the target-substrate separation.

2.1.7) THE SPUTTERING GAS

The effects of the nature and pressure of the sputtering gas on the sputtering process have been discussed extensively in the literature.[41] The gas pressure, ionic mass and radius are pertinent to the thermalization process, i.e. to the transfer of the excess momentum and kinetic energy from the sputtered atoms to the gas ions through elastic collisions as the former travel from the target to the substrate. Reaching the substrate with temperatures comparable to the

substrate temperature, the sputtered atoms can form the initial nuclei (aggregations of particles) necessary to form a continuous coating afterwards.[53] Choosing the right gas species and pressure causes the slowing down of the energetic atoms and energetic particles present, e.g. electrons. This process is important for direct synthesis of films by selecting the suitable thermalizer.[54,55]

On the other hand the sputtering yield, defined as the number of sputtered atoms per incident ion, depends on the momentum transfer from the sputtering ions to the target surface atoms, the sputtering yield of cobalt and samarium using argon ions of 500 eV energy compared to their counterparts using Kr and Xe ions of the same energy are[41] for cobalt: 1.22, 1.08 and 1.08 eV respectively and for samarium: 0.8, 1.09 and 1.28 eV respectively. The sputtering yield is known to increase with the energy of the sputtering ions except at very high energies due to depth effects. The above data shows that Xe is more effective in sputtering samarium from elemental samarium targets than Ar ions of the same energy. More importantly, however, is the close matching between the atomic masses of Xe (131.30 amu) and Sm (150.4 amu) on one hand and those of Co (58.933 amu) and Ar (39.948 amu) on the other hand. Xenon is thus believed to be a more effective thermalizer to energetic Sm atoms.

A computer simulation was used in order to study the optimum pressure for simultaneous thermalization fo Sm and Co atoms using Ar as sputterer. The model used for such calculations treats the collisions between the sputtered atoms and the sputtering gas atoms as elastic collisions between spheres having Maxwellian velocity distribution

corresponding to the temperatures T_1 and T_2 respectively and with no interaction between those species at a distance. The average energy loss of the sputtered atoms per collision normalized to the average energy of the sputtered atoms is given by:[56]

$$F = 8\ M_1\ M_2\ (1-T_2/T_1)/3(M_1+M_2)^2 \qquad (1)$$

where M_1 and M_2 are the masses (in amu) of sputtered atoms and sputtering gas ions respectively. The temperature T_2 of the sputtering gas is not assumed to be constant but rather to be dependent on the distance between the substrate and the target. The mean free path of the argon atom is given by:

$$LO = 0.225/(nxD^2) \qquad (2)$$

where n is the number of molecules per cc is given by:

$$n = 9.656x10^{18}\ P/T_2 \qquad (3)$$

with P is the gas pressure in Torr, T_2 the gas temperature in K and D the molecular diameter of Ar in centimeters (D=3.6 A). Using those values of n and D in equation (2) it reads:

$$LO = 1.8x10^{-5}\ T_2/P \qquad (4)$$

From equation (4) it is clear that even for temperatures as high as 1000 K and pressures as low as 50 microns the mean free path is only a fraction of a centimeter which is small compared to the plates (substrate-target) separation used in this work. The number of molecules between length ℓ and $\ell+d\ell$ is given by:

$$dn = .965 \cdot S \cdot P \cdot d\ell / T_2(\ell) \tag{5}$$

where P in equation (5) is in microns, and that $T_2(\ell)$ is assumed to vary in a linear fashion with the distance as:

$$T_2(\ell) = T_t + (T_s - T_t)\ell / L \tag{6}$$

with T_s and T_t as the substrate and target temperatures respectively and S is the collision cross section in A^2 and L is the target-substrate distance in centimeters. S is given by:

$$S = (R_1 + R_2)^2 \pi \tag{7}$$

with R_1 and R_2 as the radii of the sputtered atom and the sputtering gas atom respectively. The total number of collisions N that takes place up to distance ℓ off the target is given by:

$$N = .965 \cdot S \cdot P \int_0^{\ell} d\ell / T_2(\ell) \tag{8}$$

$$\text{i.e. } N = .965 \cdot S \cdot P \cdot L \cdot \text{Log } (1 + (T_s - T_t)\ell / LT) / (T_s - T_t) \tag{9}$$

So the energy of the sputtered atoms after N collisions in length ℓ is given by:

$$T_3(\ell) = (T_2 - T_2)\ (1-F)^N + T_2 \tag{10}$$

The energy spectra of sputtered neutral atoms exhibit a maximum at a few eV, the value of that maximum is dependent on the binding energy of the sputtered atoms to the surface from which they have emerged. For example the velocity distribution of neutral Sm atoms

sputtered from the Sm target using 20 keV Ar ions showed a maximum at 2 Km/sec which is equivalent to an energy of 3.0 eV and extending to higher energies up to about 12 Km/sec that is about 100 eV.[57]

Figure (4) shows the effect of different pressures of argon on the thermalization of Co and Sm atoms as they proceed from the target to the substrate. A pressure of 150 microns has proven to be high enough for Co and to some extent for Sm atoms to transfer their excess momentum and kinetic energy to argon through mainly elastic collisions before they reach the substrate so that they reach it with temperature comparable to its own temperature.

The sputtering gas pressure has also an effect on the deposition rate through its effect on the discharge current. As the gas pressure increases the discharge current increases as well leading to an increase in the deposition rate, however, using higher gas pressures may offset this effect due to backscattering.

Gas incorporation during film growth depends on many factors,[41] one of which is the gas pressure. It has been observed[58,59] that gas incorporation decreases as the sputtering gas pressure increases. The pressure of 150 microns used in this work together with the high substrate temperature have the effect of minimizing the argon content in our films. It is well known that films exhibit the same crystallographical structure as the bulk materials and hence forming new structures in film form which is not existing in bulk has been rather a rare case. Therefore observing new lines in the diffraction pattern of films can be traced to the formation of compounds with residual gases in the deposition chamber. For example such phenomenon has not

been observed in this work and all diffraction lines were identified according to the bulk diffraction patterns. Trapping gas atoms also causes the film to be porous, such porosity if severe evidently degrades the quality of the magnetic films and allow gases to get easily into the film after removing from the vacuum chamber.

2.1.8) THE TARGET POWER

Keeping all sputtering conditions practically the same and varying the target power leads to increasing the sputtering rate and in general to increase the deposition rate of the films.

We have sputtered $SmCo_5$ films from the $SmCo_5$ bulk targets described in section 2.1.3, under practically the same conditions with the exception of the target power.[50] Films with two different textures were synthesized from that set of targets using relatively high and low deposition rates, namely about 5, 1.5 and 0.5 Å/sec. The highest rate resulted in very thick films about 4.7 microns in a sputtering time of about 2 hours.

Films which developed (200) preferred orientation were sputtered directly onto heated substrates at temperature 600 C and in argon pressure of 150 micron, the target selfbias voltage in this case was 900 volts. Using the same sputtering conditions but with only 700 or 400 V target potential and slightly lower temperature, films which showed (110) texture were synthesized. The deposition rates 0.5, 1.5 and 5 Å/sec were obtained using target voltage of 400, 700 and 900 V respectively.

Figures (5a) and (5b) show the microstructure of the (110) and (200) films respectively as revealed by SEM. The (110) film microstructure is finer than that of the (200) film, both of them however are uniform and the (200) film is clearly very dense. The x-ray diffraction patterns of the same samples of Figs. (5a) and (5b) are displayed in Figures (6) and (7) respectively using Cukα and 1 deg slit source. Data has been collected using long dwell time per channel together with the slowest motion of the goniometer in an attempt to promote the statistics.

The grain sizes of the two films have been calculated from the observed diffraction profiles using (FWHM) as a measure of the broadening (Chapter 4), and the diffraction profiles of our $A\ell_2O_3$ substrate as a measure of instrumental broadening effects. The latter broadening is small enough relative to our sample broadening. Thus the use of the simple method of Warren is justified. This yielded a value of 150±25 Å as determined from the (200) line broadening of the (200) film sputtered from $SmCo_5$ targets using 5 Å/sec rate, while values of 150±25 and 90±15 Å have been obtained for the 1.5 Å/sec rate deposited (110) film from the (200) and the (110) reflections respectively.

The 5 Å/sec rate sputtered film is clearly of strong (200) texture, the intensity ratio of (200) to (110) is about 10:1 as compared to 1:1 for its counterpart from the $SmCo_5$ randomly oriented powder file. On the other hand the low rate sputtered film has two reflections, however the intensity ratio of (200) to (110) is about 0.5 and the (111) to (110) ratio is about 2.78 for the powder. For both films however the

(002) intensity is at the background level. The relatively strong reflection of the (110) compared to (200) for the low rate sputtered film shows that the fraction of grains which have relatively smaller size is larger than those with relatively larger sizes and hence the overall microstructure of (110) film is finer than that of the (200) film.

It must be mentioned at this point that the diffraction pattern of the (110) $SmCo_5$ film of Fig. (6) is not the original pattern. The original pattern contained some of the substrate lines for this 1.6 micron thick film. Two of these lines were overlapped, one with the (110) film reflection and the other, but to only a minor extent, with the (200) line of the film. These substrate lines were subtracted using the data from a bare substrate collected under conditions practically identical to those used in collecting the film data but corrected for the attenuation that both of the primary and the diffracted beams suffer in passing through the $SmCo_5$ film thickness. The correction depends on both the diffraction angle and the absorption coefficient of the $SmCo_5$ matrix.

The number of monolayers of argon gas per second reaching the target can be calculated roughly as follows: assume the degree of ionization of argon to be[42] about 10^{-4} and that most of this ionized fraction are Ar^+ ions of diameter of about 3 Å each. Assume further that the target bias voltage is about 1 kV, i.e. the maximum kinetic energy that the single ionized ions can have is 1 keV which corresponds to a velocity of about 10^6cm/sec. The number of argon ions impinging onto 1 cm^2 of the target area per second (the flux) is obtained then

by multiplying the average velocity times the number of argon ions per cc, a flux in the order of 10^{17} ions/(cm^2·sec) is obtained assuming partial argon pressure of 150 microns. On the other hand, assuming the yield of Co and Sm atoms for 1 kV argon ions to be about 1 atom/ion, and that the average energies of Sm and Co atoms are 2 and 5 eV respectively, that corresponds to average velocities of about 1.6 and 4 km/sec respectively. Assume for the elemental targets a relative area of Sm to Co targets of about 0.5, so the ratio of the Sum to Co flux reaching the substrate is about $0.5x(V_{sm}/V_{co})=0.2$, where V_{sm} and V_{co} stand for Sm and Co average velocities respectively, so the ratio of Sm to Co monolayers reaching the substrate is $0.2x(R_{sm}/R_{co})$, where R_{sm} and R_{co} are the atomic radii of Sm and Co atoms respectively. A similar calculation shows that the number of Ar monolayers reaching the substrate per second is about 10^5 assuming an Ar pressure of 150 micron and about 10^3 monolayer of oxygen per second assuming the partial oxygen pressure in the chamber to be 1 micron. The rate of Ar monolayers per second reaching the substrate is calculated assuming simply continuous argon arrival to the substrate, in addition only a fraction of that amount are accommodated in the films because the sticking probability of Ar at such high substrate temperature is low. However, we attributed the development to the different observed textures of the $SmCo_5$ films to the amount of Ar and/or oxygen accommodated in the films. We will return to this point in more detail in the section dealing with textures.

2.1.9) THE SUBSTRATE TEMPERATURE

All films directly sputtered onto heated substrates in the temperature range of about 600-1000 C have crystal structures as revealed by their well defined diffraction patterns, while films sputtered onto either water cooled substrates or onto substrates held at room temperature showed single broad peaks in their diffraction trace which is a feature of amorphous materials.

Some aspects of film formation mechanim that is nucleation and growth of thin films has been reviewed in a recent study[53] which has numerous references.

It suffices to mention here that the high temperature of the substrate enables the atoms to acquire enough kinetic energy to move on the surface of the substrate and/or previously deposited film layers, while for low temperatures the atoms have little energy to move around resulting in the absence of any crystal structure.

In addition sputtering at temperatures relatively low but high enough to directly crystallize the deposit upon reaching the substrate resulted in developing the (110) texture in the films which we attribute to more Ar incorporation at these temperatures more than that at relatively higher one.[60,61] The oxygen reaction with the Sm however takes place more effectively at higher temperatures.

The samples sectioned out from the deposited films were cut away from the edges of the substrate because of some temperature gradient at the edges, the many samples that have been synthesized and studied show systematic and reproducible properties if sputtered under the

same conditions.

The specific model of film formation has not been studied in this work, however, metallic films deposited on insulating substrates were shown to form and grow in general following the island or the Volmer-Weber model.[53]

2.1.10) TARGET-SUBSTRATE DISTANCE

The position of the substrate relative to the target has an effect on the deposition rate and on the deposit uniformity. The deposition rate increases with decreasing the target-substrate separation, assuming all other parameters are fixed, for the obvious reason of the more probable loss of the deposit atoms in their travel to the substrate. If the separation is, however, too small an insufficient number of ionization collisions will be undergone by the secondary electrons. On the other hand using very large separation has the effect of slowing down the ions through elastic collisions such that they strike the cathod (target) with energy that is not sufficient to produce more secondaries and then sustain the discharge. This, of course, depends on the sputtering gas pressure (Paschen Law).

The optimum target-substrate separation depends as well on the target area.[41] For small targets like ours the optimum separation is a few centimeters. For pressure about 100 micron and target power in the order of 1 kV we used substrate-target separation about 3-5 cm.

3.1.1) X-RAY FLUORESCENCE ANALYSIS

3.1.2) BASIC PRINCIPLES

Composition determination using energy-dispersive x-ray analysis has been widely used[62-67] as a method that offers quantitative and qualitative analysis of pure elements as well as complex alloys, the analysis is non-destructive and versatile.

Although the method is applicable to samples in either bulk or thin form, the thin samples, however, have some advantages over the bulk ones. The principle of those are:[62]

a) The function relating the analyte line intensity to the analyte concentration is linear.

b) The absence of absorption-enhancement effects which may lead to diminishing or increasing the analyte line intensity.

c) Large peak to background ratio.

d) Low and fairly constant background over wide energy range.

The intensity contributed to the total analyte line intensity of an incremental volume of an elemental sample of thickness dt at depth t is given by:[62]

$$dI = k \cdot dt \cdot \csc\phi \cdot I_o \cdot \exp(-\overline{(\mu/\rho)}\rho t) \qquad (1)$$

where $\overline{(\mu/\rho)} = (\mu/\rho)\lambda_p \cdot \csc\phi + (\mu/\rho)\lambda_L \cdot \csc\Psi$

with λ_p; λ_L: primary and analyte line wavelength respectively

Ψ: take off angle, defined as the angle between the central ray of the secondary beam and the sample surface.

ϕ: the angle between the central ray of the primary beam and the sample.

ρ,t: density and thickness of the specimen respectively.

I_0: intensity of primary beam.

(μ/ρ): mass absorption coefficient of the specimen.

$\text{tcsc}\phi$, $\text{tcsc}\Psi$: path length of the primary and secondary beams respectively in the sample.

k: is a constant.

For very thin samples equation (1) reads:

$$dI = k \cdot \csc\phi \cdot I_0 \cdot dt \qquad (2)$$

but dt is proportional to the incremental number of the analyte line atoms, dn, in the layer for constant area. This means that for "thin films" the analyte line intensity of an element is directly proportional to the number of atoms. It was demonstrated,[67] that the absorption-enhancement effects on the analyte line intensity of a particular analyte due to the presence of other elements in a specimen are absent if the specimen is "thin". The effect of film thickness on the spectral line intensity can be shown by integrating equation (1):

$$I = kI_0 \csc\phi \int_0^t \exp(-\overline{(\mu/\rho)}\rho t \, dt$$

$$\text{i.e. } I = I_\infty(1-\exp(-\overline{(\mu/\rho)}\rho t)) \qquad (3)$$

where I_∞ is the intensity for infinite thickness at which the secondary x-rays cannot emerge to the surface of the sample.

3.2.1) EXPERIMENTAL SETTING

A sketch of the apparatus used for fluorescence excitation is shown

in Fig. (8), for our energy dispersive spectrometer.

The detector-preamplifier system consists of a 512 SI(LI) detector of resolution of about 150 eV at 5.9 keV(Mn Ka) and at a count rate in the order of 1 kC/s. The relation between the resolution and the x-ray energy is given by:[66]

$$R = (2.62E+E_0^2)^{\frac{1}{2}}/E$$

where E is the energy of secondary x-ray in eV, and E_0 =100 eV is the level of electronics noise, in our system it is about the same.

A field effect transistor (FET) is connected with the counter. Its function is to amplify the pulses generated at the counter as a result of an incident x-ray photon. Both the FET and the counter must be operated at liquid nitrogen temperature (77 K). The resolution is known to degrade and the electronic noise to increase as T increases. The output of the FET is handled to the input of 513 semiconductor amplifier with pulse pileup rejector, pulse shaper with different time constans and a base line restorer. The dead time in our system is less than 5% for count rates within 2 kC/s. The amplifier output is connected to 1024 channels MCA (tracor northern TN-1705) with CRT screen for display. The first channel is the acquisition time channel. The data is then transferred to an advantage north star microcomputer for analysis and permanent storage. BASIC language proved to be good enough to accommodate the calculations needed in this work.

A GE XRD-6 diffractometer is used. Samples are mounted on its goniometer using various aluminum sample holders. Different collimating slits and point sources are available for guiding the primary beam. No

collimator, however, is used to receive the secondary radiations before entering the detector. This is because the "diffracted" radiation in energy-dispersive spectra which correspond to different sample planes is spread over the background rather than being peaked at a particular energy. A full-wave power supply GEXRD-6 is used to energize x-rays. Voltage up to 75 KVP is regulated using line voltage regulator, but there is no internal stabilizer. The current range is 1.5-100 ma, the maximum power is rated at about 4200 watts.

3.2.2) CHOICE OF EXPERIMENTAL PARAMETERS

3.2.3) PRIMARY RADIATION

The choice of experimental parameters, e.g. tube current, target voltage, count rate, collimator and most importantly the primary radiation, depends on the problem at hand. Important parameters for Sm and Co elements taken from references 58 and 62 are listed in Table 1. Some of them are in $\mathring{A}^*$ units which is considered to be angestroms except for very high accuracy work. The values of the wavelength corresponding to different absorption edges for Sm and Co elements present in Sm-Co alloys are only a few eV off the values of the pure elements.

It is well known that in order to excite the x-ray spectral lines of a given series most efficiently one must choose a primary radiation of wavelength just shorter than the wavelength corresponding to the absorption edge of that given series.[58] The primary radiation therefore must have very intense line(s) which satisfy the condition men-

tioned above in order to contribute most to the excitation, otherwise the continuous radiations contribute the most. In this work Cu radiation, i.e. Cu Kα, Cu Kβ and the continuous radiations are used, among those Cu Kα contributes the most to the fluorescence of Sm-Co films. The wavelength of Kα and Kβ lines of copper are 1.541838 and 1.392218 angestroms respectively.

3.2.4) THE OPERATING VOLTAGE

In choosing the target voltage one must at least choose a value of the peak potential that exceeds the excitation potential of an element whose characteristic spectrum is to be excited. As an example to excite the copper radiation a voltage of peak value about 8.9 kV is necessary, as long as that critical value is met the characteristic lines are present superimposed on the white spectrum with their positions are fixed to relative to the white spectrum. The change in the excitation voltage only affects their intensity relative to it, however, both the energy and the intensity of the continuous spectrum are affected by voltage fluctuations. A voltage of 40 kV has been used in all the present work.

3.2.5) TUBE CURRENT

The choice of the tube current is dictated firstly by maximum power requirements and secondly by the need of linear relationships between the count rate and the intensity. Such a relation has been studied for SmCo films at fixed tube current, tube voltage, detector-

sample distance. The linearity was preserved up to about 2 kC/s and then degraded for higher count rates. The dead time as has been already mentioned, was within 5% for all measurements within that count rate. For higher rates it was as high as 15-20%. The current used was 4 ma in all this work.

3.2.6) OTHER PARAMETERS

The detector was positioned at 114.08 degrees. Previous work[64] showed that the background scattering by $A\ell_2O_3$ substrate shows slight angular dependence in this region. The detector-sample distance was kept at 4.2 cm for all our runs to assure that the fluorescence radiations pass the same air path length.

3.2.7) CALIBRATION CONSIDERATION

The main problem in x-ray fluorescence analysis (XFA) is to convert the observed intensity ratio of the selected analyte lines into atomic ratio. This has been done first in this work for "thin" samples of known composition. The samples are in the form of filter papers which only contain light elements and hence are not efficient absorpers; those filter papers were used to absorb carefully prepared solutions of different Sm-Co compositions, namely $SmCo_2$, $SmCo_3$, $SmCo_4$, $SmCo_5$ and Sm_2Co_{17} compositions.

The solutions were prepared by dissolving highly pure carefully weighed quantities of Sm and Co elements (purity 99.99% for Sm and 99.999 for Co) into dilute nitric acid (HNO_3) and then allow known

measured quantities of the solution to dry on a filter paper of area about 1 squared centimeter in an oven of temperature about 100°C, the surface density of such samples were about 7×10^{-4} gm/cm^2. At least three samples have been prepared for each of the mentioned compositions. The thickness of those standard samples is estimated to be about 2 kÅ. The count rate of all the fluorescence events from any of those samples was at most 2kC/s. A point source has been used to guide the primary radiations. The acquisition time has been chosen long enough to achieve good statistics. Data were collected until the maximum count at the most intense peak (Cok_α) reached about 10^6 counts. Table 2 shows the data for the standard samples and Fig. 9 displays the atomic ratio of Sm to Co present in different alloys to the corresponding intensity ratio of the Sm L_β line to the Co k_α line. The second column in Table 2 shows the net intensity ratio of the L_{β_1} line of the Sm to the Co k_α line corrected for different factors to be discussed later. The L_{β_1} line of Sm has been chosen as an analyte line instead of the more intense L_{α_1} line. The reason for that is explained in the next paragraph.

The information given in Table 1 shows that the Co k_α line is of wavelength shorter than that corresponding to the absorption edge of the SmL_{α_1} line but longer than the absorption edge of the SmL_{β_1} line and hence the Co k_α line is able to excite the former but not the latter. For all our films as well as for $SmCo_5$ bulk the observed net intensity ratio of SmL_{α_1} to Co k_α lines has been different from its counterpart for the thin standard samples described above. The devi-

ation was more profound as the the thickness increases. On the other hand the Co k_β radiation is able to excite the SmL_{β_1} line and hence its ratio to the Co k_α line is affected by the film thickness as well, however the problem was less severe than that involving L_{α_1} as analyte for samarium. It is also known that the radiation which is more efficient in exciting a particular element should not only have energy larger than that of its absorption edge but its energy should be in the immediate neighborhood of the absorption edge. This means that the ratio of the mass absorption coefficient at that wavelength to that of the absorption edge should be as large as possible. For Co k_β line and the SmL_{β_1} edge the ratio is about 0.86. Using the definition of "thin sample"[67] as that satisfying the condition: $m(\mu/\rho)'<=.1$ where m is the mass per unit area and $(\mu/\rho)'$ is defined as $(\mu/\rho)\lambda_p+(\mu/\rho)\lambda_L$, where λ_p and λ_L are the primary and the analyte wavelengths respectively, to check the "thickness" of our films the ratio of the L_{β_1} to the L_{α_1} of samarium has been checked for the standard samples as well as for our films. In the former the ratio has been practically the same while in the latter it was different for different compositions on one hand, and on the other hand was different from its counterpart of the standard samples. From the previous discussion it may be concluded that the Sm-Co films in the thickness range indicated before, and of course thicker ones, are considered "thick" as far as the secondary radiation is considered. Moreover runs at different take off angles, all other things kept the same, showed that the observed intensity ratio is influenced by passing through different effective thicknesses.

From the above observation it is clear that the data given in Table 2 for the standard samples could not be applied directly to our films. The third and fourth columns in Table 2 represent the number of Sm atoms to those of cobalt as prepared in the lab and the corresponding atomic percentage of cobalt respectively. The fifth column shows the calculated percentage of Co using the observed intensity ratios. The agreement between the data in columns 4 and 5 is evident. The intensity ratios as they appear in the second column are calculated from the observed intensities but corrected for different factors. The first of these is the absorption in the filter paper themselves. In order to correct for that the linear absorption coefficient of Co k_α, SmL_{α_1} and SmL_{β_1} have been determined experimentally by observing the intensity as a function of the thickness (actually the number of stacked filter papers) for each of those radiations run, of course, separately, they are well separated in our detecting system. The values of those coefficients were calculated from the slope of the linear relation between $\log(I/I_0)$ and the number of papers. The values are $1/(6.9\ t)$, $1/(3.8\ t)$ and $1/(4.43\ t)$ in 1/cm units for the Co k_α, SmL_{α_1} and SmL_{β_1} respectively, where t is the filter paper thickness and I/I_0 is the normalized intensities. Secondly, the weak L_{γ_1} line of samarium overlaps with the high energy side of the very strong Co k_α line, and thus the observed intensity of the latter has contribution from the former, however one can show that:

$$I(L_{\beta_1})/I(K_\alpha) = c\ \ I(L_{\beta_1})/(I(K_\alpha)+I(L_{\gamma_1}))$$

where $c = (1+2I(L_{\gamma_1})/I(K_\alpha))/(1+I(L_{\gamma_1})/I(K_\alpha))$

The relative percent discrepancy between the observed ratio and the corrected one is between 2-3% for the standard samples if the net total intensity of the analyte lines is considered. It should be mentioned that because of the weak intensity of L_{γ_1} line relative to the Co k_α line, no attempt has been made to study the influence of the film thickness on the former radiation. Thirdly, there is another overlap between the high energy side of L_{β_1} line of Sm and the escape peak from the Si(Li) detector. That peak is of energy equal to the difference in energy between the Cu k_α radiation (8.041 keV) and the Si k_α radiation (1.74 keV). The intensity of the escape peak however represents at most 3% of that of the L_{β_1} line and hence its contribution has not been considered. It is worth pointing out that an uncertainty about 1% would result in the Sm percent content in the samples if the last two of the previously mentioned factors were not taken into account at all. The possible corrections to the observed intensities due to the film thickness are discussed in the next paragraph.

Equation (3) has been used to calculate the intensity of L_{β_1} line to that of Co k_α line for different film thickness and composition, the mass absorption coefficient of Sm and Co to the primary and secondary radiation as well as the atomic mass of these elements needed for the calculation are from references 62 and 66. The take off angle has always been 57.04 degrees from all our runs. Figure (10) displays that ratio calculated from equation (3) for a 2 KA film relative to

the same ratio for thicker films, as a function of the atomic percent of Co. The data itself is in Table 3. Only the Co rich Sm-Co compositions are presented. For a particular thickness the linearity is preserved for relatively cobalt poor compositions but deviation from linearity takes place more clearly as the cobalt rich regions are approached. For 25 KA thickness film the deviation from linearity represents about 0.3-2% for compositions between 77.8-89.5% i.e. between Sm_2Co_7 and Sm_2Co_{17} stoichiometries respectively. The corresponding deviation for 10 KA film is only from 0-.4%.

The correction to the possible enhancement of L_{β_1} of Sm has been considered by comparing the intensity ratio of the L_{β_1} to L_{α_1} of the standard samples to its counterpart in the films under study. This ratio has a value which is different in films, where absorption-enhancement takes place, from its value in the case of thin standard samples.

The compositions are known to be ±1 at % Co absolute and films with narrow composition gradient like those sputtered from elemental targets have been analyzed by this method. The composition of adjacent subregions about 1mm apart along the length of a single substrate have been found to differ by about 1 at %. The composition of samples of the 1:5 and the 2:17 systems have been confirmed by x-ray diffraction which indicated strong reflections of the respective phases with the absence of any major lines with any appreciable intensity that would indicate the existence of other phases with appreciable fractions in the samples. Magnetic measurements were as well compatible with the x-ray analysis as will be discussed in the last chapter.

4.1.1) X-RAY DIFFRACTION ANALYSIS

4.1.2) INTRODUCTION

The magnetic properties of ferromagnetic films in general depend on the film structure, i.e. on the degree of atomic order namely on the polycrystalline, amorphous or the single crystal nature of the film, on the crystal lattice and on the physical properties of the film such as its dimensions, size of grains and internal stresses, etc. In order to identify our films completely one should identify the phase(s) existing along the substrate either as pure and/or mixed phase regions.

In general those studies could be carried out using x-ray diffraction analysis, however microscopic examinations[40] and thermomagnetic analysis[68] have proved to be more sensitive especially in detecting a small volume fractions of a second phase. The Sm-Co phase diagram is shown in Fig. 11 and the x-ray diffraction data of the Co rich Sm-Co compounds $SmCo_3$, Sm_2Co_7, $SmCo_5$ and Sm_2Co_{17} as calculated from the lattice parameters of the bulk phases is shown in Table 4 for Cu k_α radiation wavelength 1.541838 Å. The diffraction angles as seen in Table 4 are very close to each other especially for $SmCo_5$ and Sm_2Co_7 phases.

In addition, since the C-axis in the hexagonal compounds under study in this work is the easy axis of magnetization, a study of the C-axis orientation in or out of the film plane is necessary for checking the results obtained from the magnetic measurements. Such an investigation relates the intensities of the diffraction lines to their

Miller indices as compared to randomly oriented samples.

The dependence of the magnetic properties of the R-Co alloys on the grain size has been studied extensively.[34-36] The level of sophistication of the x-ray diffraction technique and the method of calculation of the grain size depend on rough knowledge of the value of the grain size under study.[66] All of those methods depend on calculating the sample diffraction lines broadening relative to those of a material of sufficiently large grain size. The broadening of the diffraction profiles of the latter is taken to represent the instrumental broadening effects.

4.1.3) EXPERIMENTAL SETTING

Our experimental set-up is mainly the usual setting for x-ray diffractionwork using a diffractometer. However it differs from other fairly recent techniques, e.g. the time analysis diffractometry.[69] Unlike that technique in which a particular range is covered and all the angular positions of the diffraction lines within that range are measured simultaneously and then stored in a multichannel analyzer (MCA), our technique uses MCA in the scanning mode which allows the acquisition of the diffraction data of a particular range in a sequential manner. The data from only a small fraction of a degree is stored in one of the 1024 channels of the MCA, the whole spectrum of the angular range of interest is thus stored in the total of the 1024 channels with a resolution that depends on both the dwell time per channel and the Goniometer speed. The MCA displays a diffraction

pattern like that of the familiar chart pattern which could then be transferred to a small computer (North Star Advantage) for data storage, analysis and graphic display.

4.1.4) CHOICE OF EXPERIMENTAL PARAMETERS

It is well known in diffraction work that in order to get well defined diffraction patterns one must use radiation of wavelength not shorter than the absorption edge(s) of the element (alloy) present in the specimen under study. Otherwise an appreciable fluorescence will be produced and this in turn may lead to undesired distribution of background which might be of intensity high enough to obscure diffraction effects. It is generally not recommended for example to study materials containing appreciable amounts of Co or Fe using Cu radiation. The degree of that undesired effect depends on the technique used.

Our Si(Li) solid state detector allows for complete discrimination against Co fluorescence being accepted as Cu diffraction counts, the background of the Sm-Co films using this detector if fairly flat and the peaks are well identified from the background for all film thickness range (10-50 kÅ). The Cu k_β radiation is of intensity less than that of Cu k_α (1:7.5 at target) and of shorter wavelength which leads to lower angle diffraction lines compared to those using Cu k_α. However, K_α was used for its high intensity although the existence of the Cu k_α douplet, k_β has been used also, however in some of the work dealing with grain size determination. Our films are highly textured with either (200) or (110) preferred orientation and the few diffrac-

tion lines of appreciable intensity lie within about the 30-50 degree range. This, of course, imposes some limitations on the precision of the lattice parameters determination which usually requires the existence of back reflection lines. The intensities of our diffraction lines have been promoted using a slower mode of goniometer motion and long dwell time per channel.

The diffraction patterns of subregions of area in the order of 1 mm^2 have been taken using a 1 degree slit source. The beam divergence of such a source is not less than the dimensions of the samples at all detector angular positions. Those samples were mounted either on a glass holder such that the latter was adjusted as close as possible to the goniometer axis or on a special holder such that to expose the sample area only to the primary beam and thus allow the peak-background ratio to stay high. The magnetic measurements were done thus on the same samples investigated with x-ray fluorescence and diffraction analysis. At last the operating voltage of the target and the tube current were set at 40 kV and 15 ma respectively in all our runs.

4.1.5) CALIBRATION CONSIDERATION

The possible sources of systematic error in measuring the crystal plane spacing of a material using a diffractometer have been discussed in the literature.[66,70] Among those sources the displacement of the specimen from the diffractometer axis represents the largest possible source of error. High precision in lattice parameter determination is achieved using as many lines as possible in the back reflection region.

This condition, as has been already mentioned, is not present in this work. No satisfactory extrapolation function has been used, rather the lattice parameters have been calculated for different reflections and a statistical weight has been given more to higher intensity lines.

After the necessary initial alignment of the diffractometer many runs have been done using samples of materials of well known parameters, e.g. our substrate.[71] The observed locations of the diffraction lines of this material have been compared to the calculated locations for fifferent goniometer speeds and different MCS settings, the agreement has been always excellent for both of Cu k_α and Cu k_β, the existence of the doublet in the former has been considered. A calibration straight line relation has been established for each set of experimental conditions and the appropriate one was used for studying our samples.

4.1.6) COMPUTATION METHOD

A computer program in BASIC was written for diffraction data analysis. The data was in permanent storage in a digital form, the number of data points is the number of channels. In each the counts per channel are present. The program searches for the peaks by finding their 2θ value of maximum intensity rather than using curve fitting techniques,[66] computer their Bragg angles using the appropriate resolution and the starting angle of scann, the corresponding lattice spacing -d- and the integrated net intensity of the diffraction lines together with the appropriate tolerance of those quantities. The spectrum background we mentioned before is fairly flat and low relative to

the peaks for our samples. The background level has been chosen using a subroutine that searches first for the regions of minimum counts among fifty regions to which the whole spectrum was arbitrarily divided into and secondly chooses among those the value that yields the best precision in the integrated net intensity values. For example the more intense reflections having normalized intensities >=0.5 have only <5% relative percent error. Weaker reflections, however, have at most 10% relative percent error. It should be mentioned that the program does not deal with cases in which a strong overlap is present between peaks. A more elaborate curve fitting work is needed.[72]

For grain size determination Warren's method is the simplest but it has its own drawbacks.[70] The success of grain size determination depends on the ratio of broadening of the diffraction lines of a standard (chosen of large grain size) to that of lines from the sample which lie as close as possible to those of the standard, A ratio not larger than 0.5 is considered satisfactory. In addition since the pure diffraction broadening, i.e. of the sample alone excluding the instruments effects varies as $1/\cos\theta$, the choice of the angle at which experimental profiles may be taken depends on rough knowledge of the sample grain size. If the ratio mentioned above is 0.5 or smaller at relatively low angles, working in the back reflection region would not be necessary. However, if the sample grains were large enough for that ratio to be >0.5 then working becomes essential at high angles. The observed breadth is offset, however, by the natural width even for monochromatic radiation, which increases with angle. We used, thus the method of Warren for approximate grain size determination,

a guassian distribution was assumed to represent the observed profiles of our peaks. A curve fitting using a generated gaussian with FWHM equal to that of the observed profile has been utilized. The fitting was satisfactory and the pure broadening is thus given by:

$$B^2 = B_s^2 - B_t^2$$

where B_s and B_t are the broadening of the observed profile and the standard profile respectively. The grain size is related to B by the relation

$$D = 0.9\ \lambda/(B\ \cos\theta)$$

where λ is the wavelength in Å, B in radians and D in Å.

5.1.1) MAGNETIZATION

It has been already mentioned that our magnetic films were either films with fixed composition or films with wide composition gradient along the length of a single substrate. The latter kind of films provided the opportunity to study the magnetization as a function of composition.

All magnetic measurements were done using a vibrating sample magnetometer (VSM) at room temperature except where explicitly specified. The hystersis loops were measured parallel and perpendicular to film plane in order to study the easy axis relative position in the films. This has also been studied using x-ray diffraction analysis. Magnetic measurements have been done as well within film plane in order to study inplane differences.

Demagnetization factor of 4π, i.e. demagnetizing field of $4\pi M$ (kOe) has been taken into account for interpreting data measured perpendicular to films. No demagnetization factor was considered in the film plane, the latter given by $4\pi t/L+t$, with t as the film thickness (in the order of 10 KA) and L as the sample length (in the order of 1 mm), and thus it is negligibly small compared to 4π. The units used in this work are the CGS units. Magnetization is given, however in either emu/gm or in KG when the proper sample density is used.

5.1.2) DEPENDENCE ON COMPOSITION AND C-AXIS ALIGNMENT

Figure 12 displays the hystersis loop H-M measured parallel to film plane for three different crystalline compositions along the

length of a single substrate, the substrate temperature was 800°C, argon pressure was 80 microns and the base pressure was 7×10^{-7} torr.[47] These samples of Sm atomic percents 9.1, 15.1 and 22.8 exhibit maximum magnetization at 14 kOe of about 40, 25 and 15 emu/gm respectively. The remanent magnetizations are about 23, 17 and 13 emu/gm respectively. Thus both maximum and remanent magnetization increase by increasing the cobalt conent reaching their highest values at compositions near the stoichiometric composition of Sm_2Co_{17} (10.5 at % Sm) and decreasing as the relatively Sm rich regions near the $SmCo_5$ stoichiometry (16.66 at % Sm) are approached.

The hysteresis loop of the 22.8 a%Sm sample is shown in Fig. 13 both for parallel and perpendicular directions.[47] The magnetization in the latter case is less than that in the former even taking into account the shearing of the loop in that direction because of the demagnetizing field. This difference in the moments indicates that the easy axis (c-axis) lies closer to film plane.

These low maximum and remanent moments indicate relatively low density and large degree of crystal non alignment in these samples which were synthesized in the earliest stages of this study as compared to other more recent results.[49,50] The maximum possible value of the remanent magnetization M_r is the saturation moment M_s assuming that the degree of alignment and packing are 100%.

A sample of the 1:5 composition has been magnetized in a maximum field of 150 kOe in the film plane.[48] The maximum magnetic moment reached was 105 emu/gm as seen in Fig. 14. This moment is near that of bulk sintered $SmCo_5$.[31] That sample contained about 6.5 a% of

oxygen (1.4 wt%). The oxygen usually reacts with part of the samarium forming Sm_2O_3. This amount of oxygen, however did not significantly affect the total magnetic moment of the sample.

For a field of 14 kOe the maximum in plane moment for the same sample is about 70 emu/gm, i.e. about 67% of the moment at 150 kOe indicating magnetic hardness of that sample. The loop at 14 kOe is not squared with M_r=55 emu/gm. This again is due to c-axis non-alignment.

In an attempt to study the effect of applying a magnetic field during the film synthesis on the alignment of the C-axis of these crystalline films an A&NiCo permanent magnet of field 1.75 kOe has been used.[49,50] The application of a magnetic field during film synthesis has been used in previous works in an attempt to promote perpendicular texturing for crystalline Sm-Co films[33] or to promote uniaxial plane anisotropy for flash evaporated Sm-Co alloys using in-plane magnetic field fuding film synthesis.[73]

In this work the C-axis for either the (200) textured films or films with (110) texture lies in the film plane and thus the application of magnetic field in this case was not for orienting the C-axis in film plane, but rather to preferentially align it in the direction of the magnetic field we name H sputter.

Figure 15 shows the hysteresis loop of a $SmCo_5$ sample sputtered from elemental targets onto a substrate held at temperature of 650^{o}C and using argon pressure of 150 micron. The base pressure has been improved to 10^{-9} torr. No magnetic field was used during sputtering.[49] The loop in the film plane is showing significant slope at the top and

the bottom of the loop indicating that the sample is far from being saturated. The loop slopes as it enters the second quadrant showing that the alignment is still lacking, however the total moment per gram has been improved compared to the samples reported earlier in this work. Measurement of the loop for that sample in different directions within the film plane showed practically no difference indicating that the film is practically isotropic.

The x-ray diffraction pattern of the same sample of Fig. 15 is shown in Fig. 16. The only present reflections are (100), (110), (200) and (300). The C-axis is thus rigidly oriented in the film plane as it shows from the absence of any $\ell \neq 0$ lines.

The effect of the magnetic field applied during sputtering can be seen by studying Figs. 17 and 18 and Table 5. The sample in Figures 17 and 18 contains 84.5 a% Co, i.e. is slightly richer in cobalt than the stoichiometric composition. The hysteresis loop was measured with the applied field directed parallel to H sputter. The maximum in plane moment at 14 kOe is 67 emu/gm. The degree of alignment has been improved as it shows from the flat topped loop with no appreciable change of slope as it enters the second quadrant. The same sample has magnetization of 114 emu/gm when magnetized in the film plane at 150 kOe maximum field. The maximum moment at 14 kOe is thus 59% of that of the maximum moment at 150 kOe. This again indicates the magnetic hardness of the film. For less magnetically hard films one expects no large change in moments at relatively large values of magnetic fields. This is so since saturation is approached faster for soft magnetic materials. The magnetic moement of the same sample

measured perpendicular to film plane is only 25% of that measured in the film plane. The C-axis orientation of this film in the film plane has been checked as well from x-ray diffraction in Fig. 19. The ratio of the (110) reflection to the (200) reflection is 10%. The same ratio was only 5% for the sample in Fig. 16. The increase of the intensity of (110) line is attributed to more oxygen presence in the former sample.[49] This point will be discussed later in the section dealing with texture.

In Fig. 18 the magnetic field was applied parallel to film plane, but perpendicular to H sputter for the same sample in Fig. 17. The loop in this case is still square, but with maximum moment lower than that of Fig. 17. This indicates some degree of C-axis alignment in the direction of H-sputter.

Table 5 displays the inplane variation of $SmCo_5$ compound sputtered in the presence of the inplane magnetic field.[49] The ratio of the magnetization in the second quadrant to the remanent magnetization remains as high as 0.9 for fields up to 5.5 kOe. In addition M_r/M_{14}, where M_{14} is the maximum magnetization at 14 kOe field reaches values as high as 0.97. The maximum moment at 90 degress off H-sputter is about 96% of that measured paralle to H-sputter. That is relatively small degree of C-axis alignment has been achieved.

The inplane variation of such $SmCo_5$ samples magnetization is displayed in Fig. 20. The sample was rotated in constant magnetic field of 15 kOe. Again the relative effect of the field applied during sputtering is evident.[49]

Table 6 displays the data obtained from magnetic measurements on a

series of $Sm_{1-x}Co_x$ samples. The samples are subregions from a single Sm-Co film (18 kA thick) sputtered from elemental targets onto heated substrates kept at a temperature of about 600°C in the presence of the inplane magnetic field referred to earlier. The compositions have been corrected for the 2.5 at % oxygen present in the film as determined from Auger analysis. The corrections are made with the assumption that the oxygen reacts with part of the Sm forming Sm_2O_3. 1 at % oxygen (0.22 wt%) reacts with about 1.38 wt% Sm to form Sm_2Co_3. That is as much as 3.44 wt% Sm reacting with oxygen in this film.

The compositions span a range of 70-95 at % Co along the length of the same substrate. The differences in composition for the physically adjacent subregions are in the vicinity of 1 at % Co. This narrow composition gradient is a feature of films sputtered from elemental targets.[50]

The composition-magnetization ($4\pi M$) relation is plotted in Fig. 21 for the same series of Table 6. The magnetization increases as the cobalt content in the samples increases as expected and in agreement with previous studies on both crystalline[35] and amorphous samples.[70] The magnetization reaches very low value at the composition corresponding to the non-magnetic $SmCo_2$ (67 at % Co).[74,75] The decrease of magnetization as the Sm content increases is not simply because of the substitution of a heavier element of less magnetic moment, but rather because a degradation in the magnetic exchange takes place. The $SmCo_2$ is not magnetic because of the low density of states at Fermi energy.[75]

The contribution of the cobalt sublattice to the total magnetic

moment is assumed to decrease with increasing the Sm content in the samples because the Sm moment is assumed to be more localized and hence the observed values of saturation magnetization can be accounted for using the two sublattice models[1,32] with decreasing total moment per formula unit as the concentration of Co decreases. The value of metallic Co moment per atom at room temperature that yields the observed saturation value of about 17.6 kG is about 1.68 Bohr magnetons. For the R_2Co_{17} compounds most values of saturation magnetization agree closely with the two sublattice models using an average moment of 1.61 Bohr magnetons per Co atom. However Sm_2Co_{17} does not fit the model[32] but rather parallel coupling instead of the antiparallel coupling of the Sm and the Co spins is suggested. The following equation has been used to calculate the saturation magnetization of different compositions:

$$M = ((1-x)\mu_{Co} + x\mu_{Sm})/(58.933(1-x)+150.4x) \text{ Bohr magnetons per amu}$$

A value of 12.2 kG is obtained from this relation for Sm_2Co_{17} assuming parallel coupling of spins and Co and Sm moments of 1.61 and 0.7 Bohr magnetons respectively. The $SmCo_5$ saturation magnetization of about 11 kG[17] around room temperature is obtained which corresponds to 8.7 μ_B per formula unit.

Some samples have been sputtered onto substrates held at room temperature otherwise sputtering conditions were like those of Fig. 12. That resulted in amorphous films with low coercive force. Figure 22 shows the hysteresis loops of two samples of compositions 9.1 and 22.8 at %Sm. The magnetization is clearly higher than those of Fig. 12

reaching about 50 and 70 emu/gm fo 9.1 and 22.8 at %Co respectively while the intrinsic coercive force is only <0.5 kOe for these compositions.[47]

The absence of crystalline long range order in the amorphous solids in contrast to the crystalline solids is responsible for the lower coercivities observed for the magnetic amorphous compounds as compared to their crystalline counterparts. The magnetization, however, is less affected by the absence of the long range order in amorphous magnetic materials and it rather depends mainly on the alloys composition.[76]

Figure 23 displays the inplane loop of a sample containing 90.06 at %Co from a $Sm_{1-x}Co_x$ film in a field of 18 kOe parallel to H-sputter, together with the associated demagnetization relation.[50] This sample contains mostly the Sm_2Co_{17} phase as confirmed by x-ray diffraction pattern of Fig. 24 which is indexed according to the rhombohedral structure of Sm_2Co_{17},[77] the lattice parameters calculated from the observed angles are A=8.401±0.014 and C=12.318±0.018 A as compared to those of the Co rich side of the homogeneity range given by:[73] A= 8.397 and C=12.25 Å. The assigned indices are (300), (220), (006), (223) and (600) which is not shown. This shows that the C-axis of this sample lies in film plane. This has been supported by magnetic measurements in the perpendicular direction to film plane which indicated $4\pi M$ = 8 kG as compared to 14 kG in film plane. The sample is slightly richer in Co than the stoichiometric composition. A weak peak that may be identified as pure Co (012) reflection has been observed at 2θ=62.4 degrees.

Substituting the Co with the more abundant transition metals, e.g.

Fe in the pure 2:17 phase of Sm-Co system is known to increase the coercivity appreciably, but to decrease the magnetization slightly. Figure 25 displays the inplane hysteresis loop of $Sm_2(Co,Fe,Zr)_{17}$ film sputtered from $Sm_2(Co,Fe,Zr)_{17}$ targets. The film has 10 at %Sm, about 60 at %Co and about 30 at %Fe with small Zr concentration of about 3 at %. $4\pi M_{max}$ = 11 and $4\pi M_r$ = 10 kG have been measured in film plane as seen from the squared hysteresis loop of Fig. 25. The x-ray diffractometer trace of the same sample is displayed in Fig. 26. This sample exhibits a two phase 1:5 and 2:17 structure. The (110) line of Fig. 26 is due to the 2:17 hexagonal phase while (111) and (200) lines are due to the 1:5 phase.[50]

Figure 27 displays the inplane hysteresis loop of a $SmCo_5$ film sputtered from three $SmCo_5$ targets onto heated substrates at the temperature range 600-650°C using 1.5 A/sec deposition rate. The loop was measured parallel to H-sputter at -63°C in 90 kOe field. The maximum reached is about 10 kG and B_r=8.5 kG. The same sample measured in 20 kOe fields exhibited minor loops as shown in Fig. 28 where 8 kG has been reached at the maximum field. That is about 80% of the maximum magnetization at 90 kOe. Other $SmCo_5$ samples sputtered using different deposition rates namley 0.5 and 5 Å/sec showed differences in coercivities and texture but the maximum obtained magnetization is about the same.[50]

Figures 29 and 30 display the inplane loops of $SmCo_5$ films sputtered using 5 and 0.5 Å/sec deposition rates respectively from $SmCo_5$ targets onto heated substrates held at temperatures of about 600°C. Maximum moments at 18 kOe field applied parallel to H-sputter reaches

about 7 kG.[50]

Measuring the magnetization within the film plane of the $SmCo_5$ films sputtered from 1:5 phase targets indicated that the effect of H-sputter is evident as with the case of films sputtered from elemental targets. The ratio of remanent magnetization measured in film plane at 90 degrees off the H-sputter direction to the remanent magnetization measured parallel to H-sputter was found to be about 0.82 for these films.

5.1.3) COERCIVITY

We present here the results obtained from hysteresis loop measurements on films sputtered from either elemental or single phase targets and relate the observed coercive forces to the microstructure and the texture of the films.

The intrinsic coercive field is the value of the applied field necessary to reduce the magnetization $\vec{M}$ to zero. The extrinsic coercive force or the field required to reduce $\vec{B}$ to zero will be mentioned explicitly when referred to. Coercive force is given always here in kOe.

5.1.4) COERCIVE FORCE OF $Sm_{1-x}Co_x$ FILMS

As the Co concentration increases beyond 1:5 composition the coercive force decreases appreciably. This is a consequence of the fact that the anisotropy field in 2:17 compounds is one order of magnitude less than in 1:5 compounds of the same system[22,23] in

addition the coercive force in the fine grained Sm-Co materials depends on the local anisotropy.[21]

From Fig. 12 it is clear that the coercive force decreases from 10.8 to 2.5 kOe as the film composition changes from the 1:5 to the 2:17 approximate compositions.

In Table 6 we presented data of a series of Sm-Co samples spanning a composition range of about 20 at %Co. The same results are plotted in Fig. 31. The intrinsic coercive force decreases from about 9 to 5.6 kOe as the Co concentration increases 83-90 at %Co. In the entire range of composition, our samples exhibit higher intrinsic coercive force than those observed in an earlier study done on D.C sputtered thin crystalline Sm-Co films.[35] The maximum observed $_iH_c$ in that work was 4 kOe for a sample containing about 78 at %Co.

Our samples mentioned above were sputtered under the same conditions since theyare subregions from the same Sm-Co film. $SmCo_5$ samples synthesized from premixed 1:5 targets show marked coercivity dependence on some of the sputtering parameters as will be discussed next.

5.1.5) COERCIVE FORCE OF $SmCo_5$ FILMS

The microstructure, texture and hysteresis loops are shown in Figures (5a, 6, 27, 28), (5b, 7, 29) and (30,32) for $SmCo_5$ films sputtered using 1.5, 5 and 0.5 Å/sec respectively.[50] For a field of 20 kOe a minor loop was obtained for the 1.5 Å/sec deposited film with (110) texture as seen in Fig. 28. $_iH_c$ of this minor loop is 15.8 kOe measured in film plane. In an inplane field of 90 kOe and

at -63°C the same sample exhibited high $_iH_c$ of 23 kOe as seen in Fig. 27. For a (200) textured sample sputtered at 5 Å/sec a coercive force of 13 kOe has been obtained in film plane for 18 kOe field (Fig. 29). On the other hand lowering the sputtering rate to only 0.5 Å/sec resulted in (110) textured film with coercive force of 11 kOe in film plane as seen in Fig. 30.

The texture correlation to the deposition rate will be discussed in Sec. 5.4.1. Here we relate the observed coercive force with the microstructure and texture of the films.

5.1.6) COERCIVE FORCE DEPENDENCE ON MICROSTRUCTURE AND TEXTURE IN FIXED COMPOSITION $SmCo_5$ FILMS

Since these films are of fixed composition the differences in their observed coercive force are not attributed to strong deviations from the 1:5 stoichiometric composition, rather they are attributed to the differences in the microstructure and the preferred orientation developed in the films.

The coercivity is a complex function of the material structure and is very sensitive to the details of that structure,[30,33-35] in high anisotropy RCo_5 compounds where $k>>M_s^2$, i.e. the crystal anisotropy dominates the shape anisotropy. The observed values of the coercive field in these materials is low compared to the available anisotropy field, e.g. in $SmCo_5$ maximum room temperature value of about 40 kOe has been reported[33,39] coherent rotation and curling[38,78] cannot be thus considered as the magnetization reversal mechanisms. A tentative mechanism of magnetization reversal in our films will be discussed in

sec. 5.2.1. Here it suffices to mention that domain wall pinning and nucleation have been suggested as the responsible processes for reversing the magnetization.

The samples of Figs. 6 and 32 are of the same texture namely (110) but the latter has grains about 400 Å in size as compared to about 150 Å in the former. The thickness of these two films is of the same order (about 10 kA). Coercivity-thickness dependence has been reported elsewhere[34] for Sm-Co films synthesized by getter sputtering. The finer grain film as seen from its hysteresis loop has higher coercive force than that of the coarser grain films. This difference in coercivity may be accounted for on the light of the observation that fine particles are less probable to contain defects within their interior. These defects may represent centers for domain wall nucleation and thus aid magnetization reversal.[36] According to this possibility the coercive force is expected to increase with decreasing particle size.

On the other hand the film of Fig. 7 is (200) textured and is of grain smaller by a factor of roughly three than those of the sample of Fig. 32 for a (110) textured sample. However their coercive forces are not much different, apart from the difference in thickness for these two films, it is clear that the particle size is not the only factor contributing to the coercivity in these films.

The second factor is the preferred orientation of certain crystal planes. Figure 33 illustrates a schematic representation of the (110) and (200) stacking sequence in $SmCo_5$ films.[50] In the (110) texture case the 2c sites of Co lie in the same plane with the Sm sites, while in the (200) case they are not in the same plane with the Sm sites.

It has been pointed out in sec. 3.2.4 that the exchange field at the Sm sites has large contribution from the Sm-Co exchange. Neutron diffraction techniques showed that the Co-2c sites contribution to the anisotropy is larger than the 3g sites of Co.[28,79]

The magnetization vector reverses within the plane of the film rather than flipping out to the direction perpendicular to film plane and then back to film plane because of the associated demagnetizing field in the latter case. The magnetization reversal will be thus impeded more in the case of the (110) textured films due to the presence of the high anisotropy Co-2c sites in the same plane with the Sm sites in the plane of reversal.

In addition, both of the anisotropy field and the intrinsic coercive force have been shown to vary within the homogeneity range of $SmCo_5$ system. The Co rich region of that range extends from about 83.33 to 85.7 at %Co, within that range a disordered replacement of Sm atoms by pairs of Co atoms takes place leading to an observed decrease in both coercive field and anisotropy field.[29] On the other hand a peak in the coercive force has been observed in the Sm rich side of the homogeneity range at the Sm_2Co_7-$SmCo_5$ phase boundary.[40] The anisotropy field of the 2:8 phase is, although smaller than that of 1:5 is in excess of 200 kOe,[80] compared to about 100 kOe for the 2:17 phase, the Sm rich side of the 1:5 range is thus of higher available H_A. Table 4 indicates that the diffraction angles of 2:7 and 1:5 phases are very close to each other. The lattice parameters of the hexagonal phase of 2:7 phase are:[81] a=5.041 and c=24.327 Å. Since the difference in the a-parameter between these two phases is

small the 2:7 phase can precipitate on the basal plane of $SmCo_5$ matrix and so in our films with C-axis lie in or near film plane the observed intensities of the diffraction lines will be high only from the $SmCo_5$ unit cell and thus will be hard to conclude of the existence of a 2:7 phase in our films using only the x-ray diffraction technique. However we do not exclude the possibility of probable small volume fractions of the 2:7 phase in our $SmCo_5$ films.

5.1.7) ENERGY PRODUCTS OF Sm-Co BASED FILMS

It is well known that the maximum energy product of a magnetic sample is obtained by comparing BH values in the second quadrant of the sample hysteresis loop. We discuss first the dependence of energy products on the composition of Sm-Co samples. Energy products are given in MG-Oe and they all refer to the static energy product.

5.1.8) ENERGY PRODUCT VARIATION WITH COMPOSITION OF Sm-Co FILMS

Table 6 shows the variation of the inplane maximum energy products of $Sm_{1-x}Co_x$ samples measured in 14 kOe field parallel to H-sputter with the composition of the samples, the same data is plotted in Fig. 34.[50]

The energy product reaches a maximum of about 20 kOe at composition close to the Sm_2Co_{17} composition for the same sample of Figs. 23 and 24 and declines to lower values on both sides of the peak reaching a value of 10.7 MG-Oe for a 83 at %Co sample. The decline from the peak is less severe in the relatively Sm rich region of the composition range under study. We have seen that the coercive force of Sm-Co

samples decreases with increasing the Co content. This decrease is associated with an increase in the magnetization (Figs. 21 and 31). The $(BH)_{max}$ would correspond to null energy product if the Sm rich side of our relation in Fig. 34 is extrapolated to intersect the composition range at about 67 at %Co. This is corresponding to the $SmCo_2$ phase reported to be non magnetic.[74,75]

The maximum energy products in film plane but perpendicular to H-sputter are shown in Table 6 for the same composition. The effect of H-sputter on the energy product is evident. However it is small near the 1:5 composition.

Figure 35 displays the improvement in energy products of $SmCo_5$ samples. The lowest energy product of 2.6 MG-Oe is for a sample synthesized in the earliest phase of this work in about $7x10^{-7}$ torr base pressure and <100 micron argon in no inplane magnetic field onto substrate held at 800°C. The low energy product of this sample is due in part to the random orientations of the C-axis and to the low magnetization. B_r is 3.6 kG and $_BH_c$ is 3.2 kOe. The middle relation in Fig. 35 has been derived from the minor loop of Fig. 28 for a $SmCo_5$ film sputtered from 1:5 targets in the presence of 1.75 kOe field on substrate at tempeature of 600°C. The energy product of this minor loop is 7.5 MG-Oe. The corresponding $_BH_c$ is 5 kOe. The higher energy product of 18 MG-Oe is observed for the same sample of Fig. 28 but measured in 90 kOe field at -63°C (see Fig. 27 for hysteresis loop).

The value of 18 kOe mentioned above is to be compared with 21.9 MG-Oe for $SmCo_5$ samples of 16.84 at %Sm prepared by aligning, pressing and then sintering of the powder,[40] and also compared to an earlier

work[82] on nearly 100% dense and 80% aligned $SmCo_5$ samples prepared from powder, the magnetic properties of the samples in that work were: B_r = 8-9 kG, $_iH_c$ = 25 kOe and $(BH)_{max}$ = 16-20 MG-Oe measured after magnetizing in 60 kOe field.

On the other hand the Sm_2Co_{17} system with the substitution of one or more transition elements for Co has been investigated extensively in an attempt to increase the low coercivity of pure 2:17 phase and to conserve the cobalt. This has been studied in bulk[83] and film form.[33]

Samples of $Sm_2(Co,Fe,Zr)_{17}$ exhibit high energy products up to 21 MG-Oe in our work as obtained from the inplane hysteresis loop of Fig. 25. The substitution of Fe in pure 2:17 phase reduces the residual induction slightly but increases the coercive force since Fe has been found to preferentially substitute in the dumbbel site of Co.[83]

Introducing Zr in R_2Co_{17} has been observed to increase the magnetic anisotropy[84] indicating the possibility of an increase in the coercive force. The effect of introducing Zr in the 2:17 system on the microstructure and hence on the coercive force has been reported.[85]

The energy products of precipitation hardened 2:17 Sm-Co based magnets were reported to have energy products between 25-30 MG-Oe[83,86] with coercive force between 6-15 kOe. A complex heat treatment was used to achieve the hard magnetic properties of these samples. In film form[33] sputtered and heat treated $Sm_2(Co_{0.7}Fe_{0.3})_{17}$ films show coercive force of about 6 kOe and energy product of 12 MG-03 for isotropic samples.

The coercive force of pure 2:17 systems have been reported to be

very low.[33] Pure 2:17 Sm-Co films sintered with Sm-rich aid exhibited a coercive force of 9.6 kOe.[87] Our samples of Figs. 23 and 25 exhibit good magnetic properties and there is still a little room for improvement through optimizing the microstructure.

5.2.1) MAGNETIZATION REVERSAL MECHANISM

As we have already mentioned the magnetization reversal in the high anisotropy RCo compounds does not take place through coherent rotation of all the moments in unison or through non-coherent processes like curling. This is revealed for example by the fact that the measured coercivities are only one order of magnitude less than the available anisotropy field in $SmCo_5$ system.

Studies on the magnetization reversal in RCo_5 have been reviewed by Becker.[30] Further studies have been reported on single crystals,[20] on sintered magnets,[88,89] and on powder.[90] The mechanisms controlling the coercivity have been attributed to dominating nucleation process or to domain wall pinning. In both processes the crystal defects such as inhomogeneities of magnetization and anisotropy, non-magnetic inclusion, etc., may play the role of pinning or nucleating sites. It has been noted by Becker[30,37,88] that $_iH_c$ depends markedly on the maximum magnetization remains about the same while the coercivity decreases as the magnetizing field decreases. In the pinning case the coercivity remains essentially constant as the magnetizing field is varied while the remanent decreases with decreasing the maximum magnetizing field.

We have studied the variation of both M_r and $_iH_c$ with H_m in $SmCo_5$

and Sm_2Co_{17} samples in order to investigate the magnetization reversal process.[47-50] Figure 36 exhibits the demagnetization behavior of a sample sputtered from elemental targets onto a heated substrate. The sample contained about 85 at %Co. The magnetizing fields of 4,6,8, 10,12 and 14 kOe were applied in the plane of previously demagnetized samples (no H-sputter was used). The samples were demagnetized by cycling in slowly decreasing fields such that magnetization process starts from state of null magnetic moment. It is clear form Fig. 36 that both M_r and $_iH_c$ vary with H_m. The curves in addition show significant slopes as they enter the second quadrant for this sample which is lacking alignment. Such variation shows that both nucleation and pinning are taking part in the magnetization reversal.

Figure 37 displays the demagnetization curves for a $SmCo_5$ sample sputtered from $SmCo_5$ targets onto a heated substrate in the presence of 1.75 kOe inplane field. It is the same sample whose hysteresis loop is displayed in Fig. 29, indicating $_iH_c$ of 13 kOe in film plane. The curves are less steep as they enter the second quadrant and show tendency to squareness as H_m increases. In Fig. 38 a similar study is shown on a $SmCo_5$ film previously studied at 90 kOe and 20 kOe (Figs. 27 and 28). This film is magnetically harder than the film of Fig. 37 as it is clear from the steep slopes as the curves enter the second quadrant. The summary of Figs. 37 and 38 is plotted for convenience in Fig. 39. The fact that both of the remanent and the coercive force depend on the maximum applied is evident, however the remanent depends on H_m more strongly which may suggest that both nucleation and pining are contributing with the probable dominance of the pinning

mechanism.

The defects can either serve as nucleation centers and thus aid magnetization reversal, or as pinning sites which impede domain wall motion and thus increasing the difficulty with which a domain wall moves. This process increases the coercive force of the material.

Livingstron[36] has enumerated the types of defects in powders, sintered magnets and single particles that could aid or inhibit the reach to equilibrium and thus decrease or increase the coercive force. Paul[91] suggested a model to account for the coercivites observed in different materials from supermalloys to $SmCo_5$ magnets. The model is based on considering the defects, e.g. grain boundaries as pinning sites. Anisotropy and exchange constants were assumed to be different from the rest of the homogeneous materials. In his model, the intrinsic coercive force increases linearly with the defect size for small defects.

5.3.1) DEMAGNETIZATION CURVES

Figure 35 displays the demagnetization curves B-H for $SmCo_5$ samples with their associated energy product values indicating the maximum values reached at the right part of the figure.[47,50] Figure 40 displays four demagnetization curves for four $Sm_{1-x}Co_x$ samples sputtered from elemental targets.

The point of intersection between a demagnetization curve (or straight line) with the field axis represents the extrinsic coercive froce ${}_BH_c$ which is the field required to reduce the induction B to

zero. For high anisotropy RCo_5 compounds ${}_iH_c > {}_BH_c$, the maximum value of the latter is B_r in such case the demagnetization curve becomes a straight line extending from B_r on the B-axis to a value of H numerically equal to B_r. For higher Co content samples one expects higher B_r but smaller ${}_iH_c$ and hence smaller ${}_BH_c$ than for the lower Co content sample synthesized under the same conditions as those in Fig. 40.

5.4.1) TEXTURE STUDIES

In the previous sections we have seen that the preferred orientation of particular crystal planes either (110) or (200) in $SmCo_5$ films is a contributing factor to the observed coercivities in these films. These different textures have been developed in films sputtered either from elemental Sm-Co targets or single phase $SmCo_5$ targets directly onto heated substrates without any subsequent heat treatment. We have seen also that the C-axis for both kinds of films is oriented in film plane which is preferentially aligned more in the direction of the magnetic field used during sputtering. So the development of a particular texture in this work is related to the growth process itself since these same textures are observed for films synthesized in or without the inplane magnetic field.

In the elemental targets case the two distinct textures have been developed in $SmCo_5$ samples depending on the oxygen content in the films. Figure 41 displays the x-ray diffraction pattern traced using Cu k_α radiation for a $SmCo_5$ sample sputtered in 50 micron argon.[48] The oxygen content in this sample as determined from Auger analysis is 9.7

at %O which is equivalent to 2.1 wt. %O. The sample is clearly entirely (110) textured with (002) reflection at the background level. Figures 42 and 43 display the Cu k_α diffractometer trace of two $SmCo_5$ samples sputtered from the same elemental targets but in 150 micron argon. The substrate temperatures were maintained at 650 to 800°C. The oxygen at % content in the samples in Figs. 42 and 43 are 6.5 and 1.4 at %O respectively.

The deposition rate for these samples is in the range of 1Å/sec, however, increasing the argon partial pressure increases the deposition rate and decreases the foreign atoms arrival and entrapment in the growing films. The (200) to (110) intensity ratio for the sample of Fig. 42 is about 0.3 while the (110) is absent for the sample in Fig. 43. For both, the (002) reflection is absent. These results demonstrate that the particular developed texture depends on the level of oxygen present in the film.

On the other hand in films sputtered from 1:5 targets the same textures have been developed as a result of varying the target RF power while using the same argon pressure. Target self bias voltages of 900, 700 and 400 V resulted in deposition rates of about 5, 1.5 and 0.5 Å/sec respectively. The x-ray data for three samples sputtered using the above mentioned conditions are shown in Figs. 6, 7 and 32 respectively.[50]

Those results just mentioned for the elemental and the $SmCo_5$ targets are consistent and can be interpreted on the light of foreign atoms incorporation in the growing films. Figure 33 illustrates a schematic representation of the (110) and (200) crystal plane stacking

sequence in $SmCo_5$ system. The stakcing sequence leading to form (110) preferred orientation is a three stage sequence, while that of (200) is a five stage sequence. The intensity of a particular reflection in x-ray diffraction work is known to increase with increasing the number of the lattice planes whose orientations are parallel to the surface of the sample, which is the film plane in our case. The predominance of either (110) or (200) texture is therefore manifested in the relative intensities of the respective lines. A measure of the strength of a texture in a sample is obtained by comparing the intensity ratio of the (110) and (200) reflections in the sample to its counterpart in a sample of complete random orientation of the crystal planes, e.g. powder sample.

Forming a $SmCo_5$ deposit with (200) texture requires relatively low level of foreign atoms arrival and hence probable entrapment in the growing film. This is so since the five stage sequence, as compared to the shorter three stage sequence, requires less disturbance of deposit formation by the incoming foreign flux of atoms. Increasing that flux is assumed to disturb the longer sequence and the developed texture switches to the (110).

This explanation is supported by x-ray diffraction data which indicates that the diffraction angle corresponding to the (110) reflection tends to shift toward lower values in the (110) strongly textured films which indicates larger d-spacing. This is consistent with the observation that (110) texture growth is facilitated when relatively higher levels of gas entrapment are present. The atoms of the inert argon gas do not interact chemically with the film material,

but rather they get into the intersticial regions of the crystal. On the other hand oxygen interacts with Sm to form Sm_2O_3 at the Sm sites.

6.0.0) CONCLUSIONS

Ferromagnetic films of Sm-Co based systems have been synthesized directly onto heated, polished $A\ell_2O_3$ substrates, by selectively thermalized radio frequency (RF) sputtering from a set of three targets simultaneously.[47-50]

Films with composition gradients along the length of a substrate were synthesized from high purity arc-melted targets, two of which are Co and one of Sm.[47-50] In another configuration premixed compounds have been used as targets which resulted in large area films of a single composition.[50]

In most cases an inplane magnetic field of 1.75 kOe was applied during the deposition across the width of the substrate.[49,50] In the cases when no magnetic field was used during sputter synthesis,[47,48] a relatively high degree of magnetic isotropy has been obtained in film plane. Low saturation moments were measured perpendicular to film plan indicating strong orientation of C-axis within the plane of the deposits. This is supported by x-ray diffraction results. The (002) reflection intensity is 0.67 of that of the (200) line intensity in the case of a randomly oriented $SmCo_5$ powder sample compared to a ratio of 0.3 for a $SmCo_5$ RF sputtered sample synthesized in the early stages of this work.[47]

The magnetization of the samples was shown to increase as the Co content increases, but this was associated with a decrease in $_iH_c$. The relatively high degree of magnetic isotropy results in low saturation magnetization and remanent induction which led to low energy products of about 3 MG-Oe[47] in the plane of the film for samples of

composition close to $SmCo_5$.

In the selectively thermalized sputtering process, the sputtering gas, usually argon, is at a pressure high enough so that collisions between the sputtered atoms and sputtering gas atoms reduce the sputtered atoms energies to an equivalent kinetic energy of the substrate temperature. The slowing down of the energetic Sm and Co aoms as they leave the targets with average energies of several eV takes place through elastic collisions with the argon atoms along the target to substrate path. The use of selectively thermalized sputtering has profound effects on the textures developed in the synthesized films.[48-50] For $SmCo_5$ samples sputtered from elemental targets a correlation between film texture and oxygen level incorporation in the films was observed.[48] A predominant (110) texture was obtained for samples containing more than 6 at % oxygen. As the oxygen level was lowered to 1.4 at %, only a (200) texture was developed.[48]

The use of an inplane magnetic field of 1.75 kOe in the film plane during the synthesis of films deposited at substrates held at temperatures lower than the ferromagnetic Curie point of the magnetic phase resulted in a certain degree of preferential alginment of C-axis in the film plane. Films with a high degree of hysteresis loop squareness have been synthesized in the presence of that applied field.[49] $SmCo_5$ films directly synthesized onto heated substrates held at a temperature of 600^{o}C and in an argon partial pressure of 150 mTorr exhibited high remanent to maximum magnetization values of 0.97 in a direction parallel to the inplane field. The M/M_r value up to applied fields of about 5 kOe was as high as 0.9.[49] The inplane magnetization of films

so sputtered showed variation wtihin the film plane. The relative minimum of the inplane magnetization was obtained for an applied field direction at 90^{o} to the direction of the 1.75 kOe field.

The range of substrate temperatures used proved to be high enough to allow for direct crystallization of the deposit upon reaching the substrates. Well identified diffraction traces were obtained for the directly crystallized as sputtered samples.

The use of different sputtering parameters has a strong effect on the physical and crystallographical properties of the films and consequently on their magnetic properties. For the films sputtered from $SmCo_5$ targets so as to create uniform composition films, particular preferred orientations of crystal planes have been developed as a result of using different deposition rates.[50] The (110) texture is developed in films synthesized using relatively low deposition rates while relatively higher rates led to the synthesis of films with (200) texture. The formation of different textures in our films are attributed to different levels of foreign atoms, for example oxygen and/or argon, incorporation in the deposits.

Sputtering from elemental targets enabled formation of deposits with systematic composition gradients along the length of a single substrate. Magnetic properties have been studied for samples sputtered under the same conditions but having different compositions. $SmCo_5$ and Sm_2Co_{17} phases have been identified on the same substrate using x-ray diffraction and fluorescence analysis.[47-50] The absolute composition of the samples is known to ±1 % Co.

The specific (110) and (200) textures were obtained for films

sputtered from premixed $SmCo_5$ targets as a result of varying the deposition rate.[50] The (110) textured films were developed upon using relatively low deposition rates of 0.5 and 1 Å/sec, while the (200) textured films were synthesized upon using relatively higher deposition rate of 5 Å/sec. In the case of gradient composition films a distinct correlation between the oxygen content in the films and the kind of texture developed in the films was obtained.

The coercive forces ${}_iH_c$ of the $SmCo_5$ films sputtered from premixed targets show relation to both the grain size and the specific texture developed in the films.[50] Films with predominant (110) and fine grain size show large intrinsic coercive forces of 23 kOe in the plane of the film. The intensity of the (200) reflection of such films to the (110) reflection is about 0.5 compared to 1.0 for its counterpart in the case of randomly oriented $SmCo_5$ powder. The approximate grain sizes of such films are 90±15 and 150±30 Å as determined from the (110) and (200) reflections respectively. The location of the high anisotropy 2c sites of Co in the same plane with the Sm sites in the stacking sequence of films with (110) texture contributed to the large coercive force of these films by resisting magnetization reversal in the plane of the film.[50] In the (200) texture, the Co-2c sites are located in planes containing only the Co atoms which are parallel to the substrate plane. The C-axis is rigidly aligned into the film plane for both kinds of texture as revealed by magnetic measurements both inplane and perpendicular to the plane of the films. For example an inplane maximum magnetization of a (200) textured film is roughly three times larger than the magnetization of the same film measured perpendicular to film plane in the

same applied field.[50] In addition x-ray diffraction traces of both kinds of textured films indicate the absence of the (200) reflection.[50]

The magnetization reversal takes place by rotation within the film plane rather than by moment rotation out of film plane.

The coercive forces of $SmCo_5$ films deposited using 0.5 Å/sec are smaller than their counterparts in films deposited using the higher rate of 1.5 Å/sec. The former films are of grain size larger than those of the latter. Both films, however, are of the same (110) texture. This shows that the grain size is a factor contributing to the coercive force of our films. The (110) films which were developed using 1.5 Å/sec deposition rate are finer in microstructure and magnetically harder than those of the (200) textured films sputtered from elemental or fixed composition targets.[50] Varying the target power in the case of elemental targets did not seem to affect the grain size in contrast to the case of films sputtered with a uniform composition. The existence of a composition graduent along the length of a substrate could be the reason for such results. The exact mechanism has not been fully investigated.

The magnetization reversal in our films takes place through the domain wall pinning and nucleation mechanisms. Both the remanent magnetization and the intrinsic coercive force show evident dependence on the magnetizing field for films sputtered either from elemental or premixed targets.[47,50] The same mechanism has been suggested to account for magnetization reversal in the bulk materials.

The high energy products measured in the plane of the films are due to the squareness of the hysteresis loops and the high magnetic

induction of our films. A value of 18 MG-Oe has been reached for certain (110) textured fine grained films. Bulk materials prepared by the powder metallurgy technique are reported to have energy products higher than those obtained for films due to the higher degree of C-axis alignment over three dimensions achieved in bulk materials. Films of two phase 1:5 and 2:17 $Sm_2(Co,Fe,Zr)_{17}$ have been synthesized from premixed compound targets. Energy products of $\sim$21 MG-Oe have been achieved for these films.[50]

Our films have the highest energy products that we know of in Sm-Co based films. The ferromagnetic samples have been directly crystallized for the most part and the magnetic properties were measured in as sputtered samples without subsequent heat treatment. The use of an inplane magnetic field during the deposition which occurs at substrate temperatures below the ferromagnetic Curie point for these systems has allowed the synthesis of films with a high degree of hysteresis loop squareness and high energy products.

TABLE 1

COBALT (in Å units)	SAMARIUM (in Å units)
K_{α} = 1.79026	L_{α} = 2.1998
K_{β_1} = 1.62079	L_{β_1} = 1.998
K_{edge} = 1.60815	$L_{I_{edge}}$ = 1.608
	$L_{II_{edge}}$ = 1.703
	$L_{III_{edge}}$ = 1.8457
	L_{γ} = 1.726

TABLE 2

Composition	I(Sm/Co)	A(Sm/Co)	at.%Co(real)	at.%Co(cal)
$SmCo_2$	0.2643±.0007	0.4986±.0049	66.67	66.73
$SmCo_3$	0.1681±.0006	0.3373±.0033	75.00	74.77
$SmCo_4$	0.1256±.0005	0.2498±.0025	80.01	80.01
$SmCo_5$	0.0993±.0004	0.1956±.0019	83.35	83.64
Sm_2Co_{17}	0.0625±.0003	0.1956±.0019	89.45	89.31

TABLE 3

Alloy	R_2R_{10}	R_2/R_{20}	at.%Co
$SmCo_2$	0.9575	0.9169	66.67
$SmCo_3$	0.9664	0.9334	75.00
$SmCo_4$	0.9726	0.9454	80.01
$SmCo_5$	0.9773	0.9545	83.34
Sm_2Co_{17}	0.9873	0.9741	89.45

TABLE 4

hkl	1:3	2:7	1:5	2:17
100	20.30	20.34	20.52	12.16
101	20.63	20.67	30.52	14.18
110	35.55	35.62	35.94	21.15
200	41.28	41.36	41.74	24.47
111	35.75	35.81	42.74	22.39
201	41.45	41.54	47.85	25.55
202	41.96	42.05	63.53	28.58
300	63.85	63.98	64.61	37.06
303	64.97	65.10	104.3	43.47

TABLE 5

Inplane Angle deg	M at 14 kOe emu/gm	M_r/M_{14}	$_mH_c$ kOe	-H at M/M_r=0.9 kOe
0	67.5	0.966	8.9	5.5
45	67.5	0.969	7.6	5.3
90	65.2	0.962	7.5	5.5

TABLE 6

at.%Co	$(BH)_{max}$ (MG-Oe)	$(BH)_{max}$ (MG-Oe)	$4\pi M_{14}$ (kG)	$4\pi M_r$ (kG)	$_iH_c$ (kOe)	S
93.46	5	5	16	12	1	.75
91.81	13.25	11.10	15	12	2.75	.73
90.56	19.75	17.00	12	10.5	5.60	.83
86.97	14.60	11.90	9.28	7.82	7.00	.84
86.64	11.80	11.50	8.00	7.20	7.20	.90
83.01	10.70	10.70	7.50	6.75	9.00	.90
79.58	6.40	4.80	7.00	5.25	8.50	.75
76.82	4.56	3.32	5.68	4.28	9.03	.75
72.46	2.56	1.02	4.71	3.32	9.67	.70

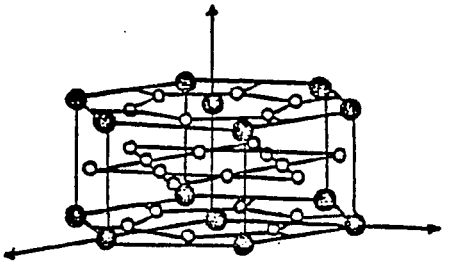

● Sm

○ Co

$SmCo_5$

Lattice Parameters:

a = 5·004 Å

c = 3·971 Å

Density = 8·58 gm/cc

One formula unit per unit cell

Figure 1

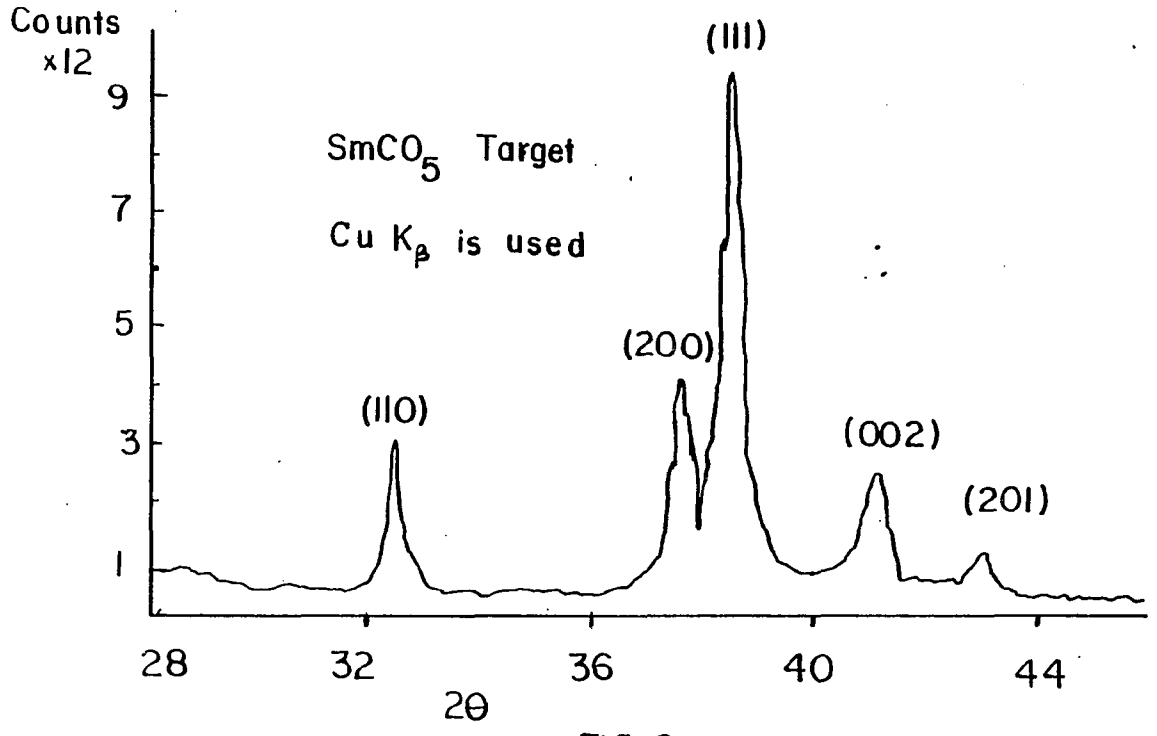
Counts
x12
9
7
5
3
1
SmCO5 Target
Cu Kβ is used
(111)
(200)
(110)
(002)
(201)
28
32
36
40
44
2θ

Fig. 2

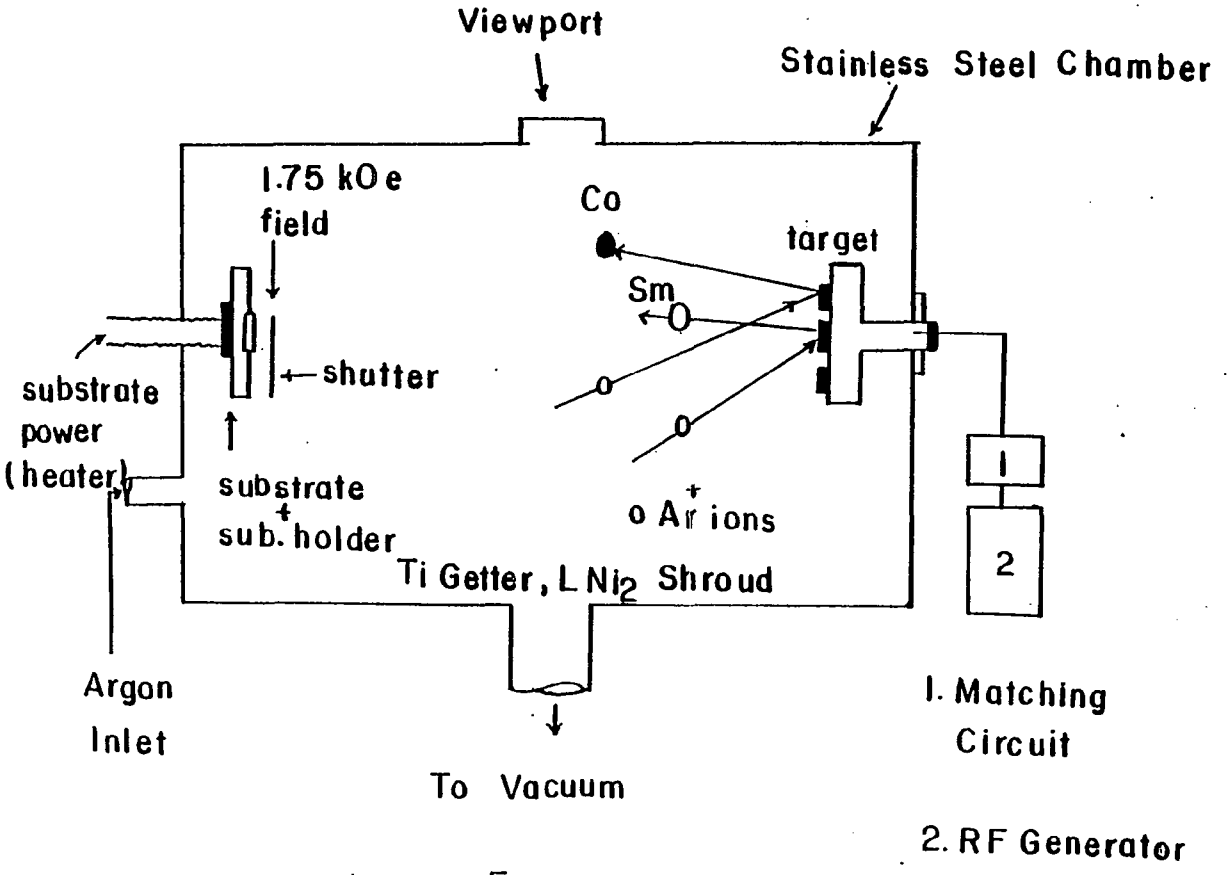
Viewport
Stainless Steel Chamber
1.75 kOe
field
Co
target
Sm
shutter
substrate
power
(heater)
substrate
+
sub. holder
o Ar+ ions
Ti Getter, L Ni2 Shroud
1
2
Argon
Inlet
To Vacuum
1. Matching
Circuit
2. RF Generator

Figure 3

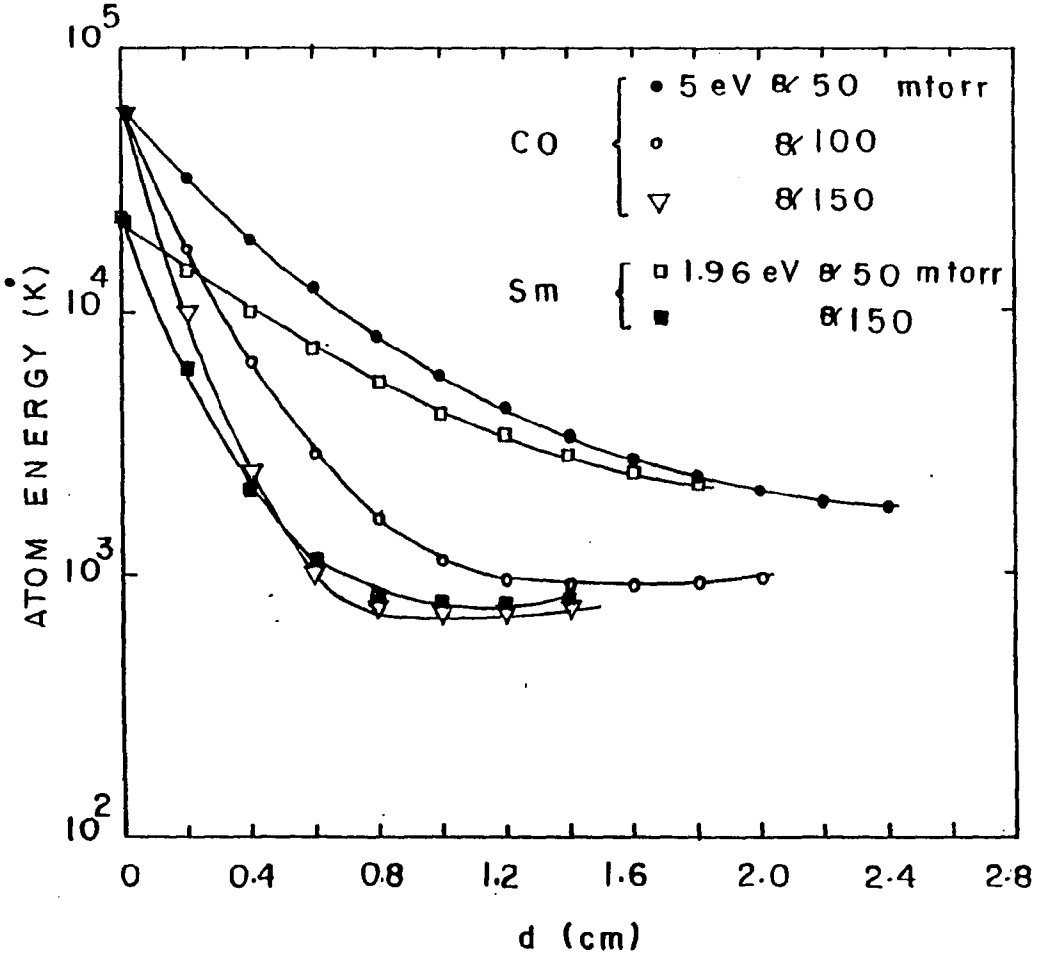
10^5
10^4
10^3
10^2
ATOM ENERGY (K)
CO
• 5 eV & 50 mtorr
o & 100
▽ & 150
Sm
□ 1.96 eV & 50 mtorr
■ & 150
0
0.4
0.8
1.2
1.6
2.0
2.4
2.8
d (cm)

Fig. 4

Fig·5 b

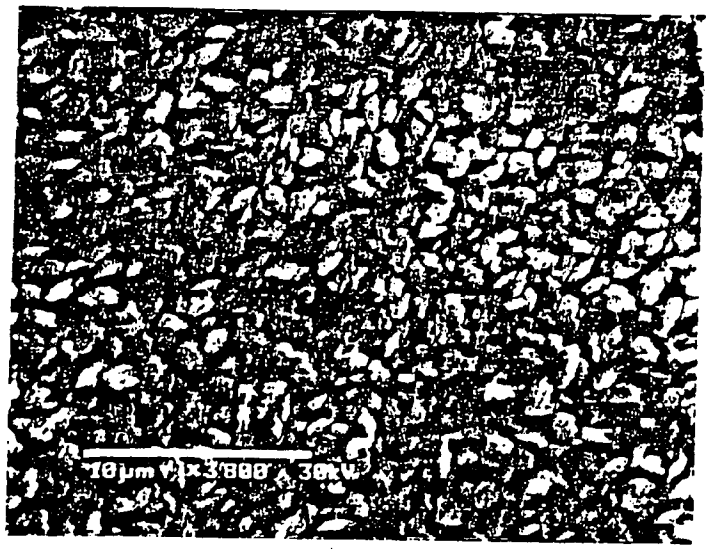

Fig·5 a

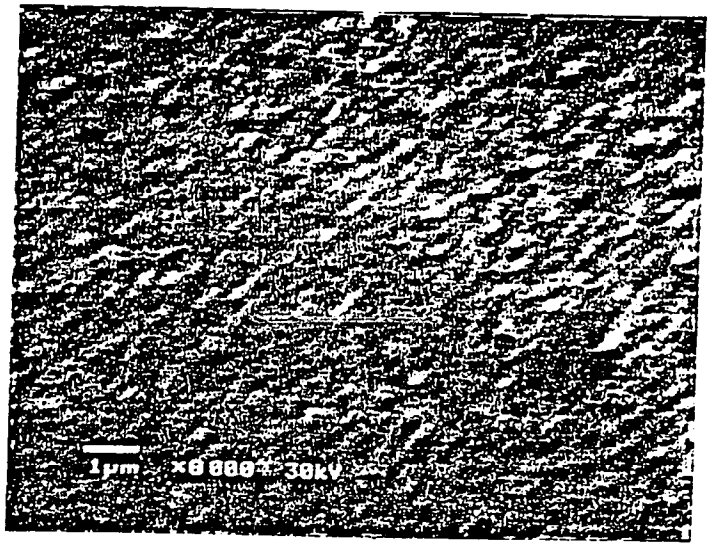

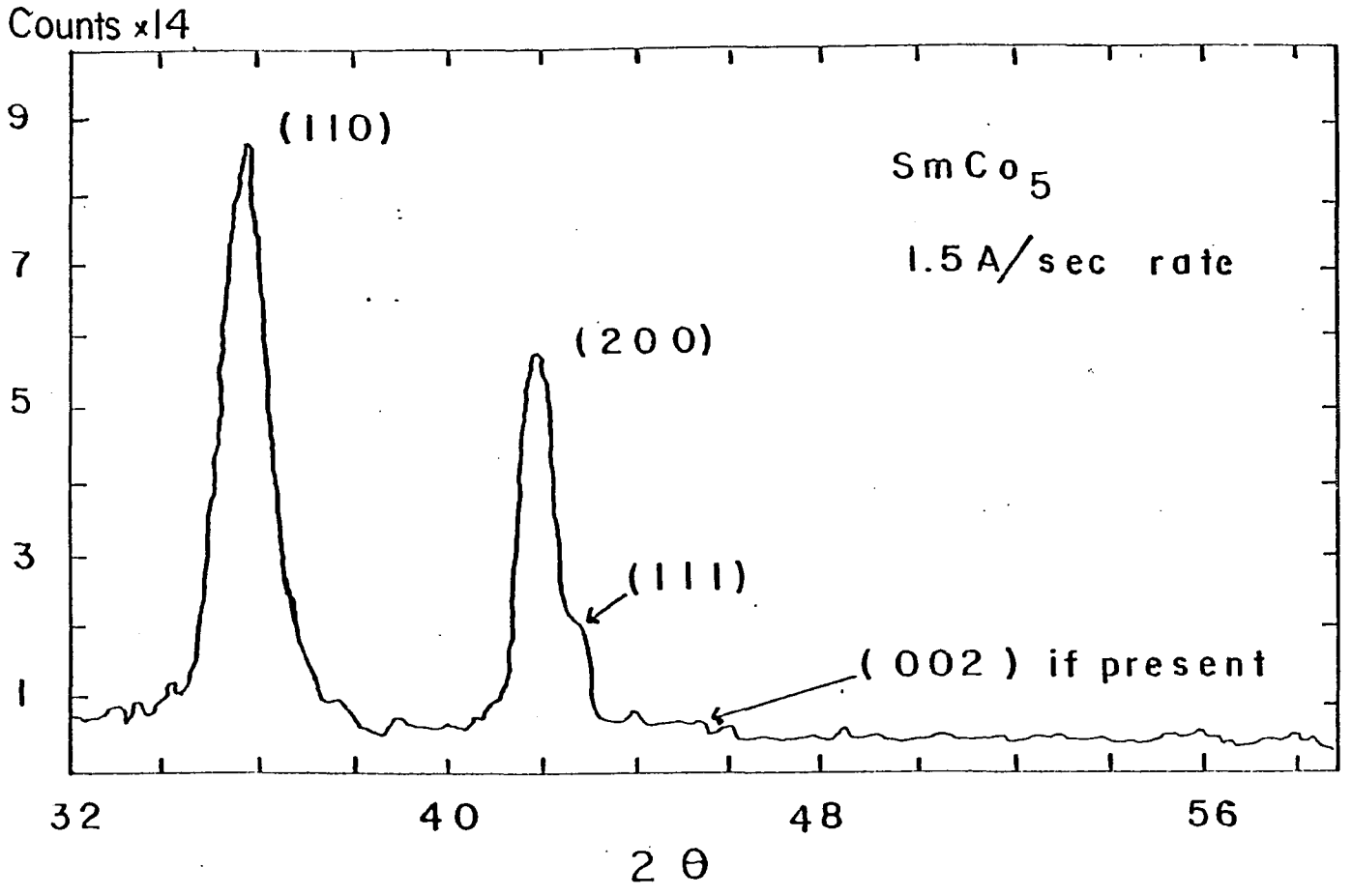
Counts x14
9
7
5
3
1
(110)
(200)
(111)
(002) if present
SmCo5
1.5 A/sec rate
32
40
48
56
2θ

Fig. 6

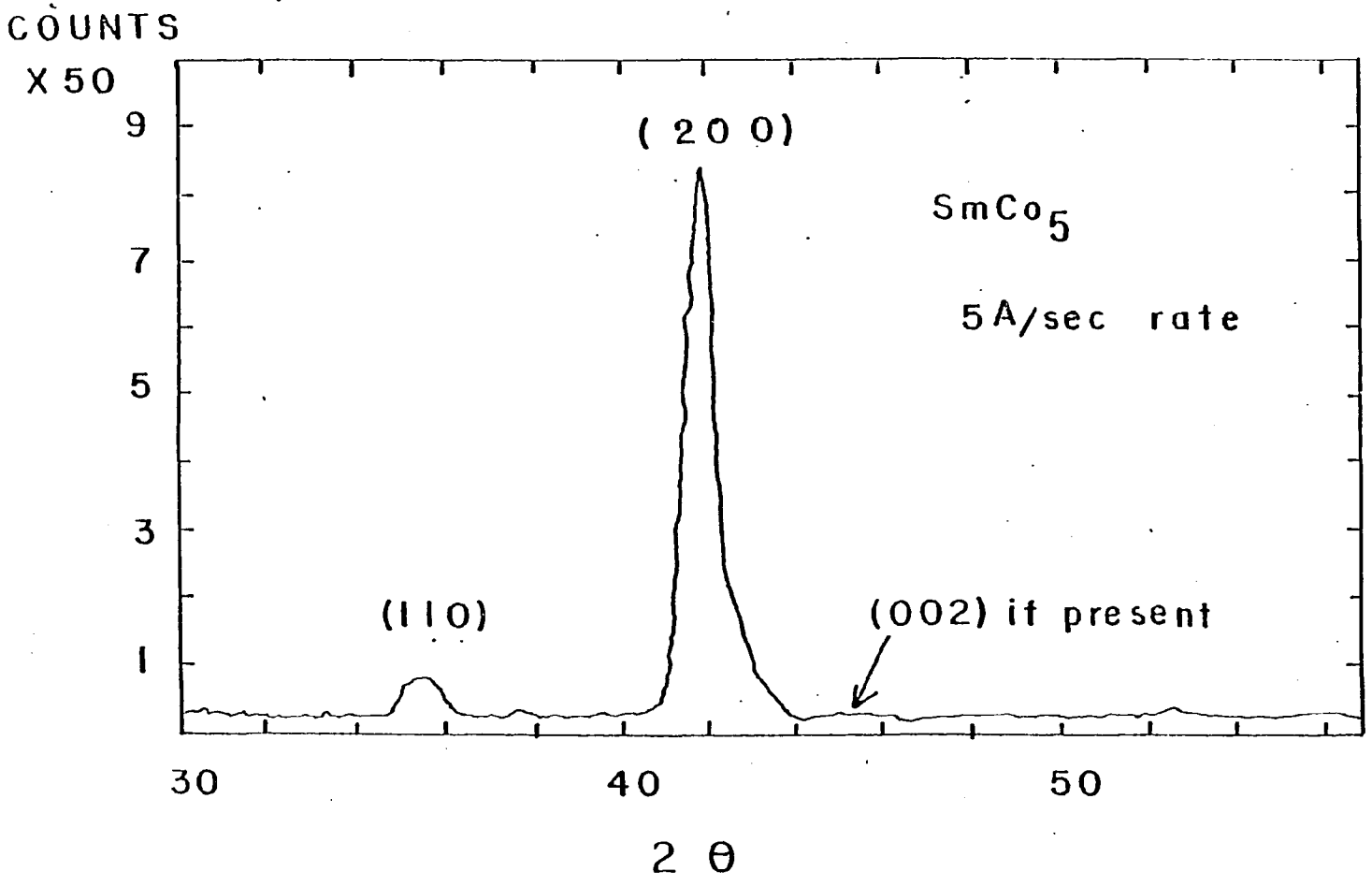
COUNTS
X 50
9
7
5
3
1
(2 0 0)
SmCo5
5A/sec rate
(1 1 0)
(002) if present
30
40
50
2 θ

Figure 7

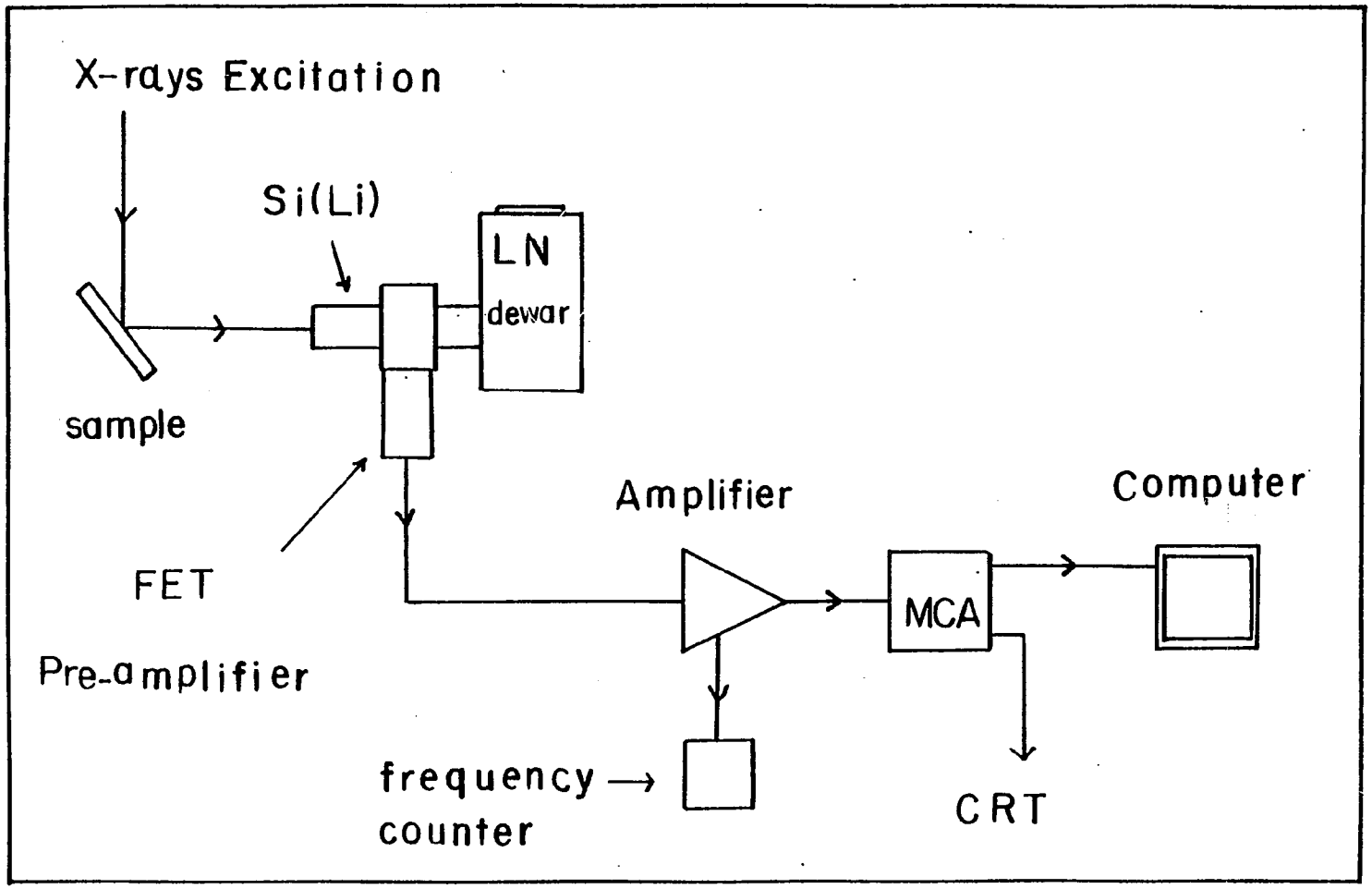
X-rays Excitation
Si(Li)
LN
dewar
sample
FET
Pre-amplifier
Amplifier
Computer
MCA
frequency
counter
CRT

Figure 8

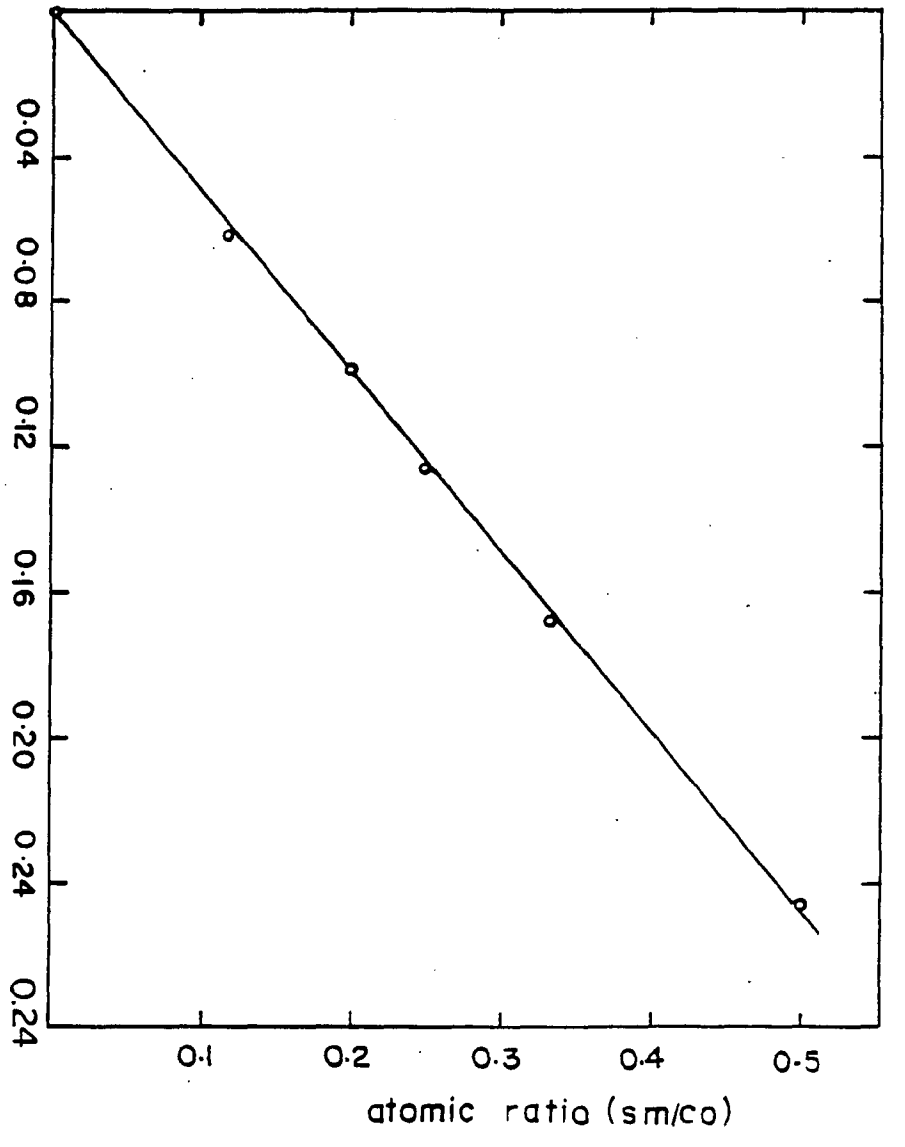

Figure 9

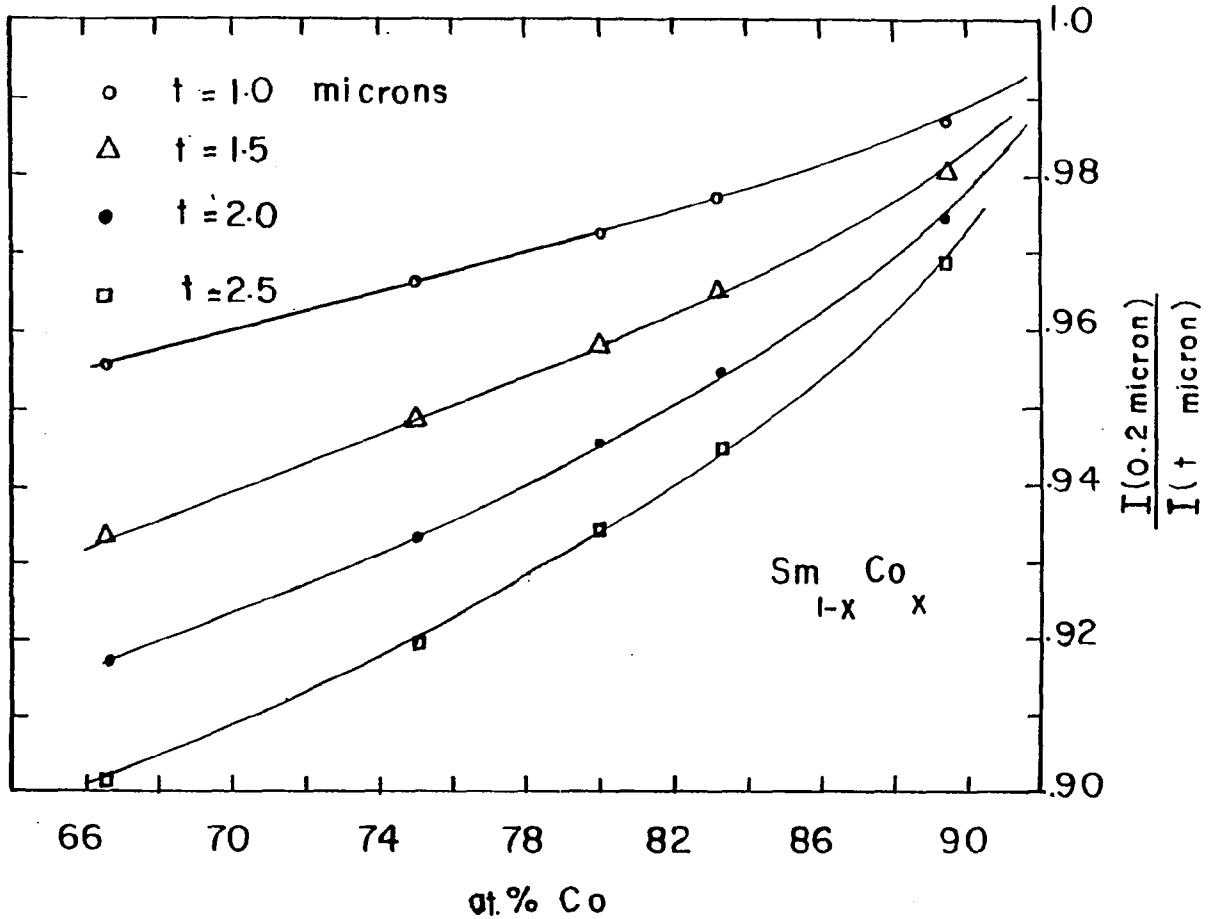
t = 1·0 microns
t = 1·5
t = 2·0
t = 2·5
Sm Co
1-x x
1·0
·98
·96
·94
·92
·90
I(0.2 micron) / I(t micron)
66
70
74
78
82
86
90
at.% Co

Figure 10

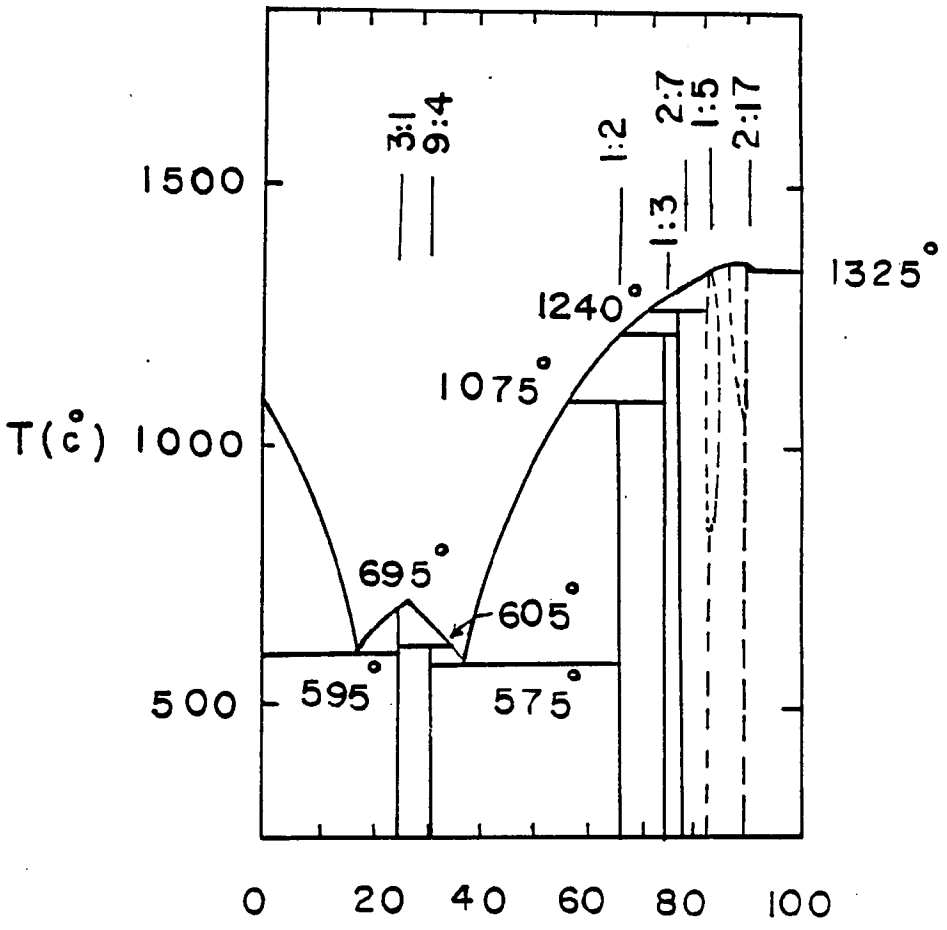
3:1
9:4
1:2
2:7
1:5
2:17
1:3
1500
1325°
1240°
1075°
T(c°) 1000
695°
605°
595°
575°
500
0
20
40
60
80
100
a% Co

Figure II

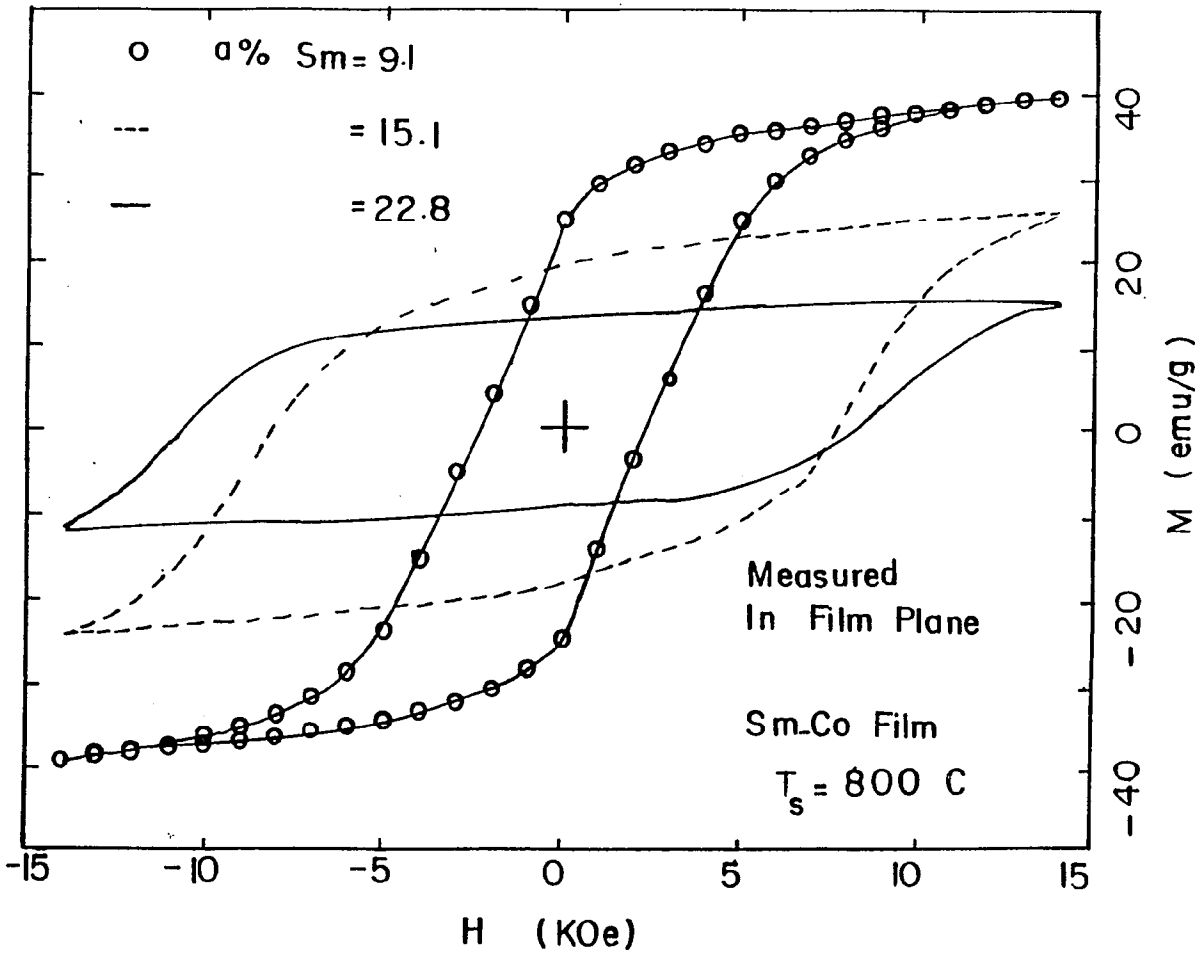
o a% Sm= 9.1
--- =15.1
— =22.8
Measured
In Film Plane
Sm-Co Film
T_s = 800 C
-15
-10
-5
0
5
10
15
H (KOe)
40
20
0
-20
-40
M (emu/g)

Figure 12

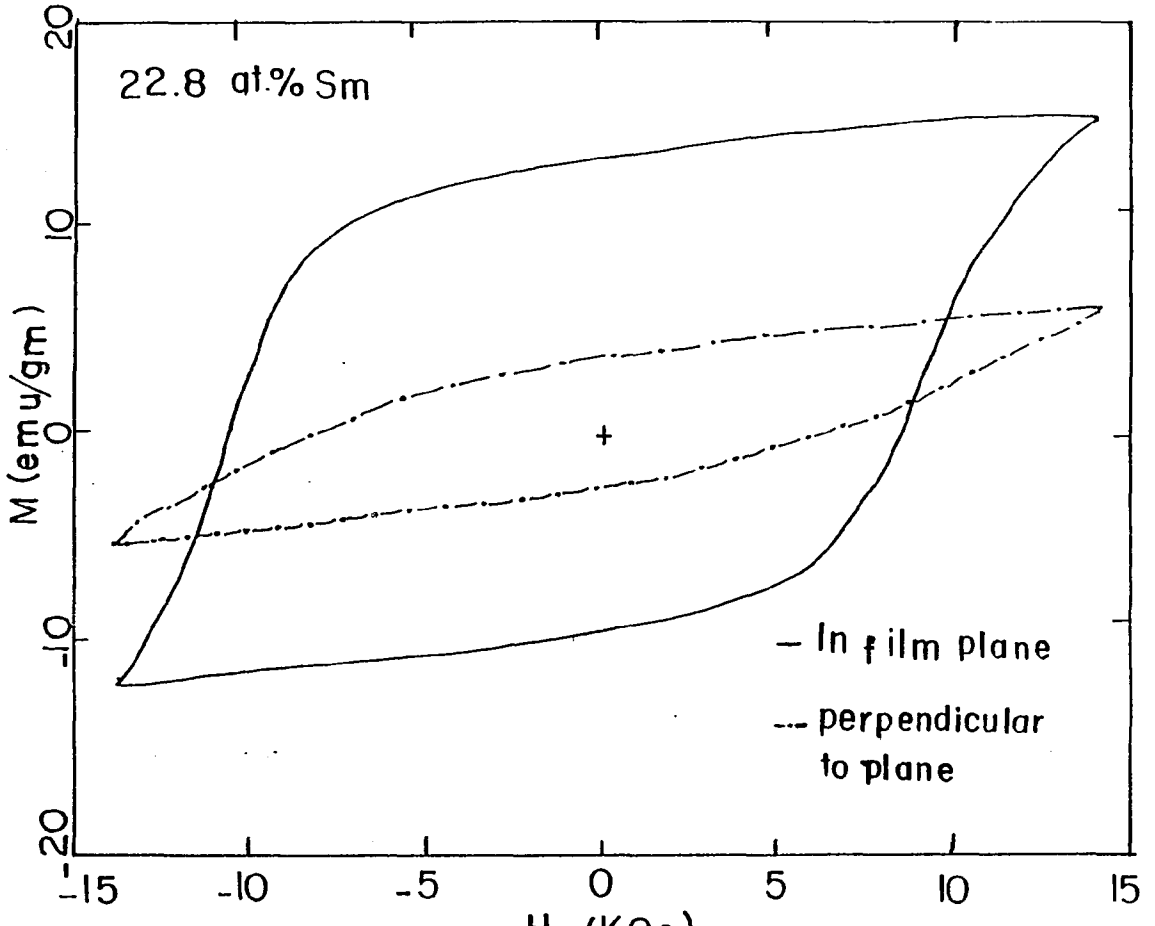
22.8 at.% Sm
M (emu/gm)
H (KOe)
20
10
0
-10
-20
-15
-10
-5
0
5
10
15
— In film plane
--- perpendicular to plane

Figure 13

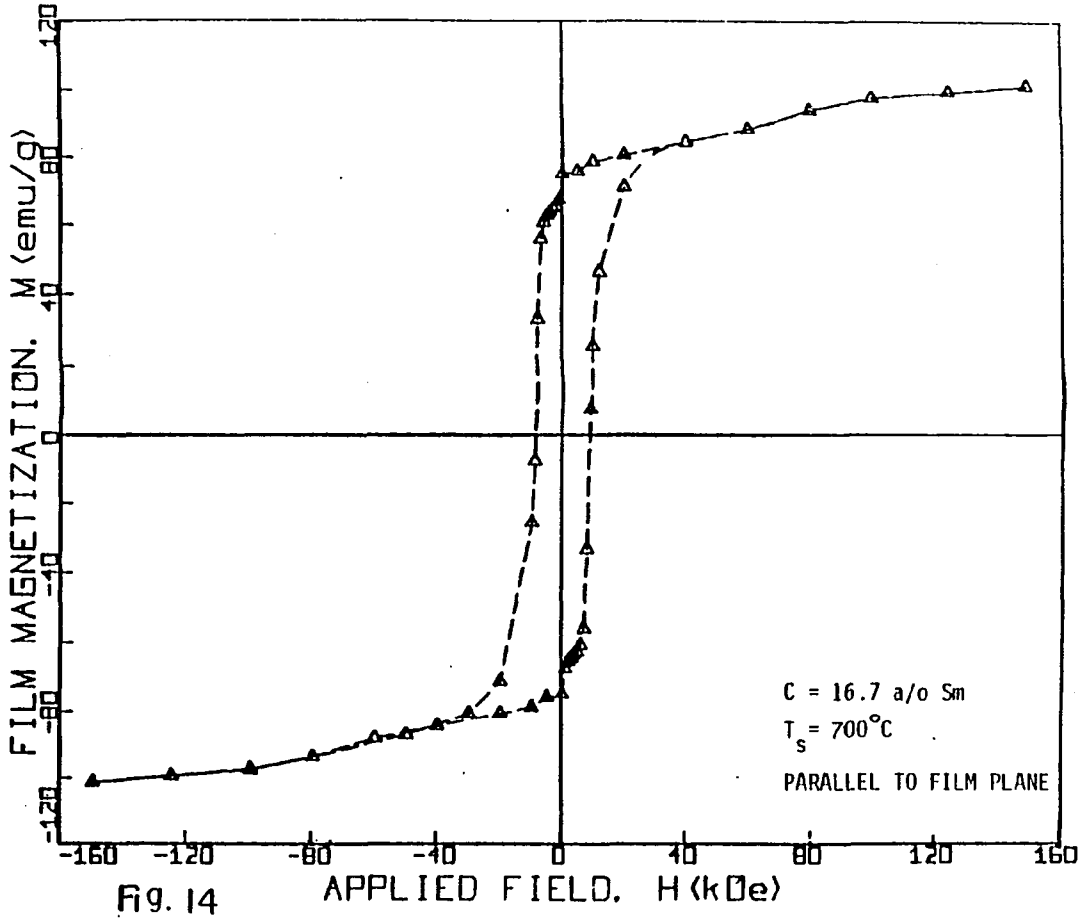
FILM MAGNETIZATION. M (emu/g)
120
80
40
0
-40
-80
-120
-160
-120
-80
-40
0
40
80
120
160
APPLIED FIELD. H (kOe)
C = 16.7 a/o Sm
T_s = 700°C
PARALLEL TO FILM PLANE

Fig. 14

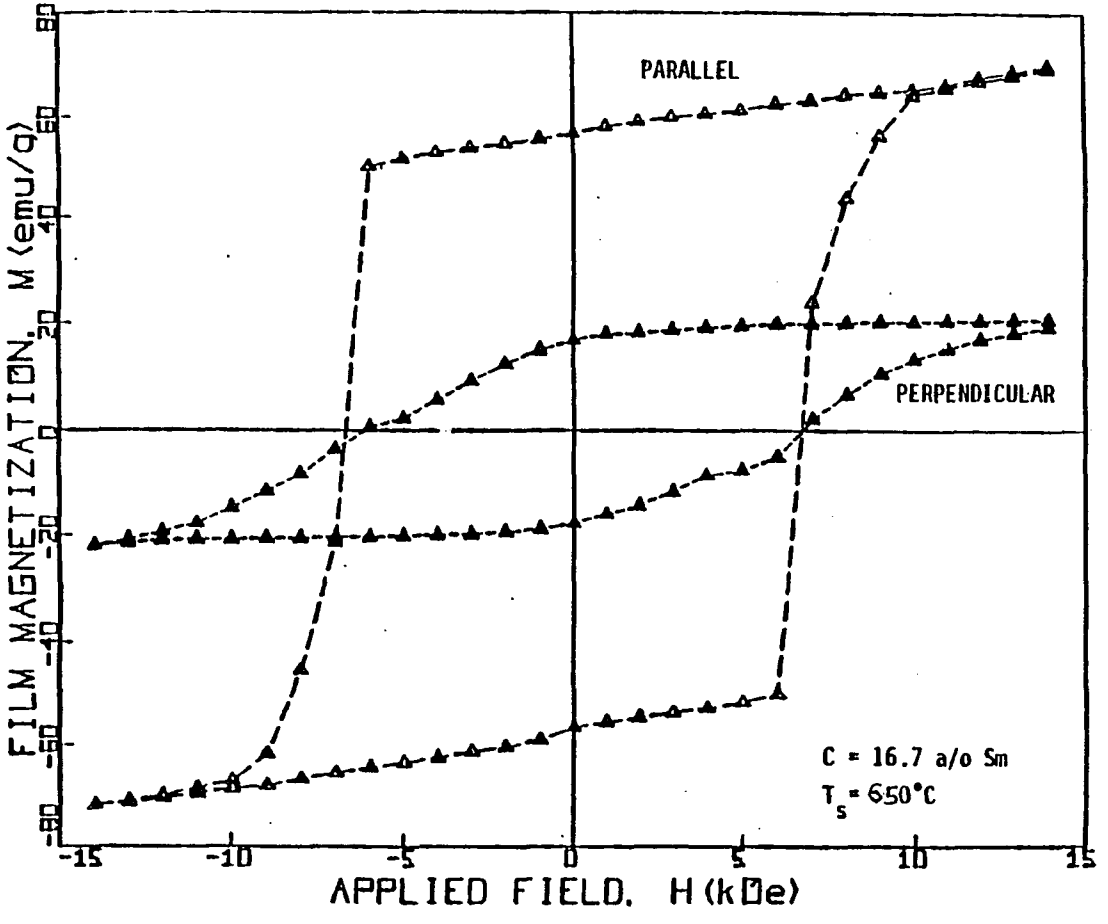
PARALLEL
PERPENDICULAR
C = 16.7 a/o Sm
T_s = 650°C
FILM MAGNETIZATION, M (emu/g)
APPLIED FIELD, H (kOe)
80
60
40
20
0
-20
-40
-60
-80
-15
-10
-5
0
5
10
15

Figure 15

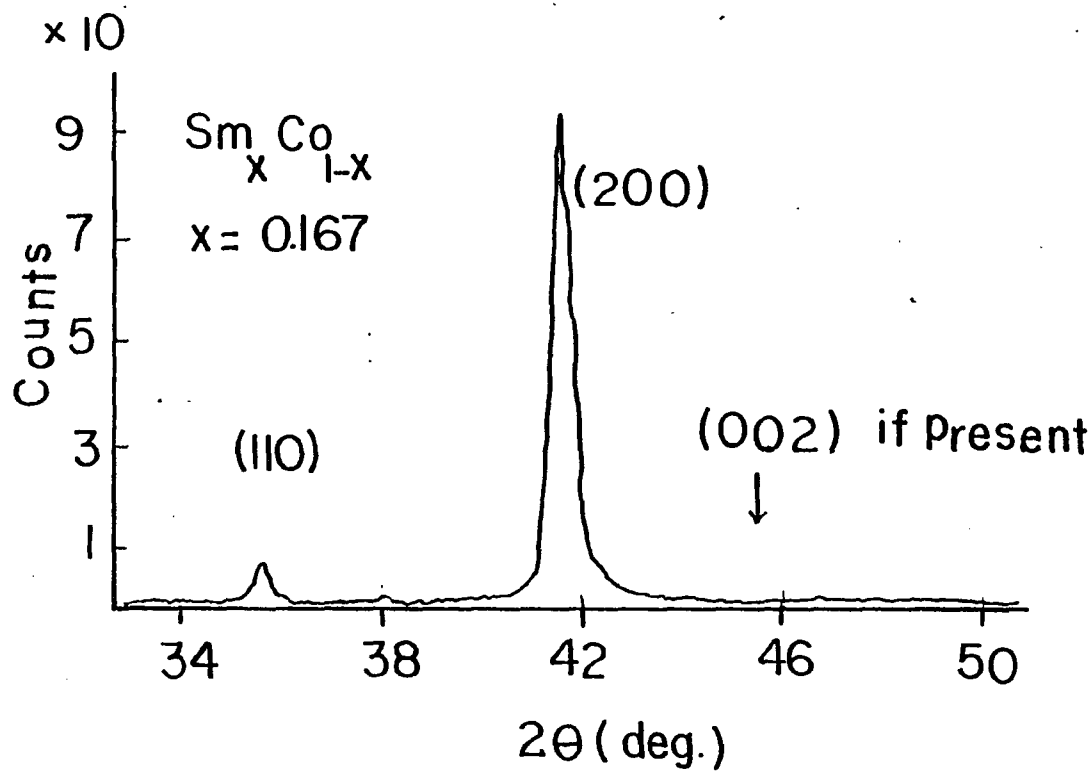
x 10
9
7
5
3
1
Counts
$Sm_x Co_{1-x}$
x = 0.167
(110)
(200)
(002) if Present
34
38
42
46
50
2θ (deg.)

Fig. 16

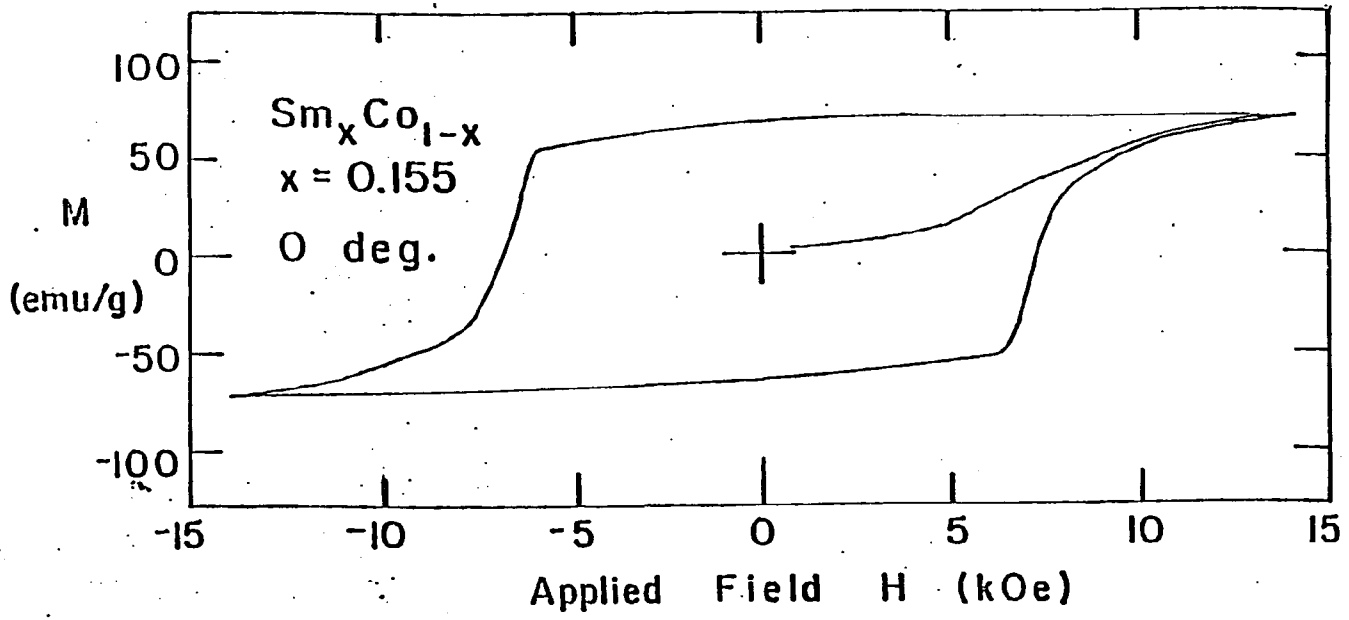
100
50
0
-50
-100
M
(emu/g)
Sm_xCo_{1-x}
x = 0.155
0 deg.
-15
-10
-5
0
5
10
15
Applied Field H (kOe)

Figure 17

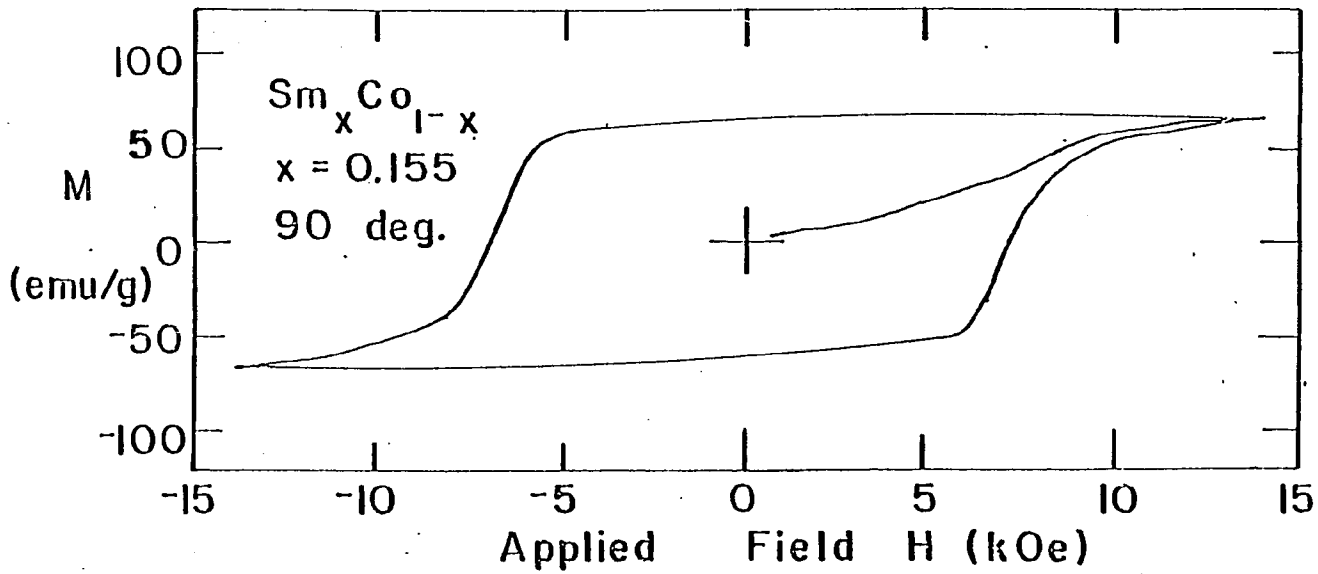
100
50
0
-50
-100
M
(emu/g)
Sm_xCo_{1-x}
x = 0.155
90 deg.
-15
-10
-5
0
5
10
15
Applied Field H (kOe)

Figure 18

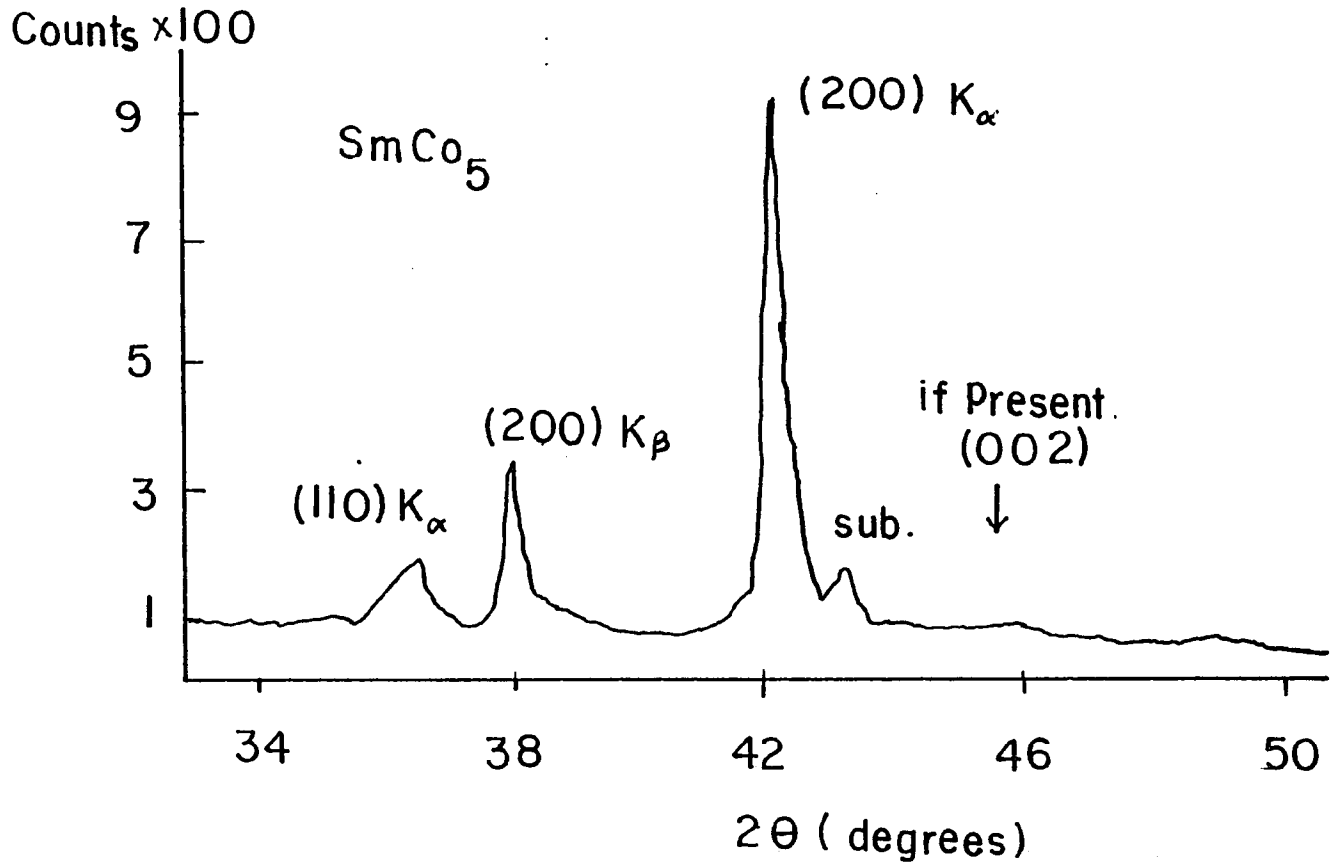
Counts x100
9
7
5
3
1
SmCo5
(200) Kα
(200) Kβ
(110) Kα
sub.
if Present
(002)
34
38
42
46
50
2θ (degrees)

Figure 19

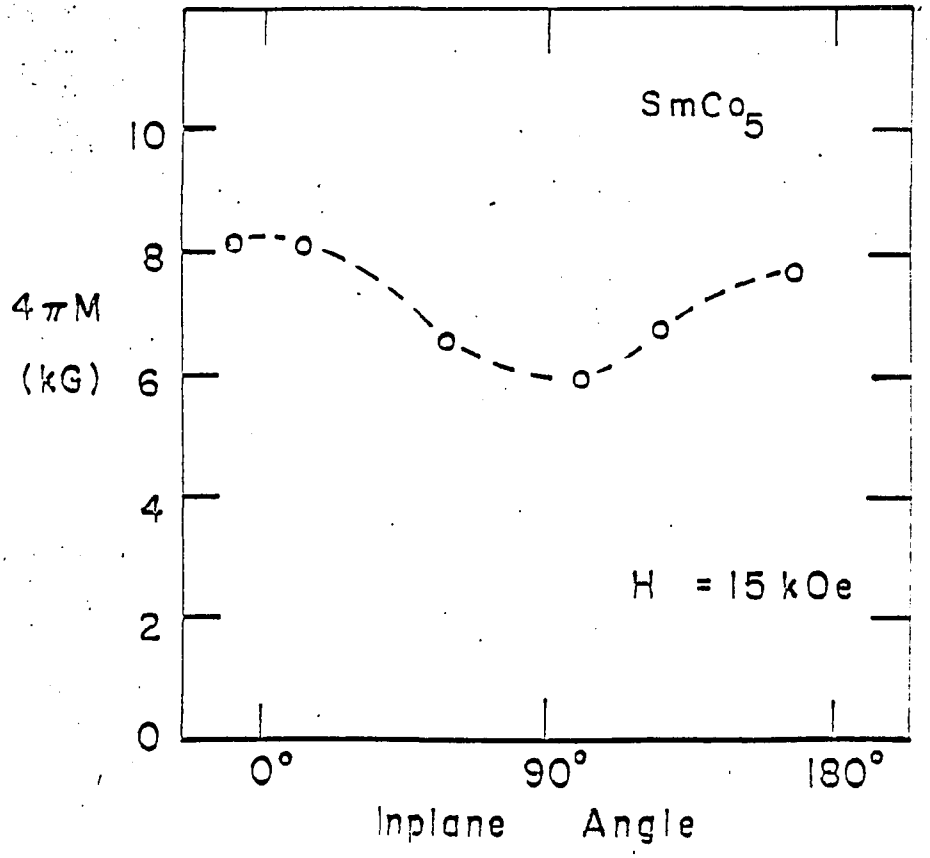

Fig.20

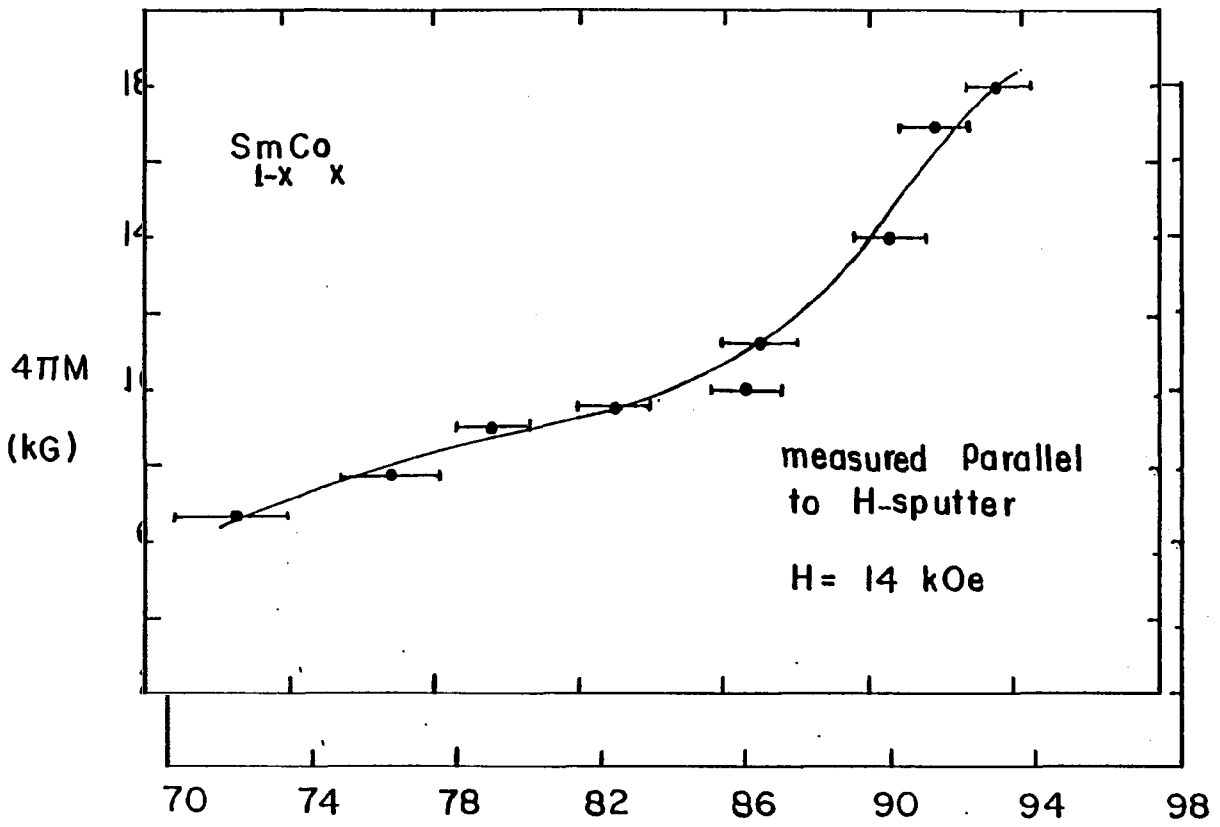
SmCo
1-x x
4πM
(kG)
measured Parallel
to H-sputter
H= 14 kOe
70
74
78
82
86
90
94
98
Co concentration (at%)

Fig.21

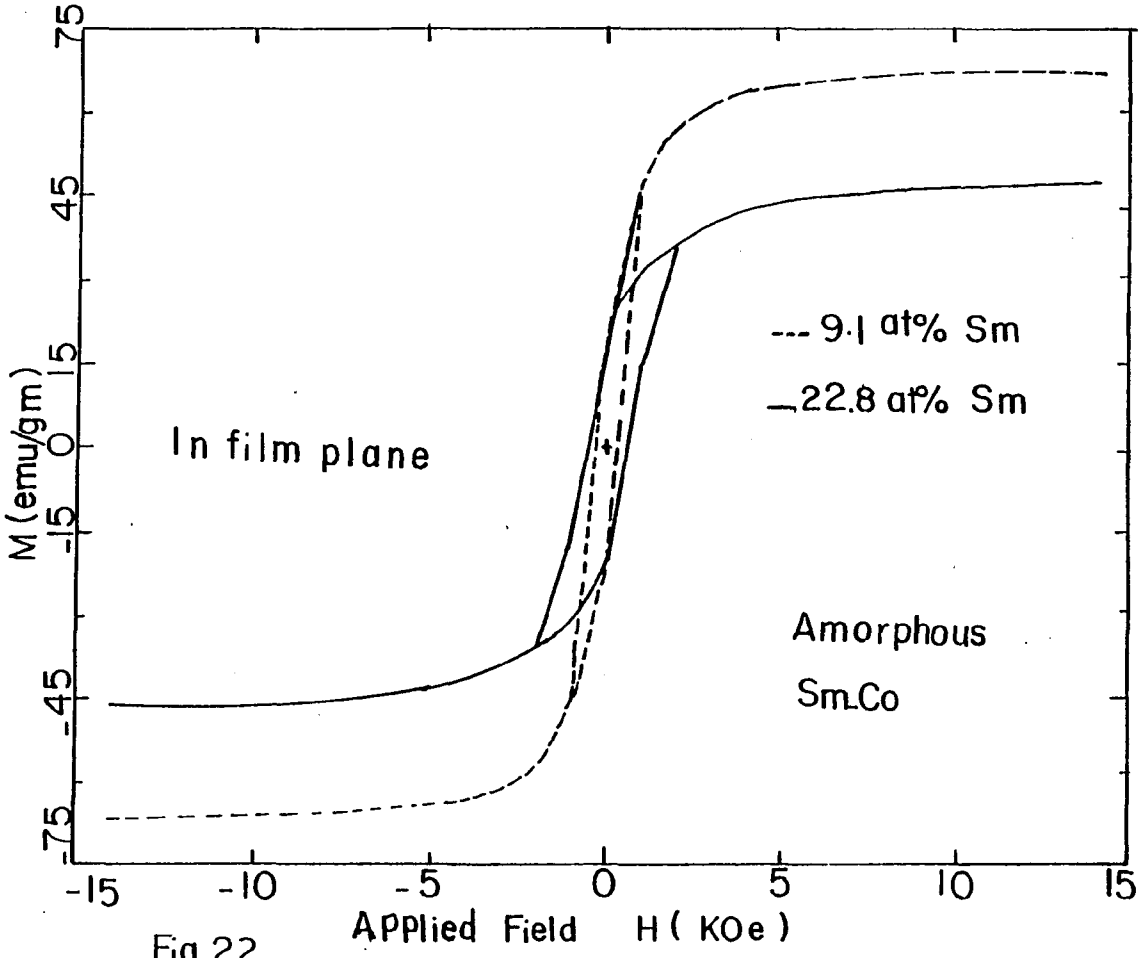
75
45
15
0
-15
-45
-75
M (emu/gm)
--- 9.1 at% Sm
_22.8 at% Sm
In film plane
Amorphous
Sm.Co
-15
-10
-5
0
5
10
15
Applied Field H (KOe)

Fig.22

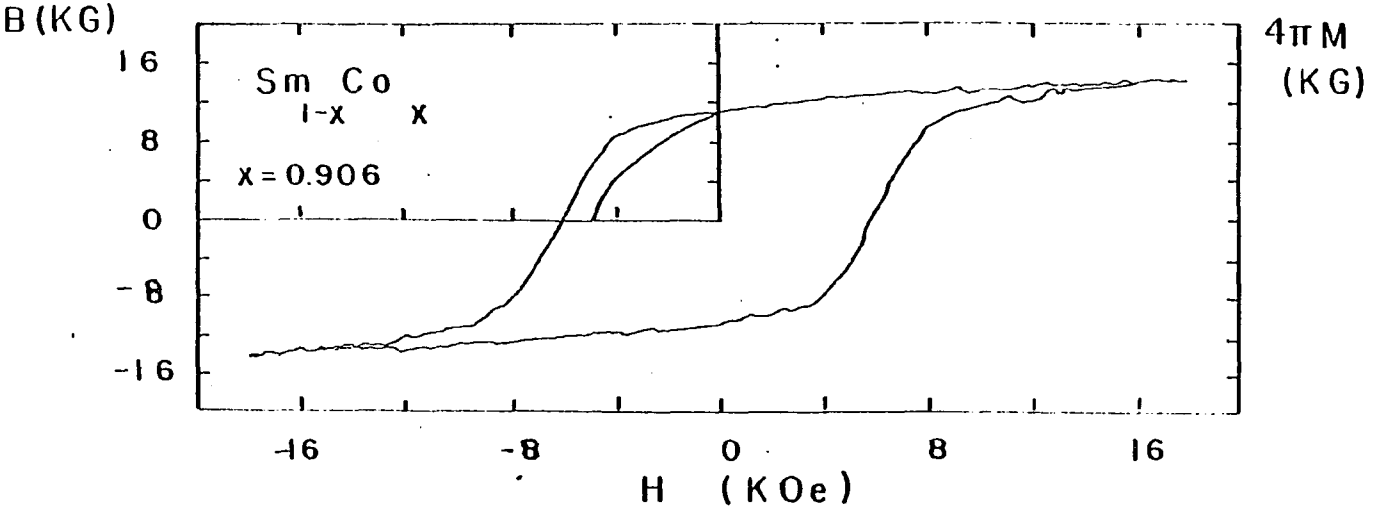

Fig. 23

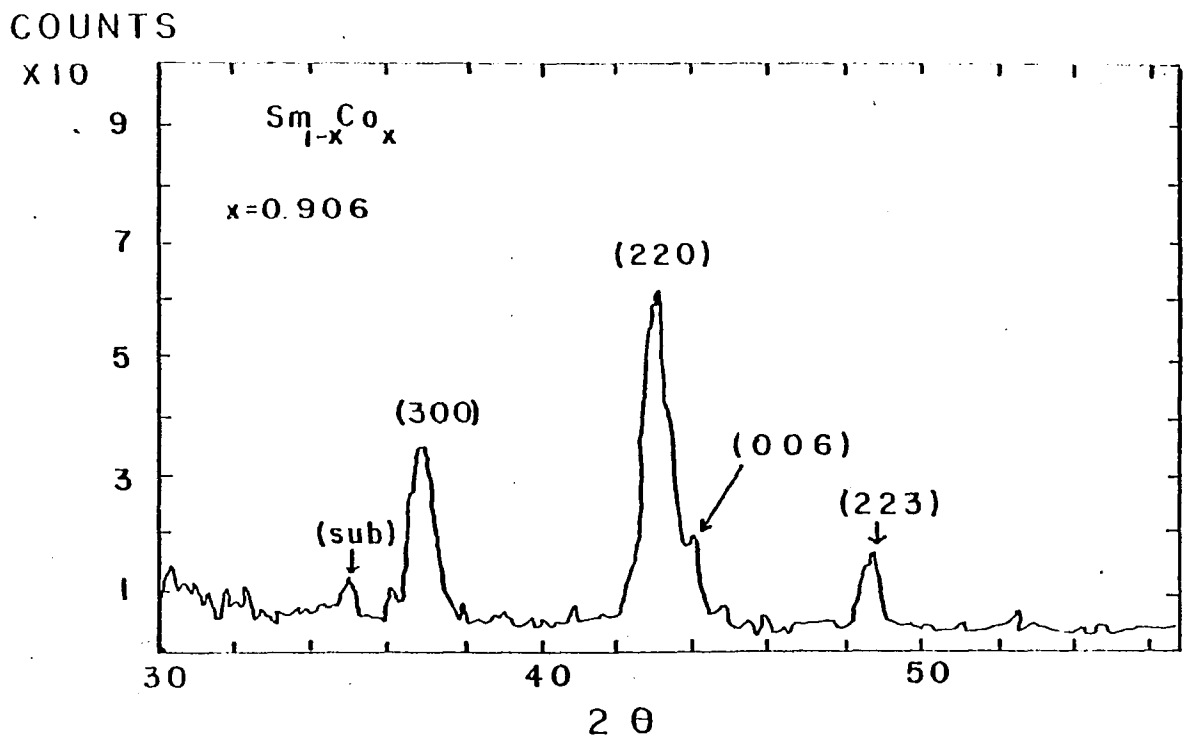

Figure 24

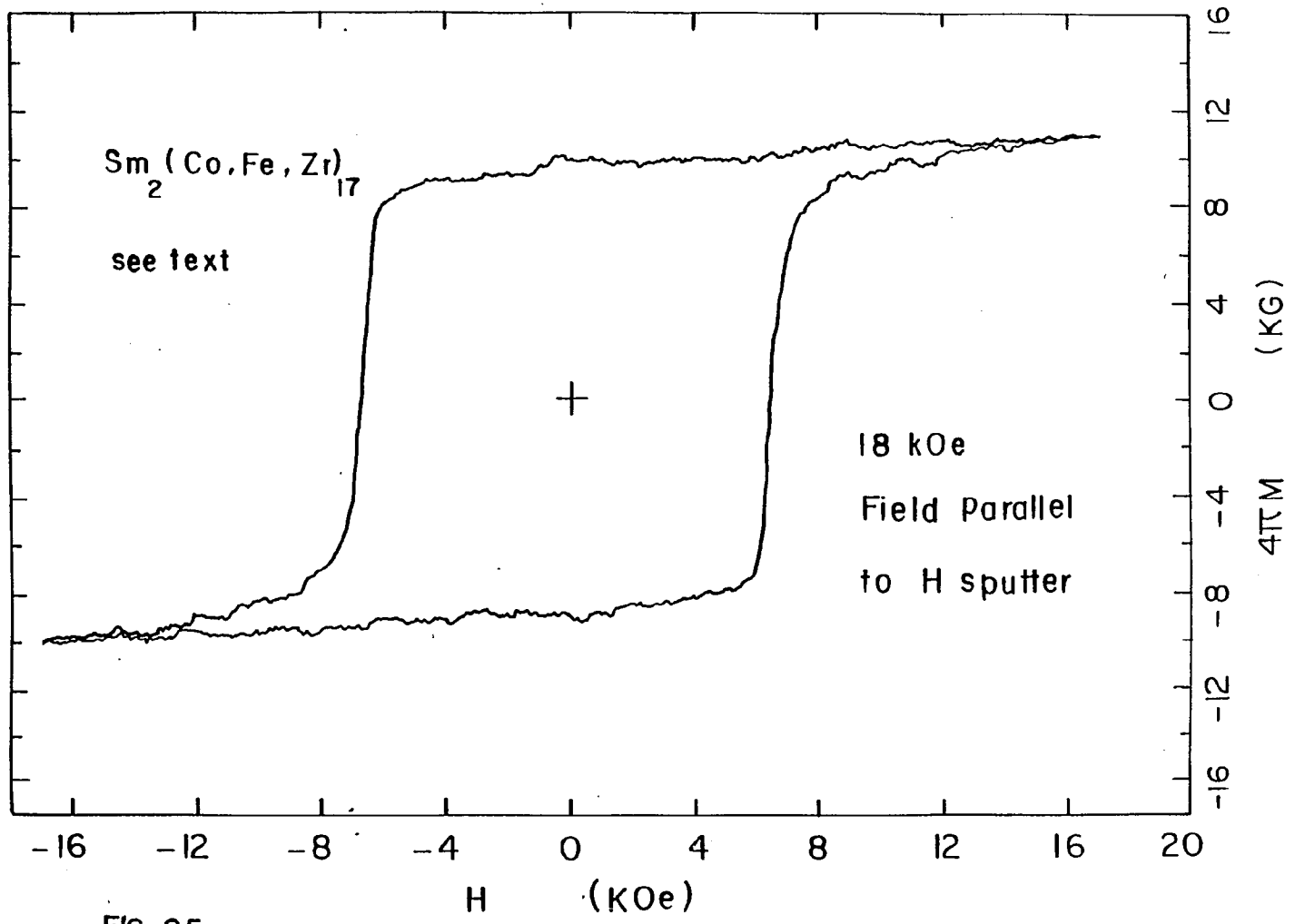
Sm2(Co,Fe,Zr)17
see text
18 kOe
Field Parallel
to H sputter
-16
-12
-8
-4
0
4
8
12
16
20
H (KOe)
16
12
8
4
0
-4
-8
-12
-16
4πM (KG)

FIG. 25

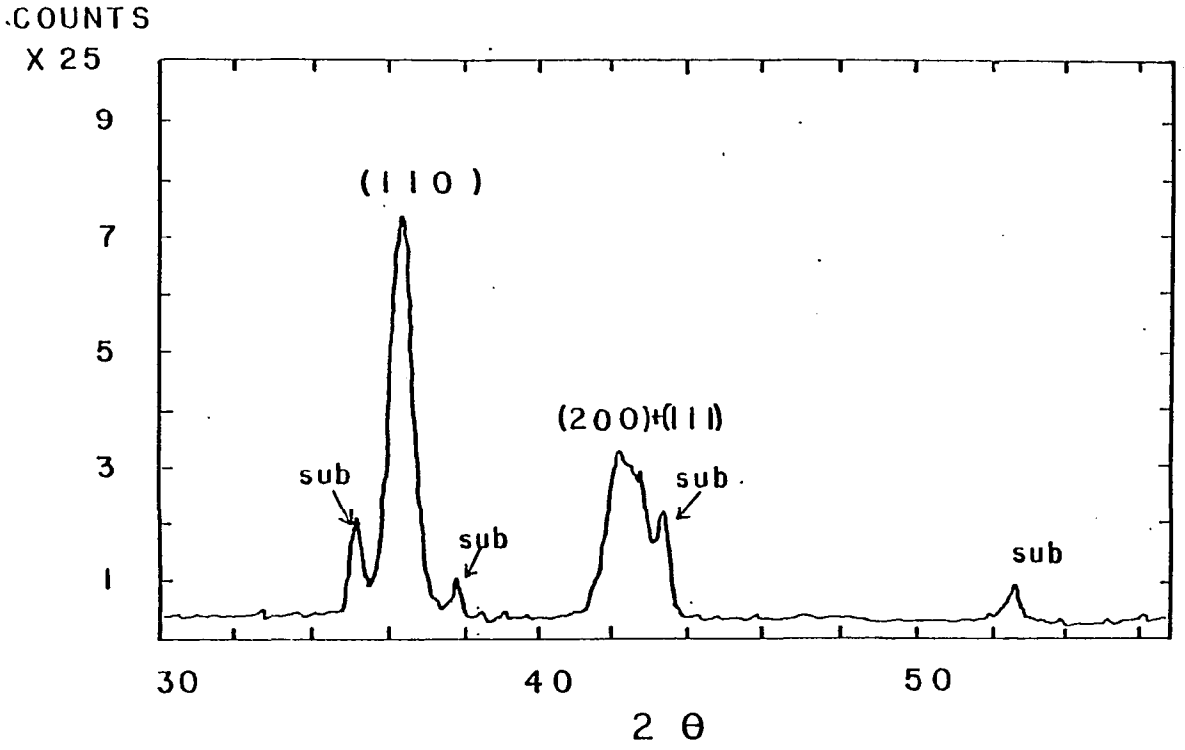

Figure 26

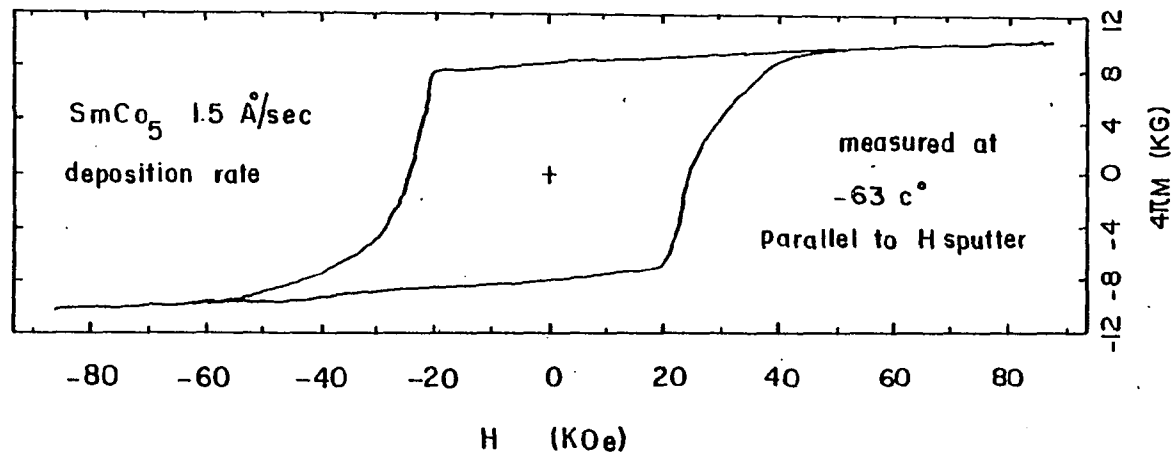
SmCo5 1.5 Å/sec
deposition rate
+
measured at
-63 c°
Parallel to H sputter
-80
-60
-40
-20
0
20
40
60
80
H (KOe)
-12
-8
-4
0
4
8
12
4πM (KG)

Fig. 27

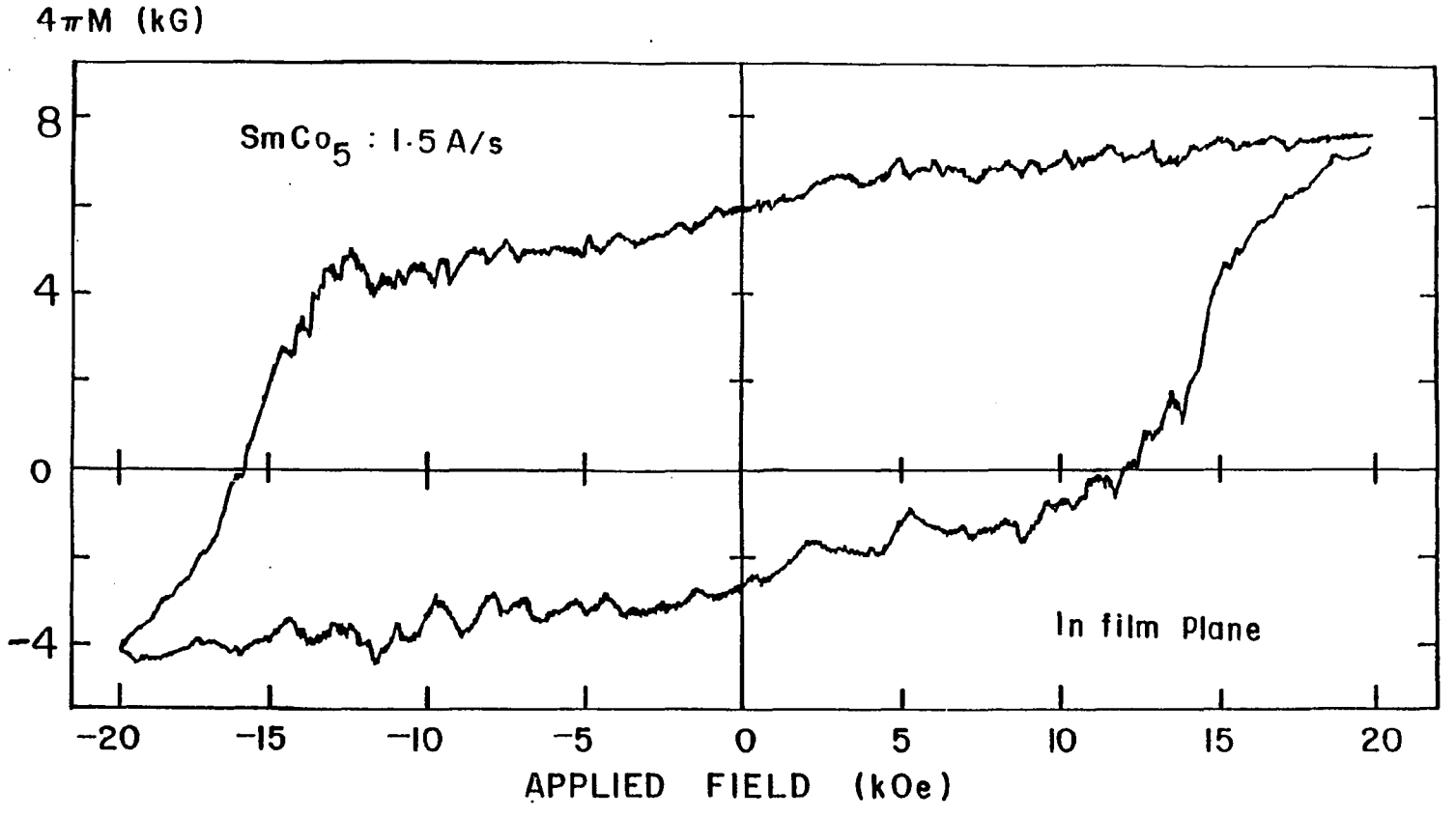
4πM (kG)
8
4
0
-4
SmCo5 : 1·5 A/s
In film Plane
-20
-15
-10
-5
0
5
10
15
20
APPLIED FIELD (kOe)

Fig. 28

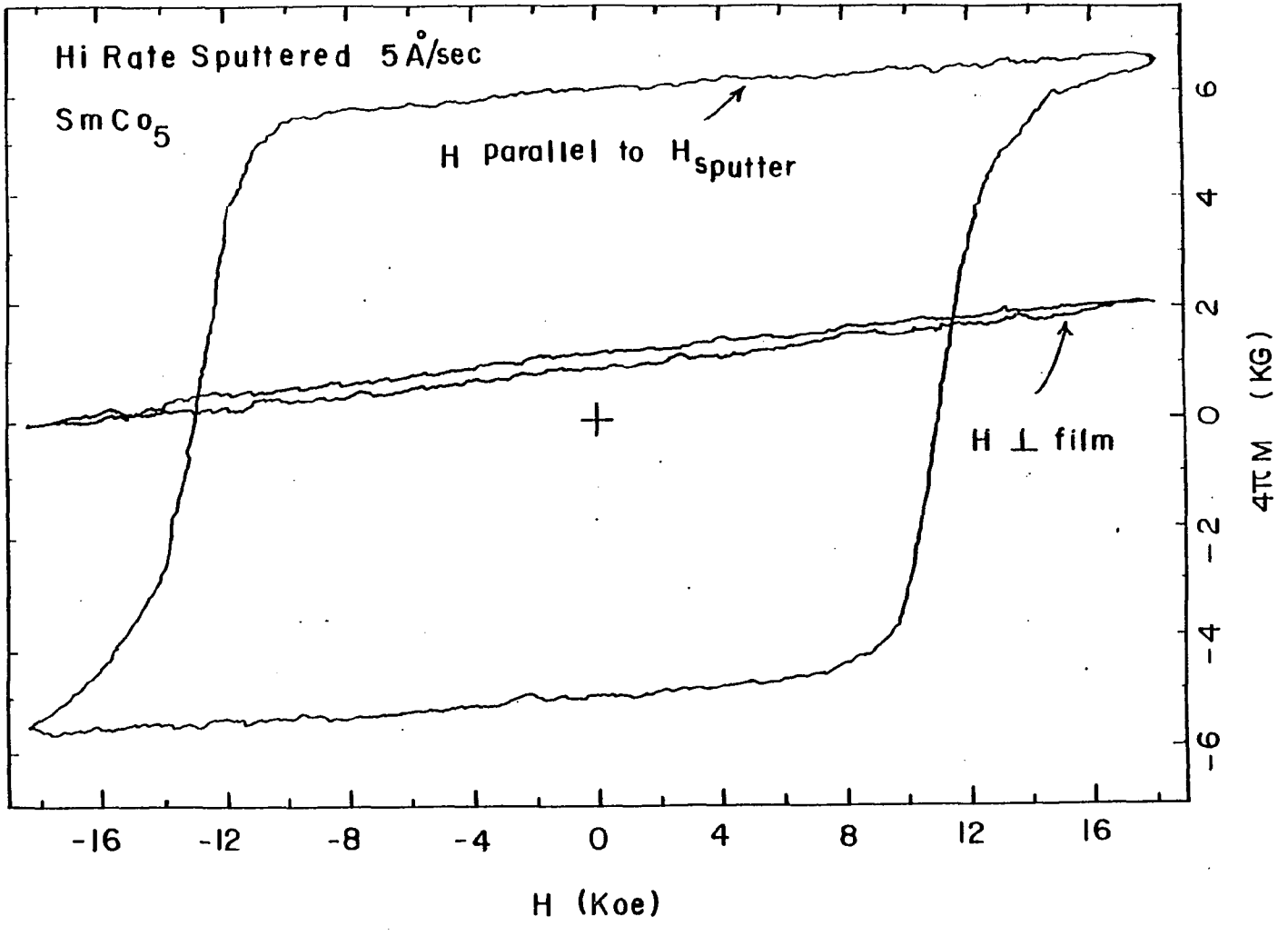
Hi Rate Sputtered 5 Å/sec
SmCo5
H parallel to Hsputter
H ⊥ film
-16
-12
-8
-4
0
4
8
12
16
H (Koe)
6
4
2
0
-2
-4
-6
4π M (KG)

Figure 29

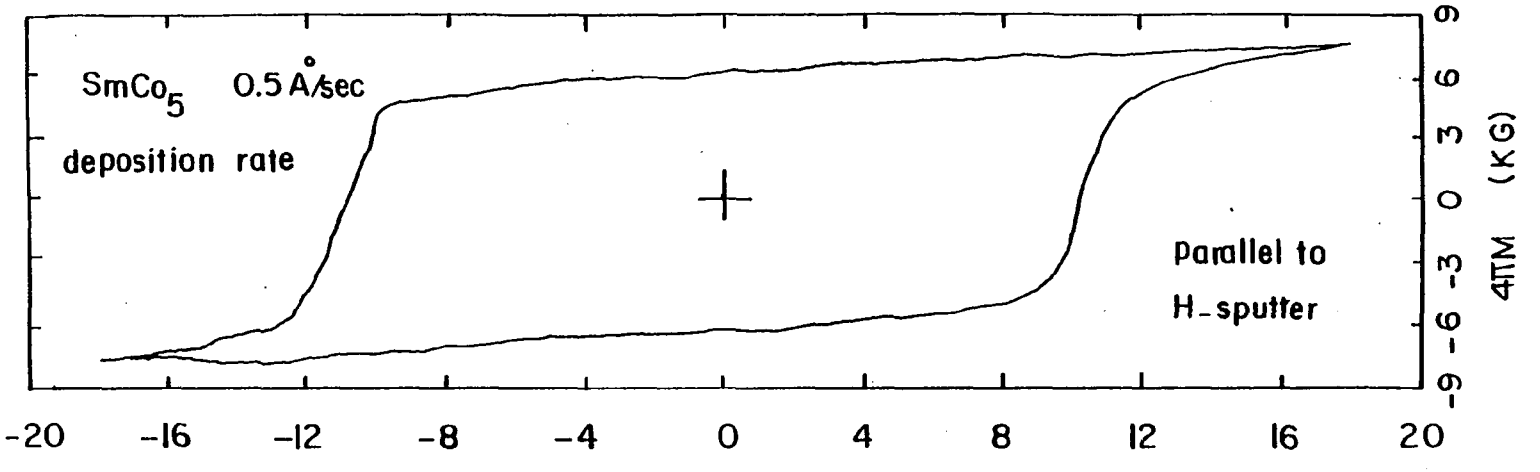
SmCo5 0.5 Å/sec
deposition rate
Parallel to
H-sputter
-20
-16
-12
-8
-4
0
4
8
12
16
20
9
6
3
0
-3
-6
-9
4πM (KG)
H (KOe)

FIG. 30

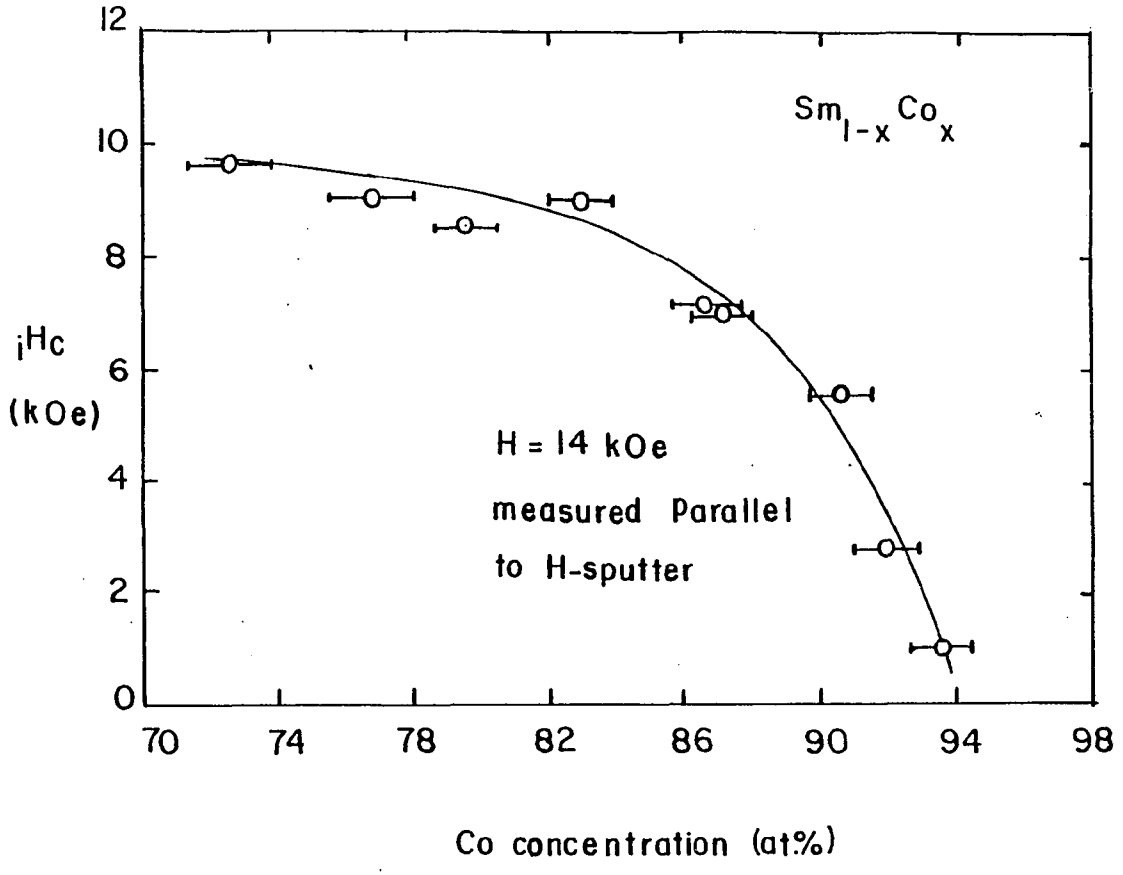
12
10
8
6
4
2
0
iHc
(kOe)
Sm1-xCox
H = 14 kOe
measured Parallel
to H-sputter
70
74
78
82
86
90
94
98
Co concentration (at%)

Fig. 31

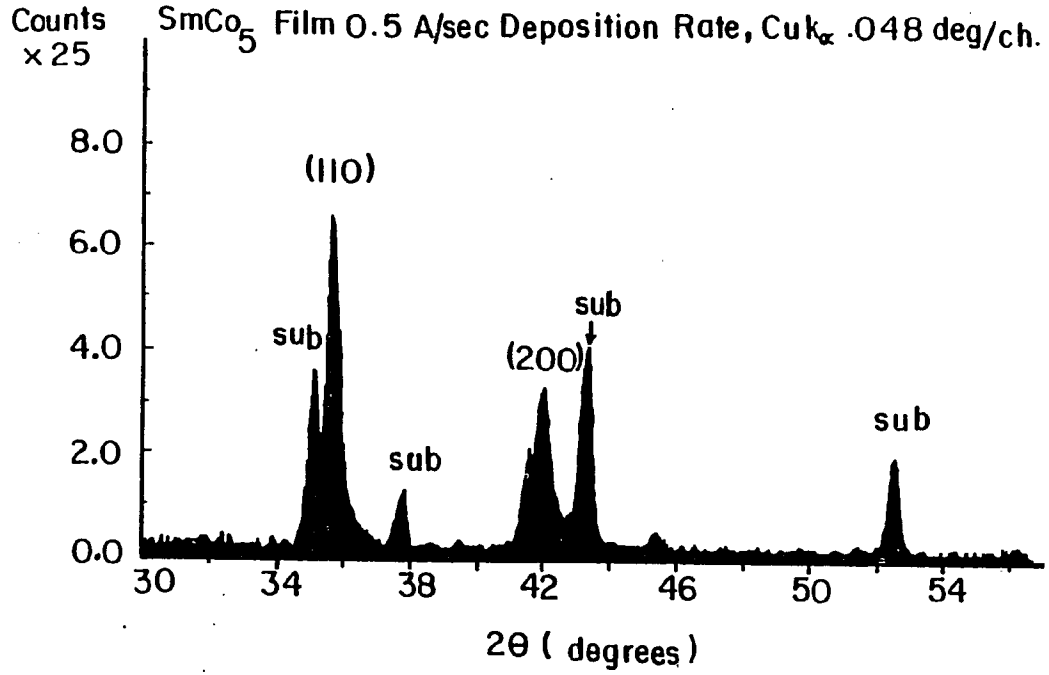
Counts
×25
SmCo5 Film 0.5 A/sec Deposition Rate, Cuk∝ .048 deg/ch.
8.0
6.0
4.0
2.0
0.0
(110)
sub
sub
(200)
sub
sub
30
34
38
42
46
50
54
2θ (degrees)

FIG. 32

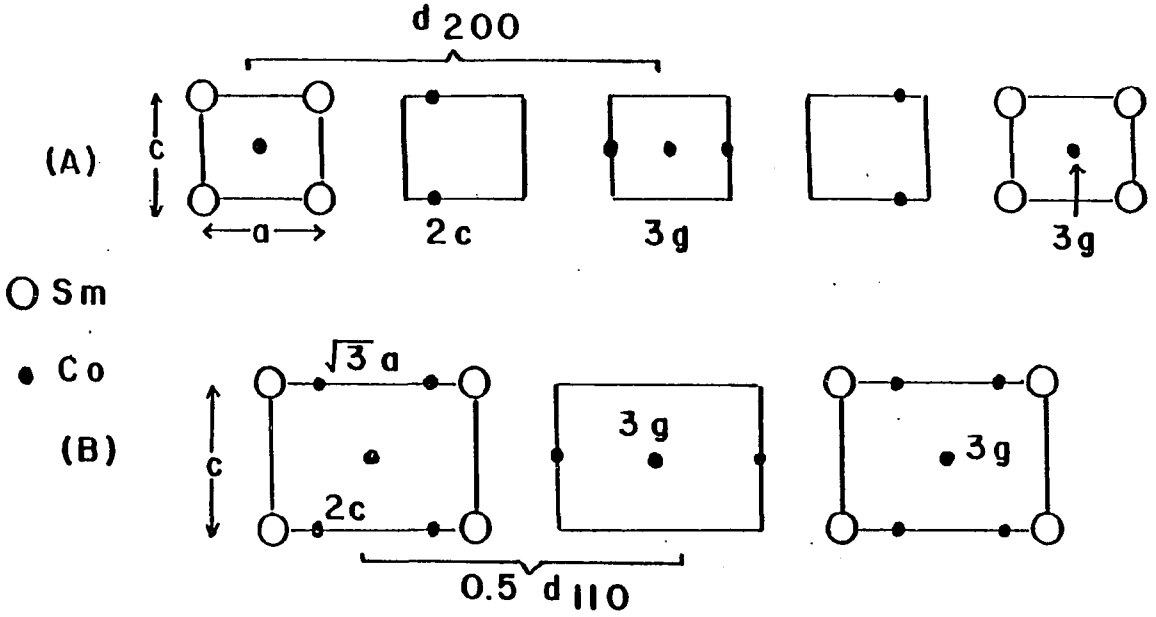

(A) 200
(B) 110
} stacking sequence of $SmCo_5$

Figure 33

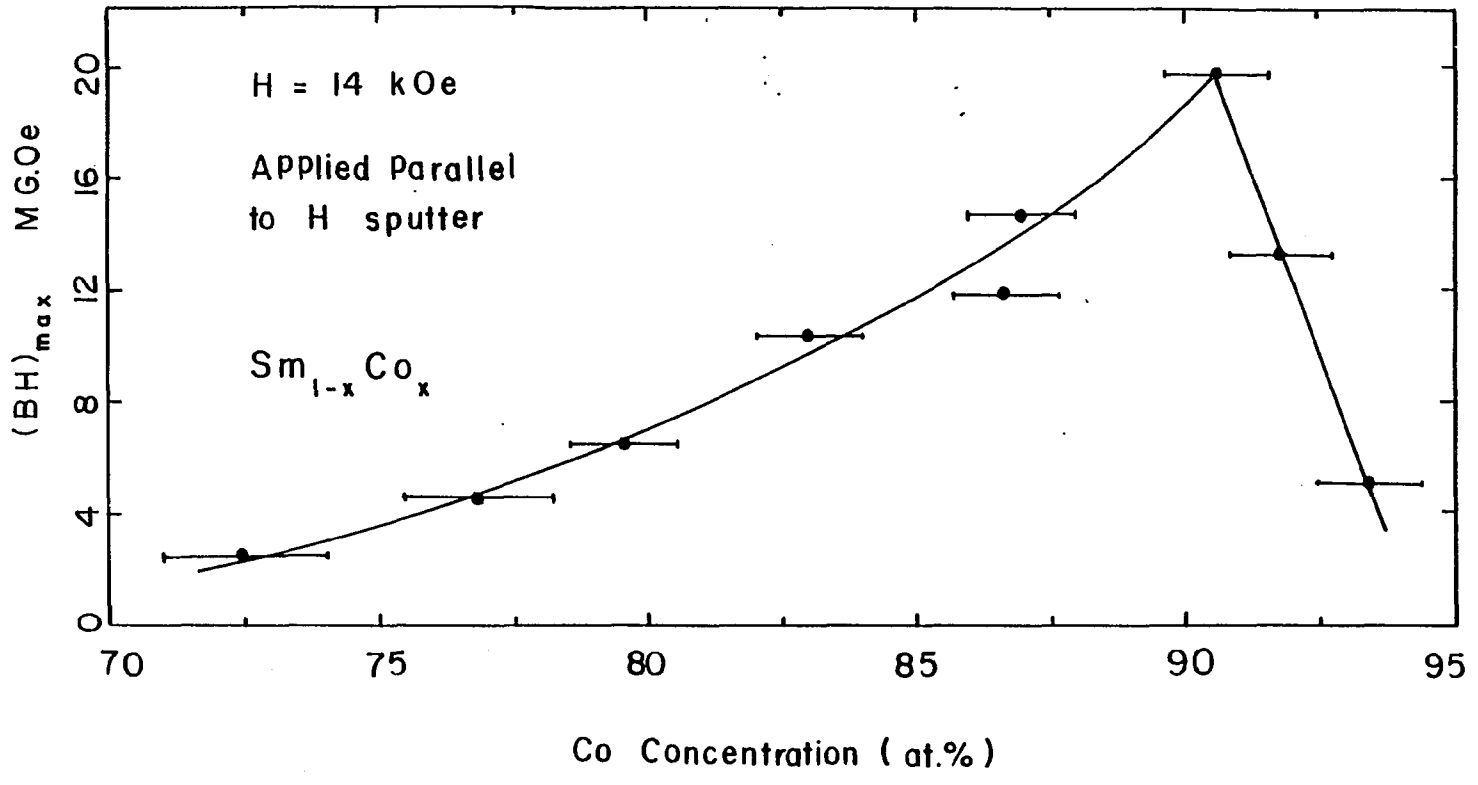
H = 14 kOe
APPlied Parallel
to H sputter
$Sm_{1-x}Co_x$
$(BH)_{max}$ MG.Oe
0
4
8
12
16
20
70
75
80
85
90
95
Co Concentration (at.%)

Fig.34

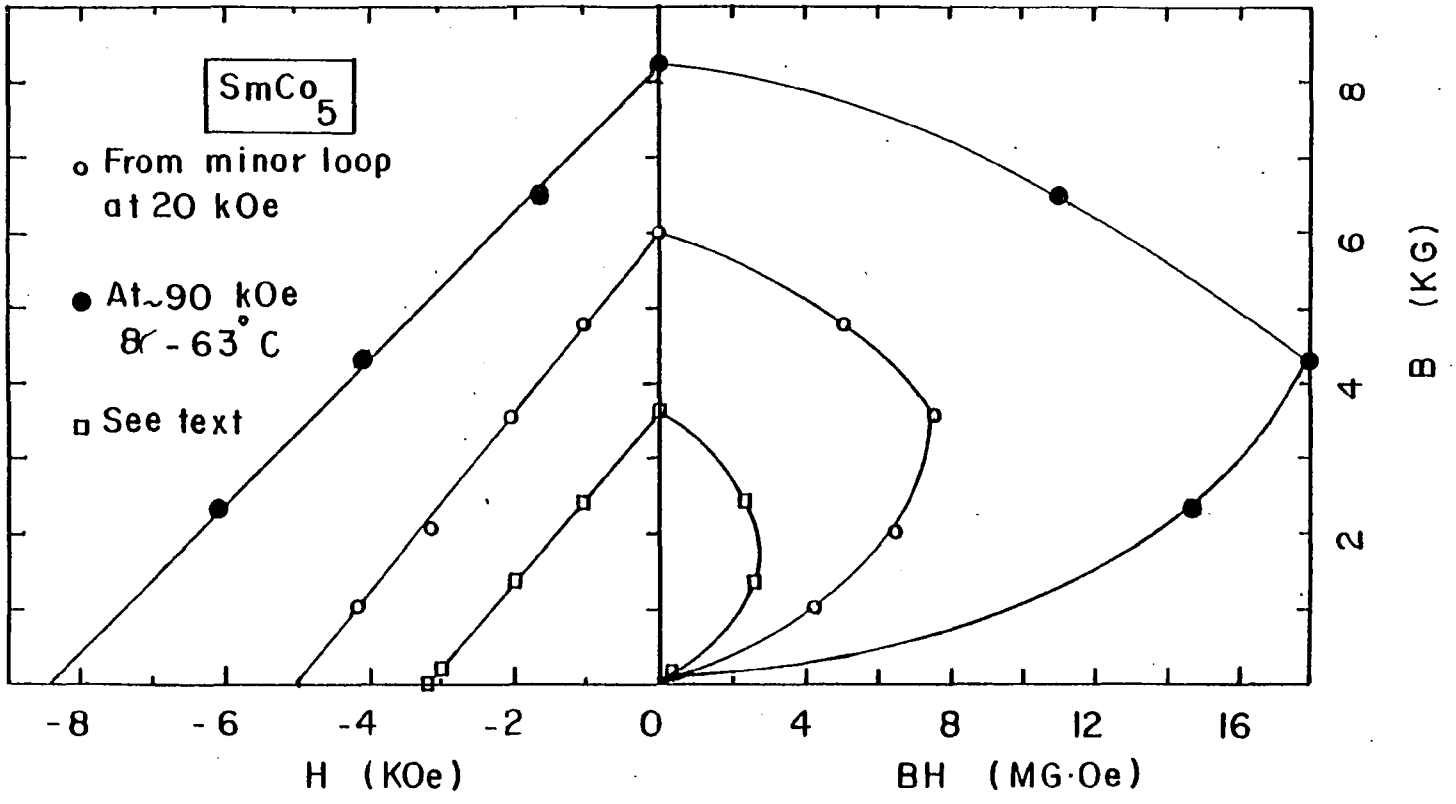
SmCo5
o From minor loop at 20 kOe
● At~90 kOe 8r - 63° C
□ See text
-8
-6
-4
-2
0
4
8
12
16
H (KOe)
BH (MG·Oe)
2
4
6
8
B (KG)

Figure 35

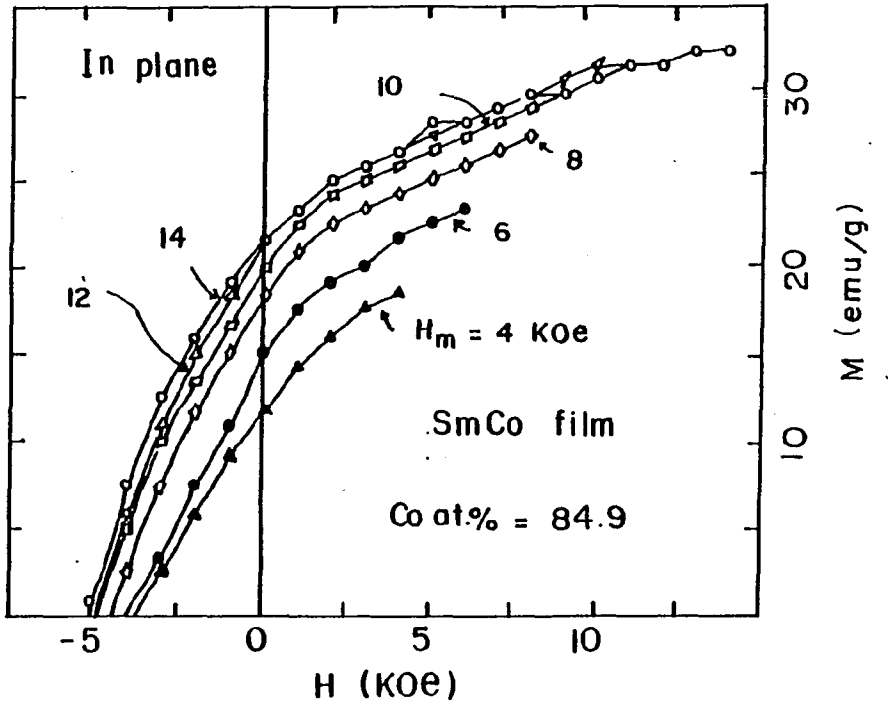
In plane
10
8
6
14
12
H_m = 4 KOe
SmCo film
Co at.% = 84.9
-5
0
5
10
H (KOe)
10
20
30
M (emu/g)

Figure 36

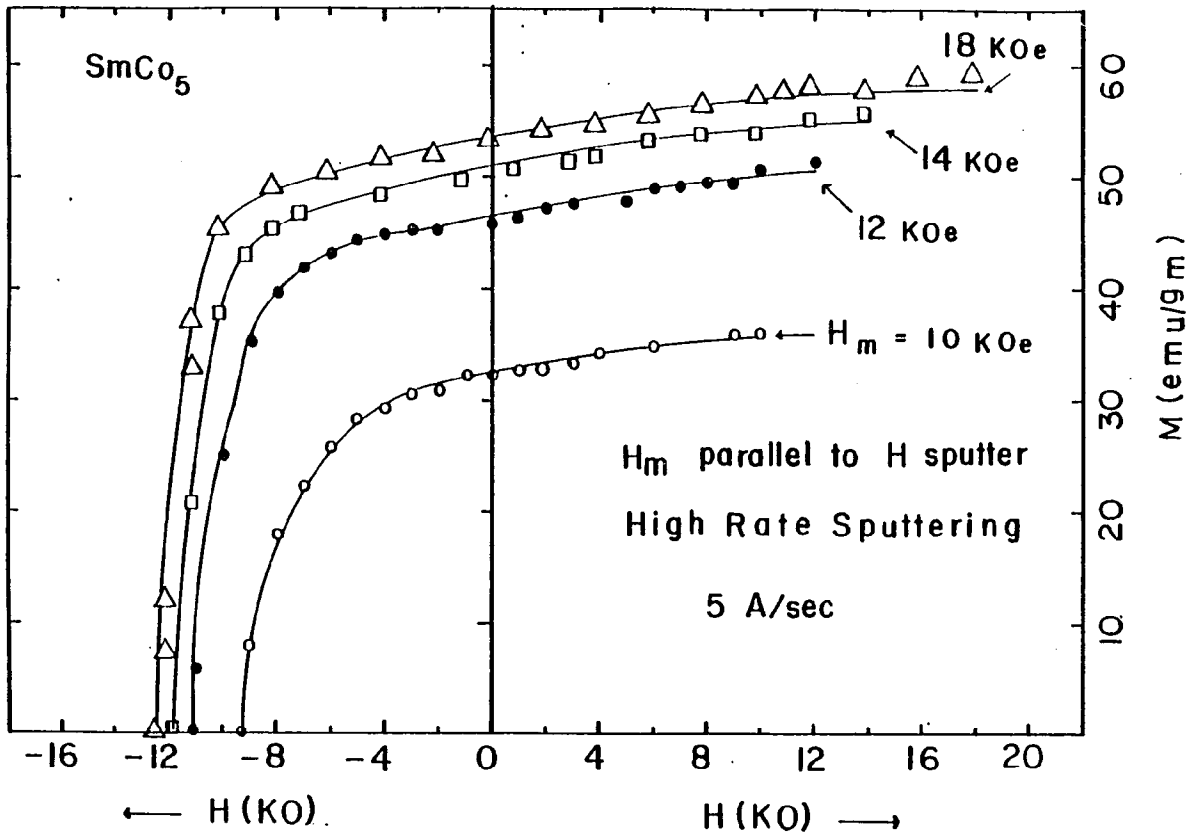
SmCo5
18 KOe
14 KOe
12 KOe
Hm = 10 KOe
Hm parallel to H sputter
High Rate Sputtering
5 A/sec
M (emu/gm)
10
20
30
40
50
60
-16
-12
-8
-4
0
4
8
12
16
20
← H (KO)
H (KO) →

Figure 37

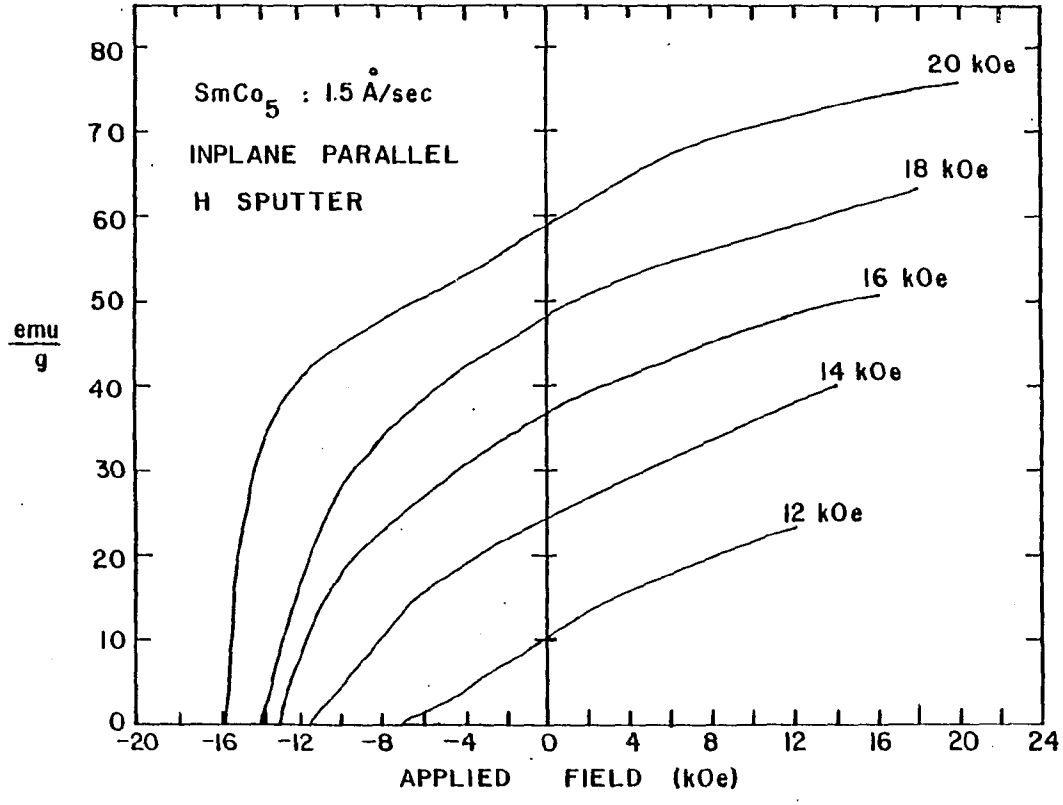
SmCo5 : 1.5 Å/sec
INPLANE PARALLEL
H SPUTTER
20 kOe
18 kOe
16 kOe
14 kOe
12 kOe
emu/g
80
70
60
50
40
30
20
10
0
-20
-16
-12
-8
-4
0
4
8
12
16
20
24
APPLIED FIELD (kOe)

Fig.38

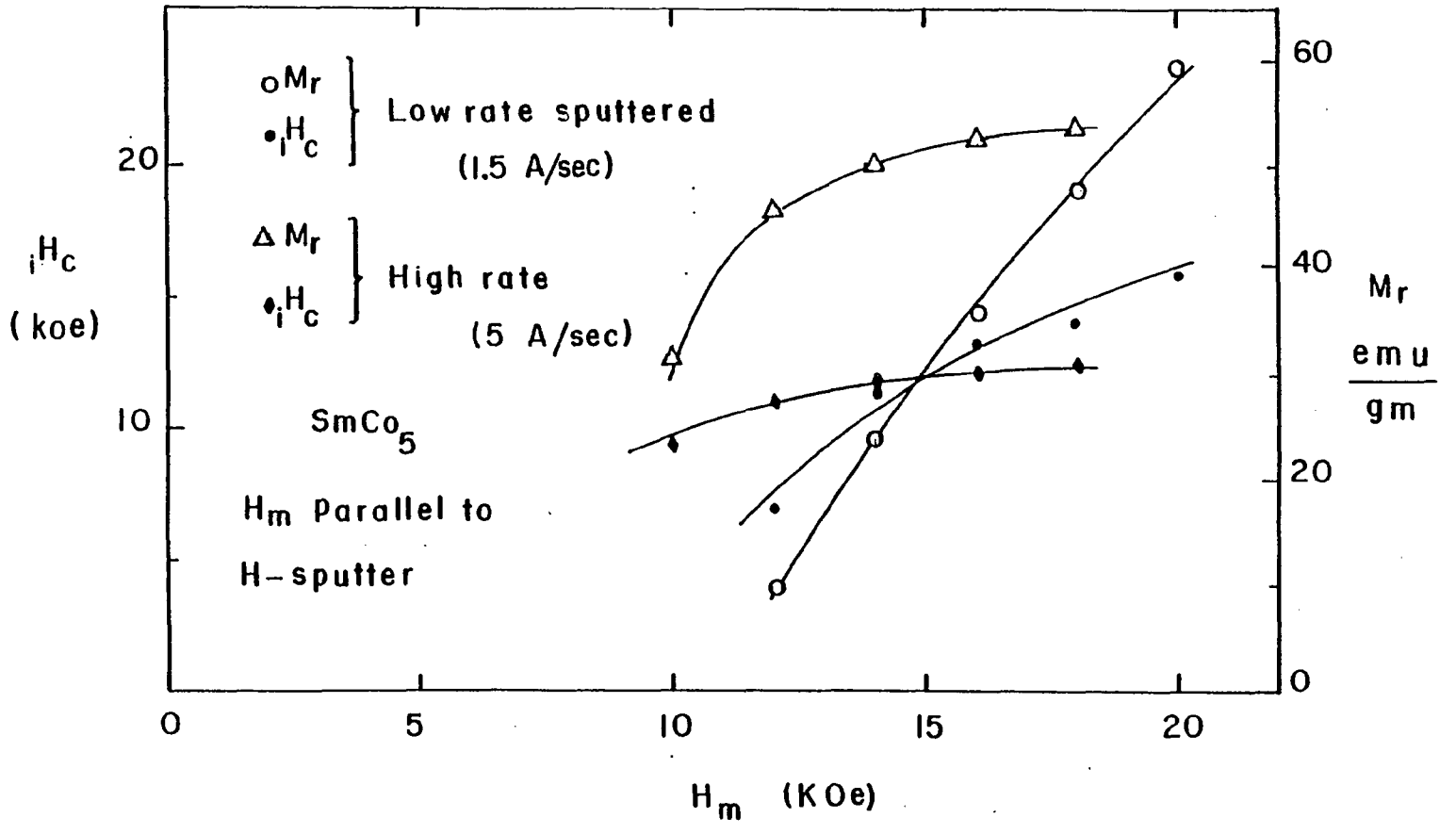
oMr
•iHc
Low rate sputtered
(1.5 A/sec)
ΔMr
•iHc
High rate
(5 A/sec)
SmCo5
Hm Parallel to
H-sputter
iHc
(koe)
Mr
emu
gm
Hm (KOe)
0
5
10
15
20
60
40
20
0

FIG. 39

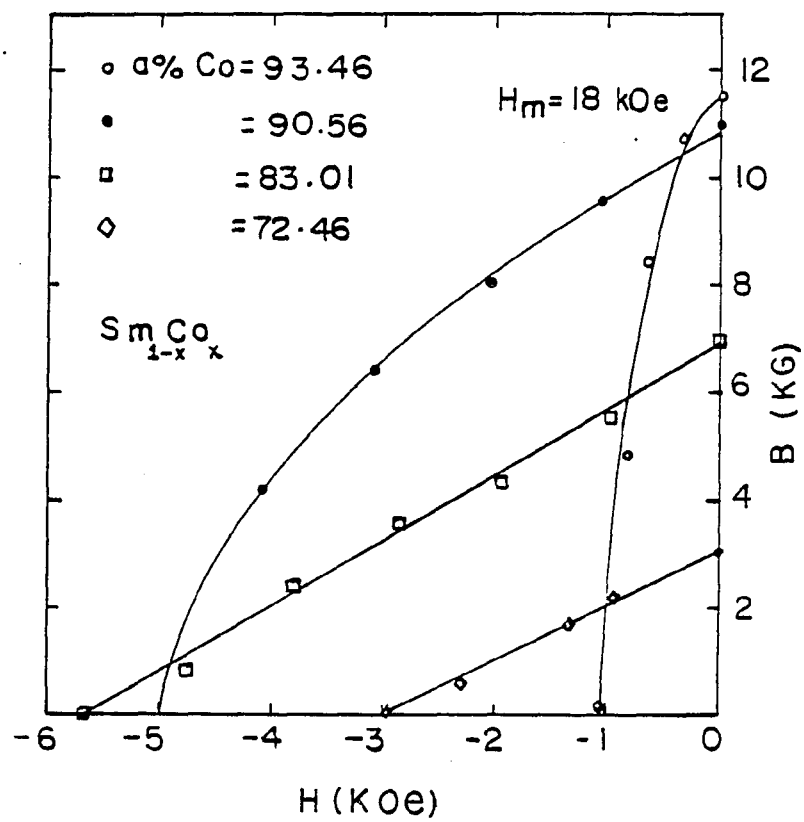
o a% Co = 93.46
• = 90.56
□ = 83.01
◇ = 72.46
Hm = 18 kOe
Sm1-xCox
12
10
8
6
4
2
B (KG)
-6
-5
-4
-3
-2
-1
0
H (KOe)

Figure 40

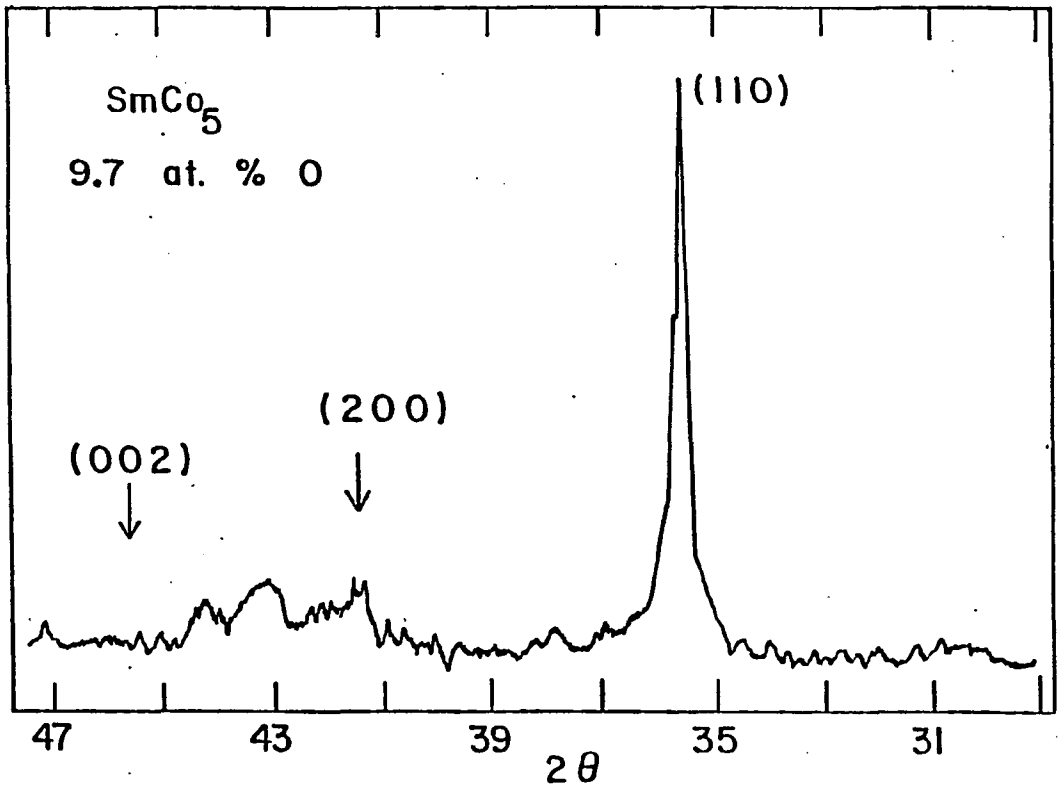

Fig. 41

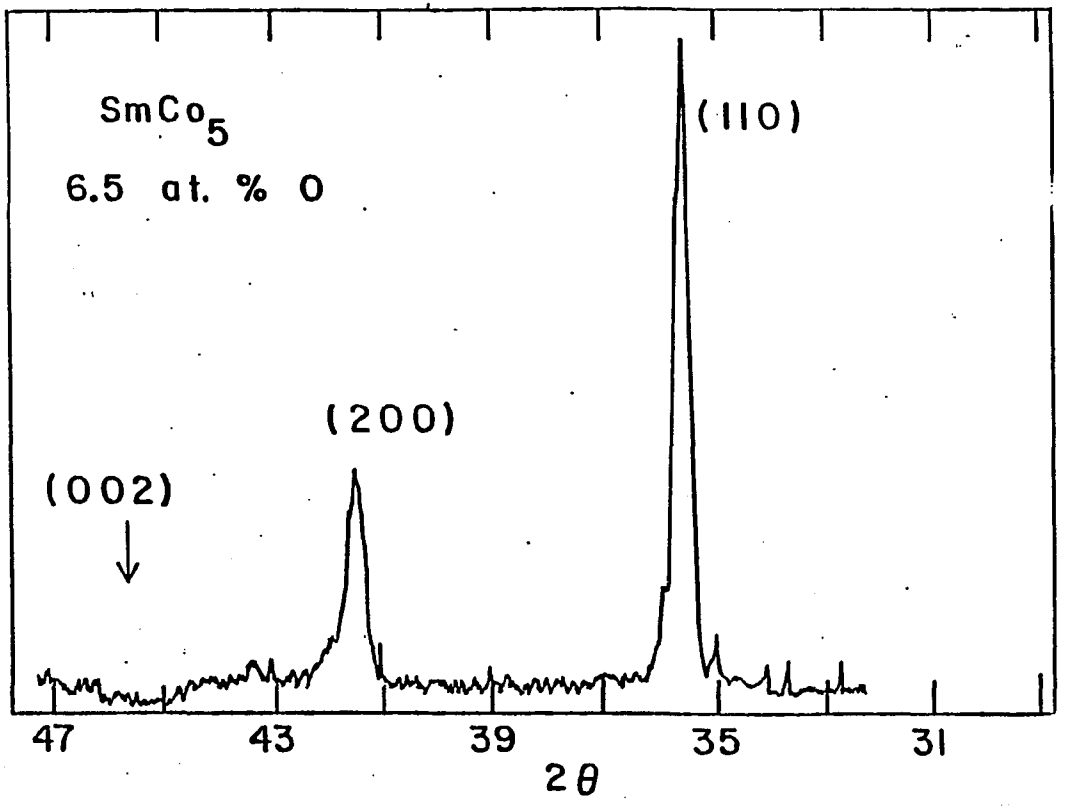

Fig. 42

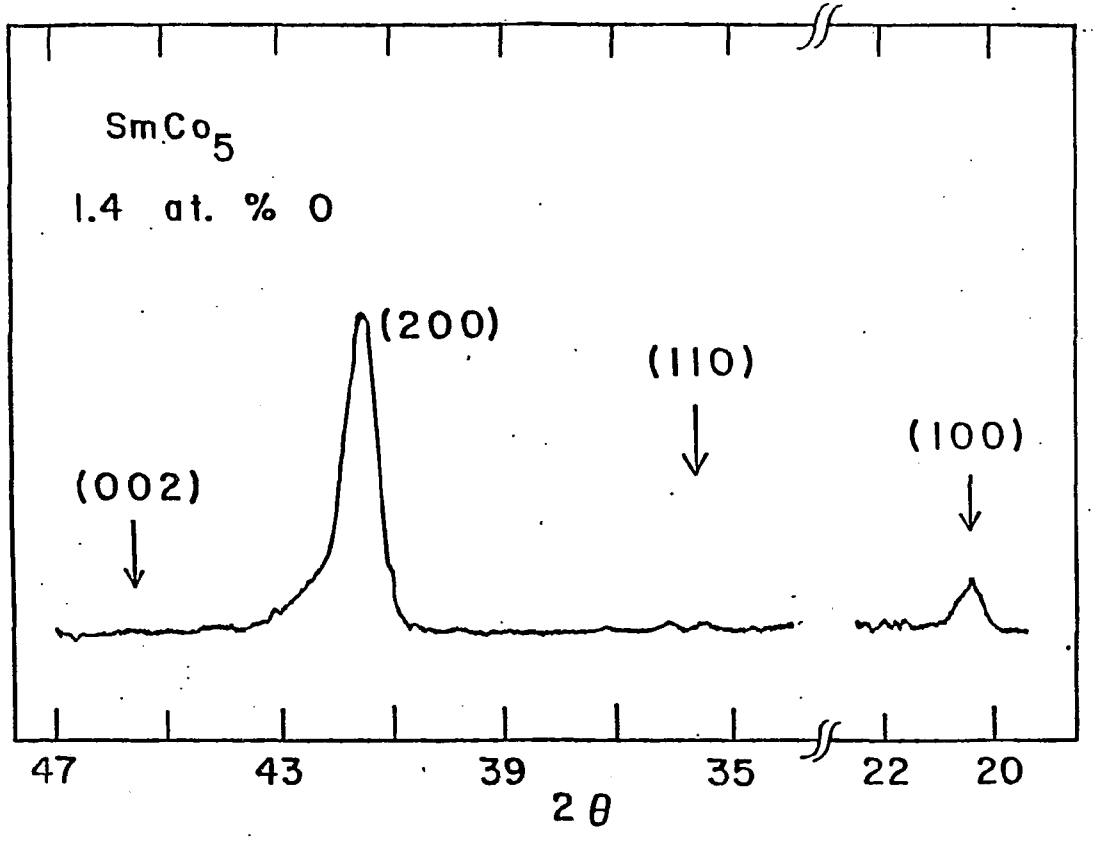

Fig 43

REFERENCES

1) E. N. Nesbitt and J. H. Wernick, Rare Earth Permanent Magnets, Academic Press, (1973).

2) R. J. Elliot, Magnetic Properties of Rare Earth Metals, Plenum Press, N.Y., 1972.

3) R. M. White and T. H. Geballe, Long Range Order in Solids, Solid State Physics Supplement 15, Academic Press (1979).

4) D. H. Martin, Magnetism in Solids, London (1967).

5) K. N. Taylor, Advances in Physics 20, 551, (1971).

6) B. J. Buschow, Report in Progress on Physics, 40, 1179 (1977).

7) S. K. Malik, F. Arlinghaus and W. E. Wallace, Physics Review B, 16, 1242 (1977).

8) S. K. Malik, R. Vijayaraghavan and W. E. Wallace, Physical Review B, 19, 1671 (1979).

9) S. G. Sankar et al. Physical Review B, 11, 435 (1975).

10) W. E. Wallace, Prog. Rare Earth Sci. Tech, 3, 1 (1968).

11) I. A. Campbell, J. Phys. F: Metal Phys. 2L, 47 (1972).

12) W. E. Wallace, Rare Earth Intermetallic, Academic Press, N.Y. (1973).

13) J. E. Greeden and V. U. S. Rao, J. Solid State Chem, 6, 387 (1973).

14) E. C. Stoner, Proc. Royal Soc. A, 165, 372 (1938).

15) K. J. H. Buschow, Phys. Status Solidi. A, 7, 199 (1971).

16) E. Burzo, D. P. Lazar and M. Ciorascu, Phys. Status Solidi B, 65K, 145 (1974).

17) H. P. Klein, A. Menth and R. S. Perkins, Physica 80B, 153 (1975).

18) R. Kutterer, H. R. Hilzinger and H. Kronmuller, J. Mag. Magn. Mater. 4, 1 (1977).

19) G. Hoffer and K. Strnat, J. Appl. Phys. 38, 1377 (1967).

20) T. Shibata and T. Katayama, J. Mag. Magn. Mater. 31-34, 1029 (1983).

21) H. Kronmuller, Proc. Second Int. Symposium on Mag. Anisotropy and Coercivity in RE-TM Alloys, San Diego (1978).

22) R. L. Berger, H. A. Leupold, J. T. Breslin, F. Rothwarf and A. Tauber, J. Appl. Phys. 50, 2349 (1979).

23) H. F. Mildrum, M. S. Hartings, K. J. Strnat and J. G. Tront, AIP Conf. Proc. Mag. Magn. Mater. 618 (1972).

24) J. H. Van Vleck, Rev. Mod. Phys. 17, 27, (1945).

25) K. H. J. Buschow and A. M. Van Diepen, Solid State Comm. 15, 903 (1974).

26) K. H. J. Buschow and R. P. Van Atapele, J. Appl. Phys. 41, 4066 (1970).

27) Y. Khan, Physica Status Solidi a, 23 K151-154, (1974).

28) J. Deportes, D. Givord, J. Schweizer and F. Tasset, IEEE Transaction on Magnetics, Vol. MAG-12, 1000 (1976).

29) J. Deportes, D. Givord, R. Lemaire, H. Nagai and Y. T. Yanaga, J. Less Comm. Met. 44, 273 (1976).

30) J. J. Becker, J. Appl. Phys. 41, 1055 (1970).

31) S. Foner, E. J. McNiff, Jr., D. L. Martin and M. G. Benz, GE Tech. Information Series Report No. 72CRD073 NY 1972.

32) K. J. Strnat, G. Hoffer, W. Ostertag and J. C. Olson, J. Appl. Phys. 37, 1252 (1966).

33) R. D. Nelson, Research in Productio of Rare Earth Cobalt Permanent Magnet Material by Sputter Deposition, AFML F33615-73-C-5012, Wright Patterson Air Force Base, OH (1974).

34) H. Theurer, E. A. Nesbitt and D. D. Backon, J. Appl. Phys. 40, 2994 (1969).

35) Steven Bendson and J. H. Judy, IEEE Trans. on Magnetics, Vol.-MAG 9, 627 (1973).

36) J. D. Livingston, AIP Confer. Proced. 10, p. 643 (1973).

37) J. J. Becker, IEEE Trans. Mag. Vol. MAG-12, 965 (1976).

38) B. Cullity, Introduction to Magnetic Materials, second edition Addison-Wesley, 1972.

39) K. H, Buschow, P. A. Naastepad and F. F. Westendorp, IEEE Trans. on Magnetics, 6, 301 (1970).

40) D. L. Martin, M. G. Benz and A. C. Rockwood, AIP Confer. Proced. on Mag. Magn. Mater. 10, 583 (1973).

41) J. L. Vossen, Thin Film Processes Ch. 1, Acadmeic Press (1978).

42) B. Chapman, Glow Discharge Processes: Sputtering and Plasma Etching, Wiley Interscience Publishers (1980).

43) J. S. Logan et al., J. Vac. Sci. Tech. Vol. 14, 1, (1977).

44) J. A. Thornton, J. Vac. Sci. Tech. Vo. 11, No. 4, 34 (1974).

45) J. A. Thornton, J. Vac. Sci. Tech. Vol. 11, p. 666 (1974).

46) Clark W. Searle, Appl. Phys. Letters, 24, 1 (1974).

47) F. J. Cadieu, S. H. Aly and T. D. Cheung, J. Appl. Phys. 53, 2401 (1982).

48) F. J. Cadieu, T. D. Cheung, S. H. Aly, L. Wickramasekara and R. G. Pirich, J. Appl. Phys. 53, 8338 (1982).

49) F. J. Cadieu, T. D. Cheung, S. H. Aly, L. Wickramasekara and R. G. Pirich, IEEE, Vol. MAG-19, 2038 (1983).

50) S. H. Aly, T. D. Cheung, L. Wickeramasekara and F. J. Cadieu, J. Appl. Phys. 47, 2147, (1985).

51) F. J. Cadieu, L. F.,Cooley and D. H. Douglass, Jr., Rev. Sci. Instr., 42, 587 (1971).

52) J. S. Logan et al., J. Vac. Sci. Tech. 6, 120 (1969).

53) J. A. Venables, G. D. T. Spiller and M. Hanbuker, Reports on Prog. in Phys. 47, 4, (1984).

54) F. J. Cadieu and N. Chencinski, IEEE Trans. on Magnetics, MAG-11, 227 (1975).

55) F. J. Cadieu and N. Chencinski, J. Low Temp. Phys. 28, 535 (1977).

56) Austin M. Garath, Phys. Rev. 36, 248 (1930).

57) R. Bruckmuller et al., Radiation Effects, Vol. 45, p. 199 (1980).

58) J. J. Cuomo and R. Gambino, J. Vac. Scie. Tech. 14, 152 (1977).

59) W. W. Lee and D. W. Oblas, J. Appl. Phys. 46, 1728 (1975).

60) D. Matox and G. J. Kominiak, J. Vac. Scie. Tech. 8, 194 (1971).

61) G. C. Schartz and R. E. Jones, IBM J. Res. DEV. 14, 52 (1970).

62) Eugene P. Bertin, Principles and Practice of X-ray Spectrometric Analysis, Second Edition, Plenum Press (1975).

63) R. Jenkins and J. L. De Vries, Practical X-Ray Spectrometry, Springer-Verlag, N.Y. (1967).

64) L. Bergel and F. J. Cadieu, X-Ray Spectrometry, Vol. 9, 19 (1980).

65) L. S. Birks, X-Ray Spectrochemical Analysis, First Edition, Interscience Publisher, N.Y. (1969).

66) B. Cullity, Elements of X-Ray Diffraction, Second Edition, Addison-Wesley, 1978.

67) J. R. Rhodes, American Lab 5(7), p. 57 (1973).

68) T. Nishio et al., Proceedings of the 4th Inter. Workshop on Rare Earth Cobalt Permanent Magnets, p. 271, 1979, Hakon, Japan.

69) S. B. Byram et al., Advances in X-Ray Analysis, 20, 529 (1977).

70) H. Klug and L. Alexander, X-Ray Diffraction Procedures, Chapter 5, 9 (1954).

71) Handbook of Chemistry and Physics, 56th Edition, CRC Press (1976).

72) W. Parrish, IBM Research Report #RJ 2774 (35440) 1980.

73) M. Gronau, H. Goeke and S. Methfessl, Proc. 4th Confer. on Rapidly Quenched Metals, Sandia, 1981.

74) M. Gronau et al., IEEE Trans. on Mag. Vol-MAG-19, 1653 (1983).

75) D. Givord, J. Mag. Mater. 31-34, 191 (1983).

76) N. Kazama and M. Kameda, AIP Confer. Proced. 34, 307 (1976).

77) K. H. Buschow, J. Less Comm. Met. 14, 323 (1968).

78) D. J. Craik and R. S. Tebble, Ferromagnetism and Ferromagnetic Domains, Wiley and Sons, N.Y. 1965.

79) D. Givord, J. Laforest, R. Lemaire and Q. Lu, J. Mag. Magn. Mater. 31-34, 191 (1983).

80) K. H. J. Buschow, J. Less. Common. Met. 33, 311 (1973).

81) K. H. J. Buschow and A. S. Van Der Goot, J. Less Comm. Met. 14, 323 (1968).

82) D. K. Das, IEEE Trans. Magnetics 5, 214 (1969).

83) R. W. Lee, J. Appl. Phys. 52, 2549 (1981).

84) W. E. Wallace, H. Fuji, M. V. Satyanarayana and S. Hirosawa, 3rd Inter. Sympo. on Magnetic Anisotropy and Coercivity in RE-TM Alloys, Baden, Austria, p. 537 (1982).

85) G. C. Hadjipanayis, J. Appl. Phys. 52, 2517 (1981).

86) R. K. Mishra et al., J. Appl. Phys. 52, 2517 (1981).

87) K. J. Strnat, IEEE Trans. on Magn., MAG-8, 511 (1972).

88) J. J. Becker, J. Appl. Phys 39, 1270 (1968).

89) K. J. Strnat, D. Li and H. F. Mildrum, J. Appl. Phys. 55, 21000 (1984).

90) H. Zijlstra, J. Appl. Phys. 41, 4881 (1970).

91) D. I. Paul, J. Appl. Phys. 53, 2362 (1981).